On the link level performance verification method of dual-polarized MIMO capable mobile antenna

Yong-Sang Cho

The Graduate School

Yonsei University

Department of Electrical and Electronic Engineering

On the link level performance verification method of dual-polarized MIMO capable mobile antenna

A Dissertation

Submitted to the Department of Electrical and Electronic Engineering

and the Graduate School of Yonsei University

in partial fulfillment of the

requirements for the degree of

Doctor of Philosophy

Yong-Sang Cho

August 2012

This certifies that the dissertation of Yong-Sang Cho is approved.

_____

Thesis Supervisor: Woo-Young Choi

_____

Dong-Ku Kim

_____

Hyun-Yong Choi

_____

In-Kyung Kim

_____

Joo-Hee Lee

The Graduate School
Yonsei University
August 2012

To my parents
And my family

Acknowledgements

First of all, I want to thank the LG Electronics Inc. Their funding over a period of three years made this thesis possible. I want to acknowledge the strong support of my supervisors, Dr. Inkyung Kim, and Dr. Joohee Lee with their insightful advises and technical leadership. I also want to express my special thanks to Youngryul Kim, who build the MIMO OTA system with myself since 2009, Hyejung Sim, who automated the system with her brilliant skills, Seoungpyo Noh, who provided valuable comments, Junhyung Park, who assisted me for this work, Sanghun Lee, who provided excellent antenna designs, MehdiMuhammad Taqi Raza and Bilal Zafar who advised me with editorial corrections of this thesis, Sangjo Park, Jihyuk Park, Junkyu Park, Eunbit Cho, Changun Lee, Harry Jang, Daeyun Kim, and Jungrak Kim for their strong supports. I am also very grateful to Dr. Pekka Kyosti, Jukka-Pekka Nuutinen, and Tommi Jsamsa at Elektrobit Corp., Finland. I am truly grateful for our cooperation over years. Special thanks to Dr. Pekka Kyosti, or my friend for his generous help with the mathematics and channel modeling. Very special thanks to my supervisor, Prof. Woo-Young Choi for his strong support on this work for guiding me with extra efforts even though he is on his sabbatical year. I am also very grateful to Prof. DongKu Kim, for encourages and qualification of the thesis through valuable advises. I also want to thank Prof. Hyun-Yong Choi for his valuable advices. Last, I want to thank my family and my friends. Special thanks to my grandmother even though she passed away many years ago for raising me with her prayer. I also want to thank my father and mother who supported with love and trust. I also want to thank to my father-in-law and mother-in-law for their help in every way. I want thanks to my friends, Taehong Park, Jinpyo Jun, Kwangjung Kim, and Patrick. Finally, I want to say thank you for your love, my wife, Hyewook, my lovely daughter, Yoonseo, and my son Soowhan!

List of figures

List of tables

List of Abbreviations

2-D	2 Dimensiona
3GPP	3G Partnership Project
AMC	Adaptive Modulation Coding Scheme
AN	Antenna
AoA	Angle of Arrival
AoD	Angle of eparture
AS	Angular Spread
AUT	Antenna Under Test
AWS	Advanced Wire ess Service
BLER	Block Error Rate
BS	Base Station
CDF	Cumulative Distribution Function
CDL	Clustered Delay Line
COST2100	European Cooperation in Science and Technology Action 2100
CP	Cyclic Prefix
CQI	Channel Quality Indicator
CRC	Cyclic Redundancy Check
CTIA	Cellular Telecommunications Industry Association

DL	Down Link
DUT	Device Under Test
E-UTRAN	Evolved Universal Terrestrial Radio Access
GPO	General Purpose Output
HARQ	Hybrid Automatic Retransmit reQuest
H-pol	Horizontal Polarization
COST IC1004	COST action on Cooperative Radio Communications for Green Smart Environments
IMT-Advanced	International Mobile Telecommunications-Advanced
LOS	Line-Of-Sight
LTE	Long Term Evolution
MAC	Medium Access Control
MCS	Modulation and Coding Scheme
MI	Mutual Information
MIMO	Multiple Input Multiple Output
MS	Mobile Station
NF	Noise Figure
NLOS	None-Line-Of-Sight
OTA	Over The Air
PAS	Power Azimuth Spectrum
PCB	Printed Circuit Board
PDA	Personal Digital Assistance

PDSCH	Physical Downlink Shared CHannel
PDU	Packet Data Unit
PHY	Physical Layer
PIFA	Planar Inverted F Antenna
PMI	Preferred Matrix Indicator
QAM	Quadrature Amplitude Modulation
RAN	Radio Access Network
RB	Resource Block
RI	Rank Indication
RSRP	Reference Signal Received Power
RSSI	Received Signal Strength Indicator
Rx	Receiver
SCM	Spatial Channel Model
SCME	Spatial Channel Model Extension
SINR	Signal-to-Interference plus Noise Ratio
SNR	Signal-to-Noise Ratio
SRS	Sounding Reference Signal
TCP	Transmission Control Protocol
TDL	Tapped Delay Line
TGn	Task Group n (IEEE)
TM	Transmission Mode

Tx	Transmitter
UDP	User Datagram Protocol
UE	User Equipment
UL	Up Link
ULA	Uniform Linear Array
V-pol	Vertical Polarization
VSA	Vector Signal Analyzer
WINNER	Wireless World Initiative New Radio
XPD	Cross Polarization Discrimination

Abstract

On the link level performance verification method of dual-polarized MIMO capable mobile antenna

Yong-Sang Cho
Dept. of Electrical and Electronic Engineering
The Graduate School
Yonsei University

In this dissertation, comprehensive comparison studies are carried out on the LTE PDSCH link level performance of various kinds of MIMO antenna schemes and actual MIMO antenna implementations for mobile terminals. It is important to associate MIMO antenna design with link level performance in order to understand the impact of antenna characteristics of mobile stations on the overall end to end performance taking the antenna schemes at Base Station side into account.

The experimental evaluation method for LTE link level performance of mobile stations is that the recently introduced anechoic chamber based MIMO OTA test methodology. The measurement results in the MIMO OTA system are evaluated by a system model developed based on the WINNER II models and also by extensive field trials against LTE live networks.

In the first place, the concept of the MIMO OTA test methodology is evaluated by characterizing the statistical properties of the radio channels created by the method. To achieve this goal, the correlation properties of co-

polarized and dual-polarized dipole antenna arrays are investigated through measurements in the MIMO OTA system, and be compared with the numerical correlation results. For numerical calculations, a simplified PAS model and the CDL based WINNER II channel models are used. It is found that the correlation data measured in a MIMO OTA system is well matched to the numerical correlation data obtained from the WINNER II channel models, whereas the PAS model can be an approximated model which has a good match with the experimental data or the CDL model if the angular spreads of incident rays are as wide as Urban Macro or uniform models.

In the second place, a system model is developed based on WINNER II channel model in order to evaluate the LTE link level throughput performance associated with the MIMO antenna implementations. This dissertation introduces an effective SNR parameter to the conventional ergodic mutual information derived from the channel transfer matrices defined by the CDL model. It is found that the developed system model is able to estimate the LTE PDSCH throughput performance of MIMO antennas when the results are compared with the experimental data obtained from the MIMO OTA system.

In the third place, the LTE PDSCH throughput performance of various kinds of MIMO antenna schemes is investigated against LTE live networks and be compared with the conclusions derived from the experimental data in the MIMO OTA system. It is found that the MIMO OTA system is able to simulate both the NLOS and LOS MIMO radio channels under which the throughput performance rank of antennas under test are the same as in the live networks. This would mean that the MIMO OTA system is able to distinguish the good and bad antenna designs with reliable and repeatable manner. It can be concluded that the MIMO OTA system can be used for simulating the live network and can verify the antenna performance in conjunction with the physical layer throughput performance if proper channel models and measurement scenarios are properly designed.

In chapter 1, as mentioned, MIMO OTA system is evaluated both theoretically and experimentally. In chapter 2, hand effects on LTE physical layer performance of mobile terminals are analyzed based on the developed link level simulation model and MIMO OTA system. In chapter 3, various kinds of form factor antennas designed for various kinds of diversity schemes are characterized with the link level simulation model and measurements in MIMO OTA system. It is found that most of the mobile antennas outperform the co-polarized dipole antenna in Ricean channels due to the fact that the mobile antennas have dual-polarization properties.

In chapter 4, LTE throughput performance of co-polarized, dual-polarized dipole array, and form factor mobile antennas is compared against an LTE trial network in two different environmental characters (LOS and NLOS channels). Through statistical studies on the characteristics of antenna performance, it is concluded that the form factor antenna shows much better performance in both test routes.

Finally in chapter 5, the AUTs evaluated in chapter 3 are verified in an LTE commercial network. The conclusions achieved through the extensive measurement campaigns in MIMO OTA system and in the live networks is, that the link performance of the form factor mobile antennas is more robust than the co-polarized dipole antenna array in the case where the channel environments are Ricean channels and Tx antennas for BS are the co-located dual-polarized antenna.

Key words: MIMO, OTA, PAS, Polarization, Channel Modeling, Cluster, Antenna Diversity, Mutual Coupling, Mutual Information, Spatial Correlation, Link Level Performance, LTE, Field Test

CHAPTER 1

Characterization of correlation properties of MIMO capable mobile antenna

1.1 Introduction

There are many factors that could impact the link level throughput performance of the MIMO capable mobile terminals, which are the antenna gains embedded in the mobile terminals, correlation between antenna branches, radio channel characteristics, MIMO decoding performance the communication modem adopted by the terminal etc. Especially, the key factors related to afore mentioned antenna characteristics are strongly coupled to each other and the trade-off studies have been the key agenda for antenna engineers.

In order to characterize the antenna performance from MIMO link level performance perspective, the the mobile terminals must be evaluated under an environment where the antenna parameters and associated MIMO throughput can be measured simultaneously. One of such test environments is the live network. However, the verification of antenna performance against the commercial networks is not a trivial task due to the fact that there are a number of factors that could impact the device performance in the live networks, and thus, it is difficult to derive the antenna parameters from the gathered data in the live network. It is more efficient and beneficial if the MIMO antenna optimization can be done in a controlled lab environment, where realistic wireless channel environments are simulated.

In order to define the test methodologies that could meet such needs, many research forums and standardization groups have been discussing the

MIMO OTA test methodologies. IC1004 [1] took and continue the discussion from COST2100 [2]. In 3GPP RAN4, the MIMO OTA methods are actively discussed as a working item [3]. The same discussions are also on-going at CTIA[4]. In all groups, "Anechoic chamber with multiple probe antennas [5]" has been discussed as a baseline methodology including the other candidate methods such as reverberation chamber, two stage OTA test method. The anechoic chamber based OTA system consists of external fading emulators and multiple probe antennas from which the pre-faded MIMO OTA signals are generated at the channel emulators and transmitted. The realization of the spatial fading channels are generated based on the geometry based stochastic channel models; 3GPP SCM/SCME [7], WINNER[8] and IMT-Advanced[9].

One of the advantages of MIMO OTA system is that it can provide consistent and reproducible measurement results when compared to those obtained through field tests in the liven networks. In this regards, this study verified the anechoic chamber based MIMO OTA solution proposed in [5] by evaluating the correlation properties of half wavelength dipole antennas with different antenna spacing at MIMO OTA system and compared the results to those obtained from theoretical model.

For comparison purpose, a simplified model based on Laplacian shape PAS (power azimuth spectrum) models and CDL (Clustered delay line) mode based WINNER II channel models are used to analyze the correlation properties of AUT (Antenna Under Test). It is important to use same type of power distribution profile both in the theoretical models and MIMO OTA system because the correlation properties at the mobile antennas are mostly determined by the angular spreads. In order to evaluate the experimental data measured in the MIMO OTA system, the cross correlation coefficient of the co-polarized dipole array with various inter-element spacing is investigated for various channel models with different PAS shapes, and be

compared with the theoretical values derived by the PAS models and CDL based channel models.

In section 1.2, MIMO OTA system setup used for the measurements, and the CDL model based MIMO OTA channel models are presented. In section 1.3, back ground of CDL based channel models and the simplified PAS models and derivation of antenna performance metrics are discussed. In section 1.4 and 1.5, the concept of the MIMO OTA test methodology is evaluated by characterizing the statistical properties of the radio channels created by the method by comparing the experimental correlation co-polarized dipole array with theoretical correlation derived from the PAS models and the CDL models.

In section 1.6, a system model is developed based on WINNER II channel model in order to evaluate the LTE link level throughput performance of dual-polarized dipole array with various relative tilt angles between antenna elements. It is found that the developed system model is able to estimate the LTE PDSCH throughput performance of MIMO antennas when the results are compared with the experimental data obtained from the MIMO OTA system.

1.2 MIMO OTA system concept

1.2.1 MIMO OTA system setup

Figure 1.1 shows MIMO OTA system setup used in this study. The MIMO OTA system consists of 8 dual-polarized probe OTA antennas in a 2-D space (or Azimuthal plane). The probe antennas are connected to the channel emulators located outside of anechoic chamber for simulation of the MIMO radio channel models. The 8-probe antennas are placed with 45° angular distance between adjacent probe antennas. Each probe antenna

transmits V-polarized and H-polarized components simultaneously in order to create independent channels for each polarization state.

Spatial clusters defined in the channel models can be created by using 2~4 adjacent probe antennas with different power weights based on pre-faded signals synthesis method [5][15]. Each probe antenna radiates pre-faded signals with different power weightings in such a way that the created PAS follows the Laplacian power distributions in 2-D space, and the PAS creates the correlation between antennas in spatial domain. Such spatial fading effects are measured and presented in figure 1.2, and be compared with the theoretical 2-D spatial correlation results presented in [5]. The measured 2-D spatial correlation data near the test zone is well matched to the theoretical results presented in [5] for the case of 8-probe OTA antenna system. One important limitation of the MIMO OTA system is that it has limited number of probe antennas than the number of radio channels, and this define such area where the spatial correlation follows the Bessel function of the 1st kind. In case of 8-probe OTA antenna system, such test area is limited to 0.75λ. In 700 MHz band, the primary band to be used throughout this thesis, the test zone is around 30 cm, and therefore the size of DUT (Device under test) can be up to 30 cm.

The spatial correlation properties of AUTs can be obtained from power correlation measurements between the time samples of received powers through antenna branches. The power correlations are the correlation coefficients of squared magnitudes [6].

In the MIMO OTA system setup in figure 1.1, 2x2 MIMO downlink signals are generated from BSE (Base station emulator) and are fed to the input ports of fading emulators and then transmitted through the probe antennas into the chamber. Each branch of AUT is connected to a VSA (Vector signal analyzer) outside the chamber and to the LTE terminal as shown in figure 1.1.

The power correlation coefficient between time samples of received power from two antenna branches is given by,

$$\mathbf{P_1} = \mathbf{FFT}(\mathbf{S_1}), \quad \mathbf{P_2} = \mathbf{FFT}(\mathbf{S_2}) \qquad (\boldsymbol{Eq.1.1})$$

$$\boldsymbol{\rho_{pwr}} = \frac{\mathbf{E}\{\mathbf{P_1^* P_2} + \mathbf{P_2^* P_1}\}^2}{\mathbf{E}\{\mathbf{P_1^* P_1}\}\,\mathbf{E}\{\mathbf{P_2^* P_2}\}} \qquad (\boldsymbol{Eq.1.2})$$

$\mathbf{S_1}$ and $\mathbf{S_2}$ denote the received signal, $\mathbf{P_1}$ and $\mathbf{P_2}$ denote received power, and $\boldsymbol{\rho_{pwr}}$ denote power correlation measured at VSA. It should be noted that the power correlation coefficients are an approximation of squared amplitudes of the complex signal correlation [25].

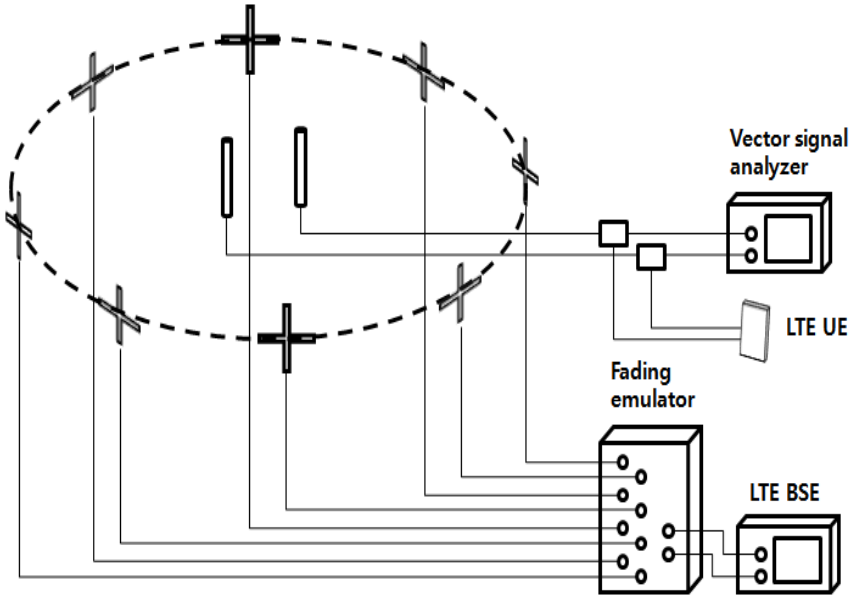

Figure 1.1 MIMO OTA system diagram to measure wireless Data through performance of LTE terminal

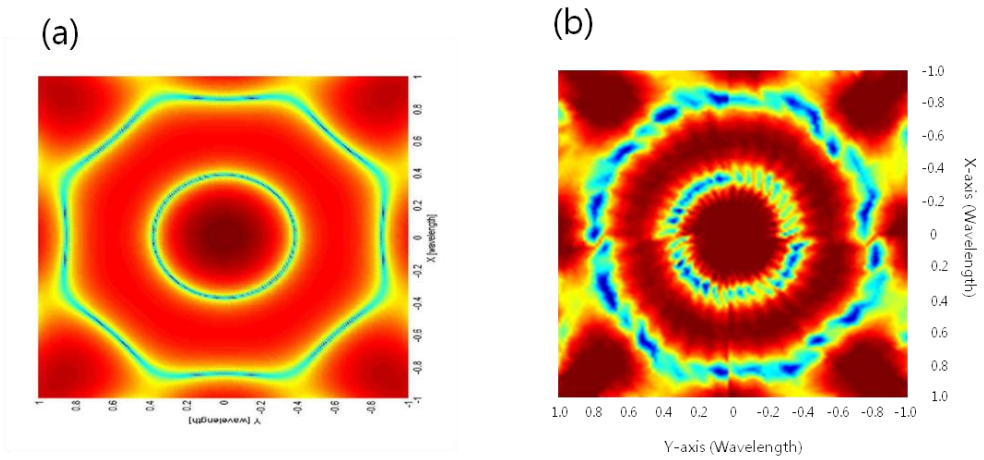

Figure 1.2 2-D spatial correlation for MIMO OTA system with 8-Probe OTA antennas obtained from a) theoretical simulation results in [4], b) measurement results

1.2.2 Geometrical stochastic MIMO OTA Channel models

1.2.2.1 MIMO OTA channel model requirements

It is necessary to define key requirements for the MIMO OTA channel models in order to satisfy aforementioned needs for MIMO OTA system. In 3GPP, key operators and device manufactures agreed to use the OTA throughput as the figure of merit of MIMO OTA testing leading that the MIMO OTA system should be able to evaluate the antenna gain imbalance, antenna correlation, intra-terminal interference, RF transceiver and baseband performance [10]. The requirements are interpreted to the relevant requirements for the MIMO OTA channel models as below.

- *Antenna pattern independency from the channel model*
- *Visible signal arrival direction from model parameters in order to validate the antenna gain and gain imbalance of MS depending on the direction of incident signals.*
- *Dual polarized channel model both for NLOS and LOS paths.*
- *XPR shall be adjustable.*

- *Signal angular spreads and arrival/departure angles shall be adjustable.*
- *Delay spread, Doppler shifts shall be adjustable.*

1.2.2.2 CDL model based MIMO OTA channel model

SCME channel model has been developed as part of WINNER project for an interim channel model for beyond-3G systems [7]. The major extended feature of SCME from SCM is bandwidth extension to 100 MHz by introducing intra-cluster delay spread. As in SCM, SCME channel model is a geometrical channel model based on the clustered delay line (CDL) model which is deemed as a spatial extension of the tabbed delay line (TDL) model. Figure 1.3 shows a graphical explanation and terminologies related to the CDL model.

The typical outdoor models in SCME are defined based on the measurement parameters for three kinds of geometrical environments (Suburban Macro, Urban Macro, and Urban Micro). There are 6 “clusters” in every scenario and each “cluster” consists of 20 “rays”. The sum-of-rays in the test zone results in correlation between antennas [15]. From the large scale parameters defined for each clusters, the signal arrival can be visualized from model and this is a clear benefit of CDL based model in a sense that the antenna engineers can validate their antenna design knowing that the directions of the incident waves and associated antenna performance.

One known limitation of SCME channel model is that it does not support horizontal polarization component for LOS path, which is very important for characterizing the dual polarized antennas of MS in Ricean fading channel conditions. Because of this limitation, SCME channel is not the best choice for MIMO OTA channel model where the Ricean channel is present. However, it is clear that SCME satisfies the other requirements for MIMO OTA channel model and can be used in case of NLOS conditions.

WINNER II model is more generalized CDL based channel model than SCME providing more scenarios such as outdoor-to-indoor scenario as well as extended features such as intra-cluster delay spread for the major clusters and enriched dynamic effects [8]. The dual polarized LOS path could be supported if the error in dual polarized LOS path term is corrected to WINNER II model. In this dissertation, MIMO OTA channel models are generated by WINNER II model based on geometrical parameters of SCME channel model.

1.2.2.3 Geometrical parameters for MIMO OTA channel model realization

The large scale parameters for the MIMO OTA channel models are important because they determine the fixed geometrical parameters to be used for channel impulse response realization.

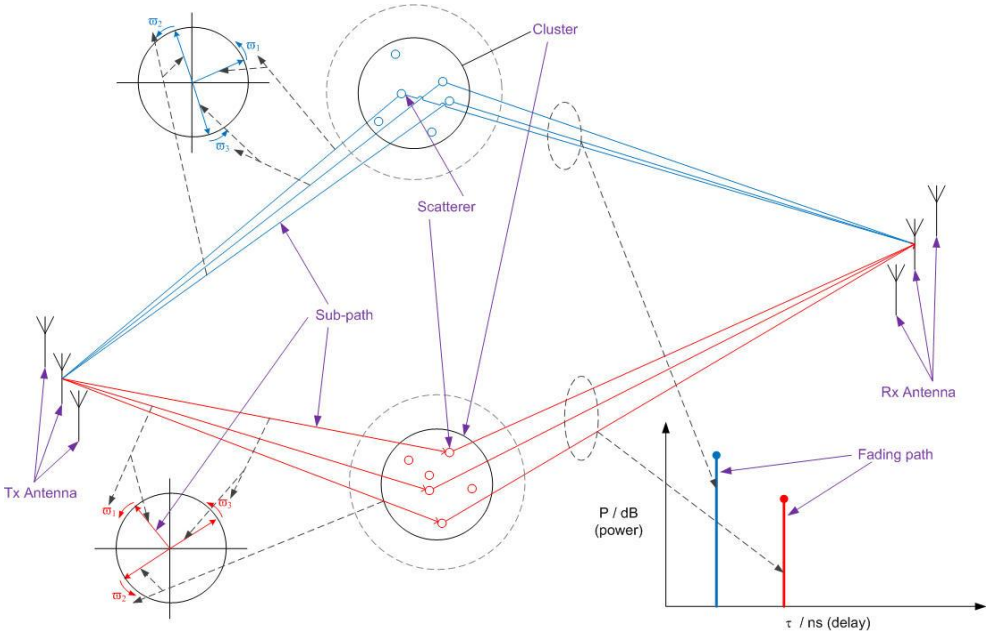

Figure 1.3 Graphical descriptions of spatial clusters for CDL channel models

The MIMO OTA channel models are realized based on the geometrical parameters defined in SCME channel models, which are summarized in appendix, table A.1 (2D-Uniform multi-path model), A.2 (Single spatial cluster model), A.3 (Urban Micro-cell model), and A.4 (Urban macro-cell model) [14].

The power distribution functions for each of channel model under discussion are depicted in the figure 1.4, which are generated from the large scale parameters in table A.1, A.2, A.3, and A.4. Signal arrival directions of the PAS are visualized in 2-D space (Azimuth plane propagation only) for better understanding of the different PAS shapes between models. Numerical method for PAS generation will be discussed in the later sections.

In case of 2-D uniform model, the multi-path parameters are adopted from the enhanced pedestrian-A channel model, and its power distribution function in Azimuth plane is uniform. Single spatial cluster model is defined based on Urban micro-cell model for each multi-path parameters but has only one spatial cluster with AoA=0° (Angle of arrival). Urban macro and urban micro models have 6 clusters with different AoAs, creating wider power distributions than the single cluster model.

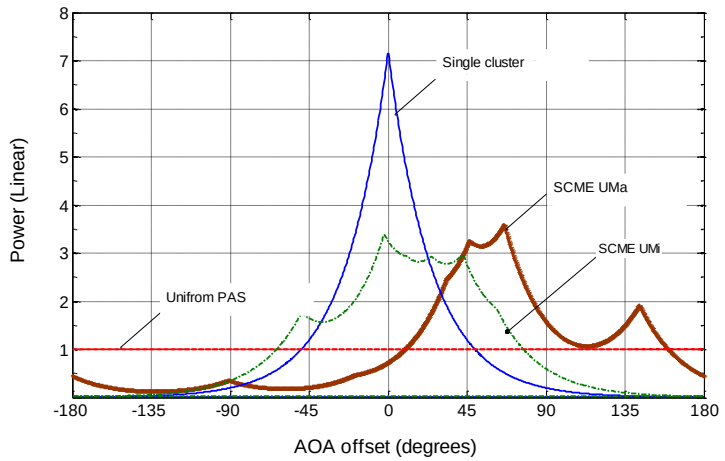

Figure 1.4 Power Azimuth Spectrum (PAS) models to compare the channel model defined for MIMO OTA test

1.3 Performance metrics of antenna in radio channels

In this section, the performance metrics of antennas taking the radio channels into account are discussed. By evaluating the selected performance measures, the experimental data obtained from the MIMO OTA system can be evaluated with the theoretical simulation results. The performance metrics to be discussed are as follows

- *Correlation coefficient*
- *Diversity measure*
- *Mutual information*
- *Physical layer throughput*

In the following sections the performance matrices will be discussed in detail and validated in case of Ricean channels as well as the Rayleigh channels.

1.3.1 MIMO radio channel

The transfer matrix of an $N_{tx} \times N_{rx}$ MIMO radio channels are defined with the time-variant channel impulse response between *j*th *tx* antenna and *i*th *rx* antenna, $H_{ij}(t,\tau)$, where *t* is time, τ is delay [17].

$$\mathbf{H}(t,\tau) = \begin{pmatrix} H_{11}(t,\tau) & H_{12}(t,\tau) & \cdots & H_{1N_{tx}}(t,\tau) \\ H_{21}(t,\tau) & H_{22}(t,\tau) & \cdots & H_{2N_{tx}}(t,\tau) \\ \vdots & \vdots & \ddots & \vdots \\ H_{N_{rx}1}(t,\tau) & H_{N_{rx}2}(t,\tau) & \cdots & H_{N_{rx}N_{tx}}(t,\tau) \end{pmatrix} \qquad (Eq.\,1.3)$$

The transfer matrix comprises the non-coherent summation of the transfer matrix of each cluster

$$\mathbf{H}(t,\tau) = \sum_{l=1}^{L} \mathbf{H}_l(t,\tau) \qquad (Eq.\,1.4)$$

H_l by the geometrical channel model can be expressed with independently separated antenna field patterns for BS and MS from the channel impulse response, h_l.

$$\mathbf{H}_l(t,\tau) = \iint \mathbf{F}_{rx}^{T}(\varphi)\mathbf{h}_{\boldsymbol{l}}(t,\tau,\phi,\varphi)\,\mathbf{F}_{tx}(\varphi)\,d\varphi d\phi \qquad (Eq.\,1.5)$$

where, φ is the average angle of departure and ϕ is the average angle of arrival of l th cluster. The dual polarized channel matrix and antenna matrices are introduced in the clustered structure of propagation channel [8].

1.3.2 Covariance matrix and spatio-temporal correlation coefficients

The correlation matrix of single-polarized MIMO channel is defined from the channel transfer matrix, H [16].

$$\mathbf{R} = E\{\mathrm{vec}(\mathbf{H})\mathrm{vec}(\mathbf{H})^{\mathrm{H}}\} \qquad (Eq.\,1.6)$$

where the superscript ^{H} designates the Hermitian transpose. For 2x2 MIMO channels, R is a 4x4 matrix.

$$\mathbf{R} = \begin{pmatrix} 1 & \rho_{tx}^{*} & \rho_{rx}^{*} & s_1^{*} \\ \rho_{tx} & 1 & s_2^{*} & \rho_{rx}^{*} \\ \rho_{rx} & s_2 & 1 & \rho_{tx}^{*} \\ s_1 & \rho_{rx} & \rho_{tx} & 1 \end{pmatrix} \qquad (Eq.\,1.7)$$

ρ_{tx} and ρ_{rx} are the transmit and receive antenna spatial correlation coefficients at the transmitters and the receivers; and s_1 and s_2 are the cross-channel correlations [17]. This spatial correlation matrix in *Eq.* 1.7

can be used for analyzing the correlation properties of co-polarized linear dipole antenna array taking into account for the channel correlation.

In case of dual polarized radio channel analysis, C. Oestges developed analytic correlation coefficient model for special cases of antenna schemes [16]. However, such model cannot be applicable to the arbitrary antenna schemes to be analyzed in this thesis.

For antenna with arbitrary polarization states, the spatio-temporal correlation coefficients for *Tx* and *Rx* can be derived from the 2x2 channel transfer matrices.

$$\rho_{rx,\bar{t}} = E\left\{\frac{H_{11}^{*}(t,\tau)H_{21}(t,\tau) + H_{12}^{*}(t,\tau)H_{22}(t,\tau)}{\sqrt{|H_{11}(t,\tau)|^2 + |H_{12}(t,\tau)|^2}\sqrt{|H_{21}(t,\tau)|^2 + |H_{22}(t,\tau)|^2}}\right\} \qquad (Eq.1.8)$$

$$\rho_{tx,\bar{t}} = E\left\{\frac{H_{11}^{*}(t,\tau)H_{12}(t,\tau) + H_{21}^{*}(t,\tau)H_{22}(t,\tau)}{\sqrt{|H_{11}(t,\tau)|^2 + |H_{21}(t,\tau)|^2}\sqrt{|H_{12}(t,\tau)|^2 + |H_{22}(t,\tau)|^2}}\right\} \qquad (Eq.1.9)$$

In the following sections the correlation coefficients obtained from the covariance matrix and from the spatio-temporal correlation coefficients will be validated with co-polarized and dual-polarized dipole arrays in case of Ricean channels as well as the Rayleigh channels.

1.3.3 Antenna pattern correlation coefficient

The pattern correlation coefficient is widely used as a measurement method of the correlation properties of antennas from measured complex patterns because of its simplicity. The pattern correlation between two receive antennas in Rayleigh channels can be defined with [11].

$$\rho_F = \frac{\int \mathrm{F}_1(\phi)\,\mathrm{F}_2^{*}(\phi)\mathrm{P}_\mathrm{L}(\phi)d\phi}{\sqrt{\int|\mathrm{F}_1(\phi)|^2\mathrm{P}_\mathrm{L}(\phi)d\phi \cdot \int|\mathrm{F}_2(\phi)|^2\mathrm{P}_\mathrm{L}(\phi)d\phi}} \qquad (Eq.1.10)$$

where, ϕ is angle in 2-D space, F_1, F_2 are the complex antenna patterns of MS antennas, P_L denotes the PAS in 2-D space defined by the Laplacian distribution function [11].

$$P_L(\phi) = \sum_{l=1}^{L} \frac{Q_l}{\sigma_l \sqrt{2}} \exp\left[\left(-\sqrt{2} |\phi - \phi_{0,l}| \right) / \sigma_l \right] \qquad (Eq.\ 1.11)$$

where , $Q_{L,k}$ is power normalization factor for the *l*th cluster, L is the number of cluster, σ_l is the converted angular spread for *l*th cluster, $\phi_{0,l}$ is the mean AoA of *l*th cluster. The PAS by *Eq*. 1.11 is polynomial fitted of RMS (Rood Mean Square) angular spreads to σ parameter of the Laplacian distribution. The angular spread to σ parameter conversion parameter was developed by Laurent Schumacher for TGn channel model [13].

1.3.4 Diversity measure

Among the conventional antenna performance metric, the diversity measure is widely discussed in literatures [16][17][18][19]. Diversity measure can be utilized as a parameter for the system to be able to select between the diversity and the spatial (or polarization) multiplexing mode. In principle, the diversity gain is inversely proportional to the multiplexing gain. The diversity measure is a generalized definition indicating how the random variable varies relative to its average value, which explains the degree of freedom of the channel to the variance of $\|\mathbf{H}\|_F$[19]. The diversity measure is derived from the covariance matrix in *Eq*. 1.7 for Rayleigh fading MIMO radio channels, with tr[·] denoting trace of the matrix and $\|\cdot\|_F$ denoting the Frobenius norm.

$$\psi(\mathbf{R}) = \left(\frac{\mathrm{tr}\,\mathbf{R}}{\|\mathbf{R}\|_F^2} \right)^2 \qquad (Eq.\ 1.12)$$

In case of correlated radio channels, the diversity measure can be derived from the original meaning of the diversity measure with

$$\Psi(\mathbf{R}) = \frac{(\mathrm{E}[\Upsilon])^2}{\mathrm{var}[\Upsilon]} \quad \text{, where } \Upsilon := \|\mathbf{H}\|_{\mathrm{F}}^2 \qquad (Eq.\ 1.13)$$

where, var[▪] denoting variance of the random variables. In the following section the diversity measure will be validated in case of Ricean channels as well as the Rayleigh channels.

1.3.5 Mutual information

System model for the input and output relations of a single link MIMO system is defined with

$$\boldsymbol{r}(t) = \boldsymbol{H}(t,\tau) * \boldsymbol{s}(t) + \boldsymbol{n}(t) \qquad (Eq.\ 1.14)$$

When the transmitter has no knowledge of the receiver, the channel impulse response, $\mathrm{H}(t,\tau)$ obtained from *Eq.* 1.5 can be normalized to constant transmit power which removes the effects of antenna gain and path loss effects [18].

$$\mathbf{H}_{\mathrm{n}} = \sqrt{\frac{N_{tx}N_{rx}}{\|\mathbf{H}\|_{\mathrm{F}}^2}}\mathbf{H} \qquad (Eq.\ 1.15)$$

N_{tx}, N_{rx} denoting the number of transmit and receive antenna, $\|\mathrm{H}\|_{\mathrm{F}}$ denoting the Frobenius norm of H. From the normalized channel transfer matrix, narrow band mutual information (MI) at time, *t* is defined as

$$\boldsymbol{I}(t) = \log_2 \det\left[\mathrm{I} + \frac{\mathrm{SNR}}{N_t}\mathbf{H}_{\mathrm{n}}(t)\mathbf{H}_{\mathrm{n}}^{\mathrm{H}}(\mathrm{t})\right] \qquad (Eq.\ 1.16)$$

In principle, the narrow band MI and the wide band MI are different. However in practice, the narrow band MI is a good approximation in case of wide band with typical delay spreads. The ergodic MI for a random H can be approximated by averaging MI over 50,000 realizations.

In the following section the ergodic MI will be validated in case of Ricean channels as well as the Rayleigh channels.

1.3.6 LTE physical layer throughput estimation

From the derived mutual information for each antenna, LTE physical layer throughput performance can be estimated based on standard link level system parameters [24]. LTE physical layer throughput can be obtained from MI with,

$$C = \mathrm{F} \cdot \mathrm{BW} \cdot \mathrm{R_c} \cdot \mathrm{I(t)} \qquad (Eq.\,1.17)$$

where F denoting correction factor, BW denoting effective bandwidth, Rc is coding rate of the frame, e denoting block error rates.

$$BW = \frac{\mathrm{N_{SC}} \cdot \mathrm{N_S} \cdot \mathrm{N_{RB}}}{\mathrm{T_{sub}}} \qquad (Eq.\,1.18)$$

The effective bandwidth, BW is total resources in a sub-frame, where $\mathrm{N_{SC}}$, denoting the number of sub-carriers in a resource block (RB), $\mathrm{N_S}$ denoting the number of OFDM symbol in a sub frame, $\mathrm{N_{RB}}$ denoting number of RBs. F includes the loss due to cyclic prefix (CP), the sounding reference channel (SRS) transmission, and reference symbols. $\mathrm{R_c}$ for MCS index 28 (0.801) is used, and 10% of BLER, and 22.5 dB of SNR is used, which is the required SNR for MCS 27.

1.3.7 Antenna schemes

The radio channels created by the channel models have a large impact on the correlation properties between the signals received by the MIMO antenna branches. Transmit antennas at BS are also part of the channel models that influences on the correlation properties of the radio channels.

Table 1.1 shows three different antenna schemes on both ends (MS and BS) to be analyzed. Slanted ($\vartheta = \pm 45°$) dual-polarized ideal dipole antennas are adopted for BS antenna patterns, and co-polarized or dual polarized dipole antenna arrays are used for receive antennas at MS. Δ_d denotes inter-element spacing of dipole array normalized by the wavelength, $(\vartheta_{1,}\vartheta_2)$ denotes tilt angle of each antenna with respect to the zenith. In case of V-polarization, $\vartheta = 0°$, and in case of H-polarization, $\vartheta = \pm 90°$.

Scheme A is selected for comparative study of the accuracy between the measurement data in MIMO OTA system and numerical methods. Scheme B and C are designed for the link level performance analysis of dipole array with arbitrary polarization states under Rayleigh fading and Ricean fading conditions.

Table 1. 1 Antenna schemes for investigation

Scheme	Parameter	BS	MS
A	Δ_l	$\{40\lambda\}$	$\{{}^1/_{10}\lambda, {}^1/_8\lambda, {}^1/_4\lambda, {}^1/_2\lambda, {}^2/_3\lambda\}$
	$(\vartheta_{1,}\vartheta_2)$	$\{(45°, -45°)\}$	$\{(0°, 0°)\}$
B	Δ_l	$\{0\lambda\}$	$\{{}^2/_3\lambda\}$
	$(\vartheta_{1,}\vartheta_2)$	$\{(45°, -45°)\}$	$\{(0°, 0°)\}$
C	Δ_l	$\{0\lambda\}$	$\{{}^1/_{10}\lambda\}$
	$(\vartheta_{1,}\vartheta_2)$	$\{(45°, -45°)\}$	$\{(0°, 0°), (0°, -22.5°), (0°, -45°), (0°, -67.5°), (0°, -90°), (22.5°, -22.5°), (45°, -45°)\}$

1.4. Analysis on correlation characteristics of co-polarized dipole based on PAS models

1.4.1 Pattern correlation analysis at fixed AoA

Pattern correlation (ρ_F) across two antennas can be derived from *Eq*. 1.10 with the complex antenna patterns and appropriate PAS models. With this method, antenna correlation properties can be investigated taking the mutual coupling effects into account. Three types of PAS models are used for analysis; 2-D Uniform, Single cluster, and Urban Macro models.

It is necessary to derive the pattern correlation in the presence as well as absence of mutual coupling effects to quantify the impact of the mutual coupling effects on the antenna correlation and to take these effects into account for comparing with the experimental data gathered from the MIMO OTA system. The complex antenna patterns are measured in two different ways.

- *Presence of mutual coupling effects*(ρ_{FC}): *two antennas are located at the test position together and one of antenna is terminated with 50 ohm load while the other is under measurements and vice versa.*
- *No mutual coupling effects* (ρ_{FF}): *radiation pattern for each antenna is measured separately.*

Figure 1.5 shows the pattern correlation properties of co-polarized dipole array obtained from the *Eq.* 1.10 and *Eq.* 1.11 as a function of inter-element spacing, Δ_l, for three types of PAS models. For reference, theoretical correlation curve obtained from the Bessel function of the first kind is depicted for each PAS model. Note that AoA=0° of the PAS is aligned to the broad side of the dipole array. It is clear from the results that the ρ_{FF} without mutual coupling effects shows similar result to the theoretical correlation function for all PAS models.

In case of 2-D uniform PAS model, ρ_{FC} in the presence of mutual coupling effects shows approximately 50% reduced correlation properties

from those of theory at $\Delta_l = 0.1\lambda$. As the antenna spacing increases, ρ_{FC} reduces and becomes flat shape close to '0'. Figure 1.5 (b) depicts ρ_{FC} in the case of single cluster PAS model. Because of the narrow angular spread, it appears that ρ_{FC} for single cluster PAS model is larger than that of 2-D uniform PAS model.

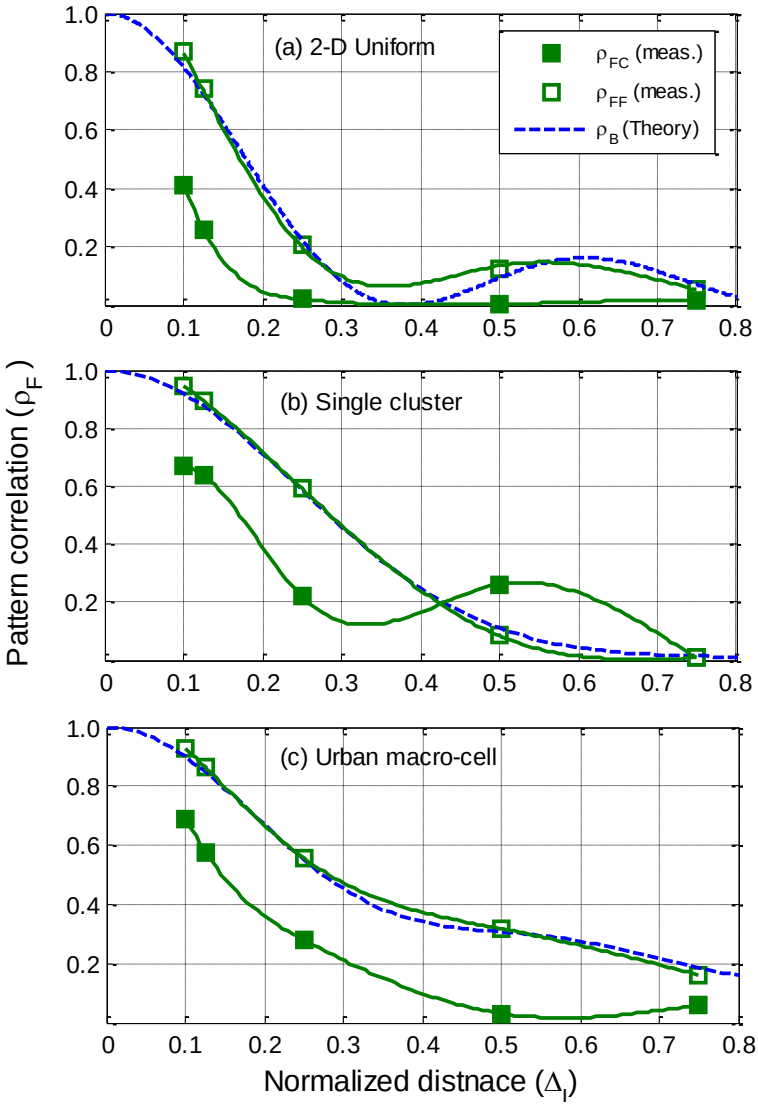

Figure 1.5 Correlation characteristics of co-polarized dipole array as a function of $\boldsymbol{\Delta_l}$. for (a) 2D uniform PAS, (b) Single cluster PAS, (c) Urban Macro PAS models

It should be noted that ρ_{FC} increases near $\Delta_l = 0.5\lambda$, where the antenna separation is considered to be sufficient to achieve low correlation. This can be observed at a particular angle of arrival due to the distorted antenna patterns by the mutual coupling effects. The observation suggests that the correlation properties for each PAS models need to be investigated over different AoA offsets in 2-D space. In case of Urban Macro PAS model, as shown in figure 1.5 (c), ρ_{FC} decreases quite linearly when we compare with the other PAS models as the antenna spacing increases. Because the cluster with shortest delay of Urban Macro PAS model is at 66° and the next one is at 46°, it shows high correlation characteristics despite the wide angular spreads. Such offset increases the correlation values. Comparing between the correlation properties obtained from different PAS models, the following observations can be made:

- *Pattern correlation obtained from the PAS model and measured complex antenna patterns is able to model the mutual coupling effects*
- *Mutual coupling effect are still dominant even at* $\Delta_l = 0.5\lambda$

1.4.2 Impact of AoA offsets on pattern correlation

Figure 1.6 shows ρ_{FF} with respect to the AoA offset, $\Delta_{AoA} \in \{-180; 180\}$ for Single Cluster and Urban Macro PAS models. The theoretical ρ_F of ideal dipole array for different inter-element spacing are presented together with the measurement results without mutual coupling effects for comparison. 2-D uniform PAS model is not included due to the fact that there is no angular dependency in the uniform model. It is clear from the results that ρ_{FF} vary as a function of Δ_{AoA} in a large degree. This would mean that ρ_{FF} should be averaged over Δ_{AoA} to be compared to the values obtained from different PAS model to prevent under estimation or over

estimation of the correlation. Comparing the results between the correlations properties obtained from two PAS models, it is clear that ρ_{FF} for the Single Cluster PAS model has much stronger dependencies on Δ_{AoA} than Urban Macro PAS model and be easier to identify the AoA creates high correlation.

Figure 1.7 shows the measured ρ_{FC} for the antenna patterns with mutual coupling effects. It is observed that ρ_{FC} decrease for all Δ_l conditions compared the case of ρ_F without the mutual coupling effects.

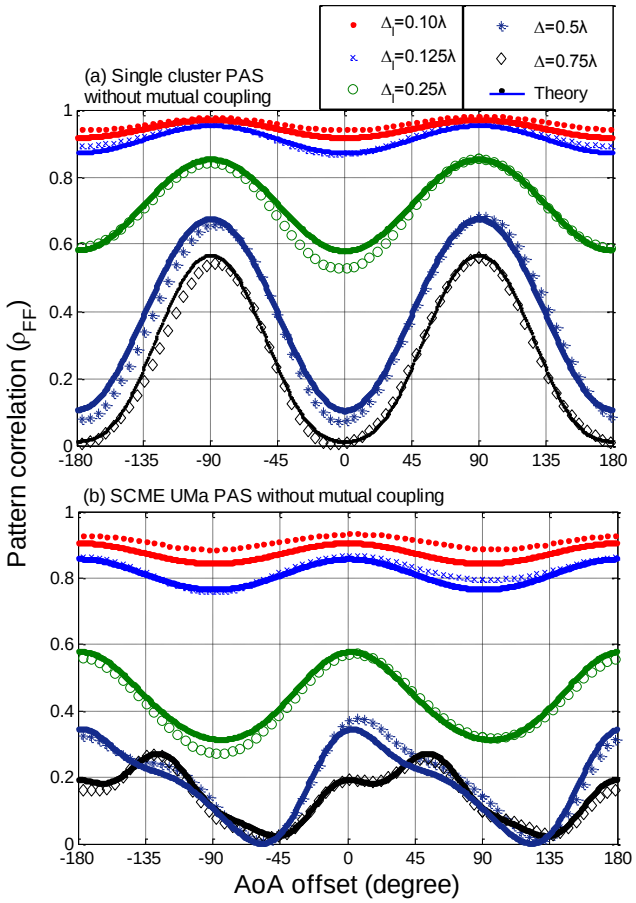

Figure 1.6 ρ_F as a function of Δ_{AoA} and Δ_l for (a) Single Cluster PAS and antenna patterns without mutual coupling effect (b) Urban Macro PAS and radiation patterns without mutual coupling effect. Solid lines show the theoretical values

It is clear from the results that the mutual coupling effects still have a large impact even at the spacing of 0.5λ and 0.75λ both for the Single Cluster and Urban Macro PAS models. This would mean that the mutual coupling effects exist in most cases especially for the mobile terminals for which operating bands are 1< GHz. For example the typical size of mobile terminal would be in the order of 0.25λ in 700 MHz band and still be under influence of mutual coupling effects.

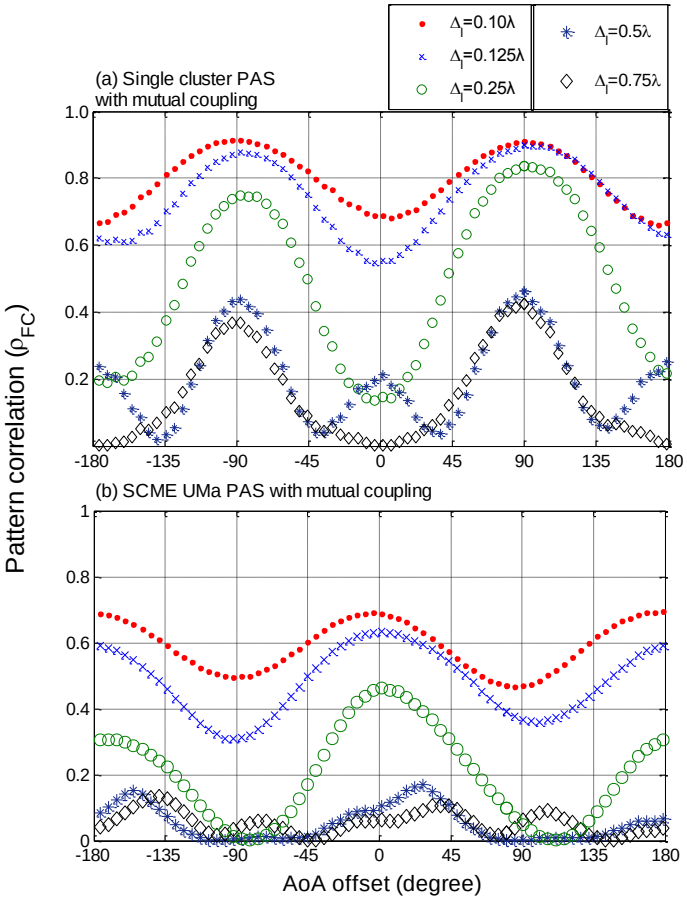

Figure 1.7 ρ_F characteristics against Δ_{AoA} and Δ_l condition under (a) Single Cluster PAS and radiation patterns with mutual coupling effect, (b) Urban Macro-cell PAS and radiation patterns with mutual coupling effect

1.5 Correlation measurement of co-polarized dipole with MIMO OTA system

1.5.1 Comparison of MIMO OTA measurement results to PAS model

Although the power spectral distribution functions of the incident rays of the channel models for MIMO OTA system is the same as in the PAS model, they are based on the geometrical stochastic channel models so called, CDL models discussed in section 1.2.2.2. The channel coefficients are defined by *Eq.* 1.5 except for the MS antenna patterns are replaced with the real antennas of DUT (Device Under Test) located at the center of the chamber. In principle, the pattern correlation results discussed in section 1.3 and 1.4 and those obtained from the MIMO OTA system are different because the correlation, in the CDL model, is jointly defined by Tx and Rx antenna patterns. However, from a practical stand point, it is worthwhile to compare the measured correlation properties of AUTs with MIMO OTA system to the pattern correlation results.

Figure 1.8 shows the comparison between the pattern correlation coefficients for the three PAS models and measured values from the MIMO OTA channel models for which power distributions in 2D space are the same as the PAS models. The correlation coefficients are averaged over Δ_{AoA}= {0°, 45°, 90°}. It should be noted that both the experimental data and values obtained from the PAS models are almost identical except for the single cluster model. This can be explained by the fact that the channel correlations become dominant in case of the power distributions of the signals are narrow. Similarly, when the angular spreads are large as in the cases of the 2-D uniform or the Urban Macro channel models, the impact of the channel correlations on the Rx correlation would be smaller.

It is important to note that the 2-D uniform PAS model which is the most widely used in antenna correlation analysis may give underestimated

values. In addition, in case of the single cluster channel model, the pattern correlations tend to be over-estimated than in the realistic conditions. However it would be useful to use it for evaluation of the antenna pattern for performance improvement purpose rather than using it as a performance metric. The Urban macro channel model can be a more practical choice for pattern correlation metric.

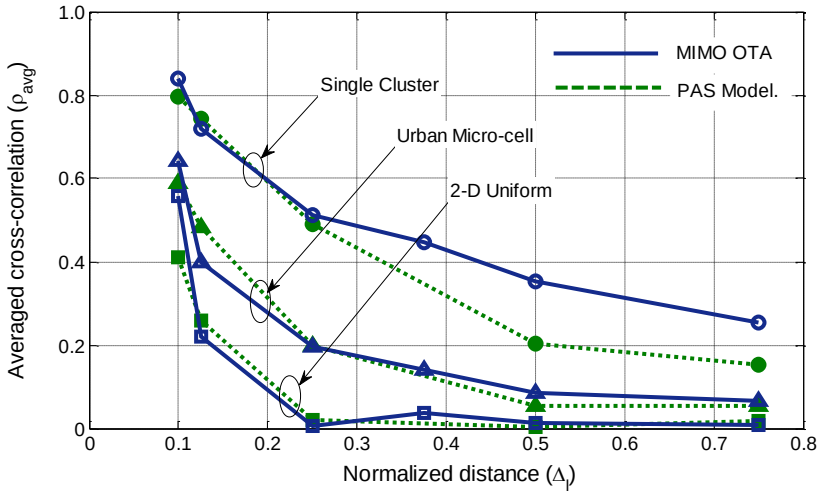

Figure 1.8 Comparison of the measured correlation characteristics in the MIMO OTA system to the correlation results obtained from the PAS model and radiation pattern with mutual coupling effects

1.5.2 Comparison of MIMO OTA measurement results to CDL model

As shown in section 1.6.1, pattern correlation characteristics derived from the PAS model can be a good approximation when the power distributions of the incident waves are wide enough. However, it is clear that the PAS model showed a large deviation from the measurement results when the PAS is narrow as in the case of Single Cluster model. In order to

clarify the cause of the error, spatial correlation properties are analyzed for the co-polarized dipole antenna array based on the CDL model.

Co-variance matrix of the 2x2 MIMO radio channel can be derived by applying the vectorized channel coefficient matrices to *Eq*. 1.6, and a normalized correlation matrix of *Eq*. 1.7 can be obtained. For 2x2 MIMO radio channel realization, antenna scheme A, in table 1.1 is used, and the measured radiation patterns of co-polarized dipole array with mutual coupling effects are used as in section 1.6.2. Channel transfer matrices are generated by the CDL channel model in *Eq*. 1.5 for two geometrical scenarios; Single Cluster with multi-path and Urban Macro channel model. Both scenarios are NLOS and their geometrical parameters are defined in table A.2 and A.3.

Figure 1.9 shows comparison results between spatial correlation coefficients obtained from CDL model and the measured values in MIMO OTA system for two geometrical scenarios. It is clear from the results that CDL model shows good match with the experimental data gathered from MIMO OTA system. The gap observed in figure 1.8 can be explained by the fact that the channel correlation becomes dominant in case of Single Cluster model. It is also important to note that the MIMO OTA system can accurately measure the correlation properties of co-polarized dipole antenna array and considered to be verified as an evaluation methodology of antenna performance.

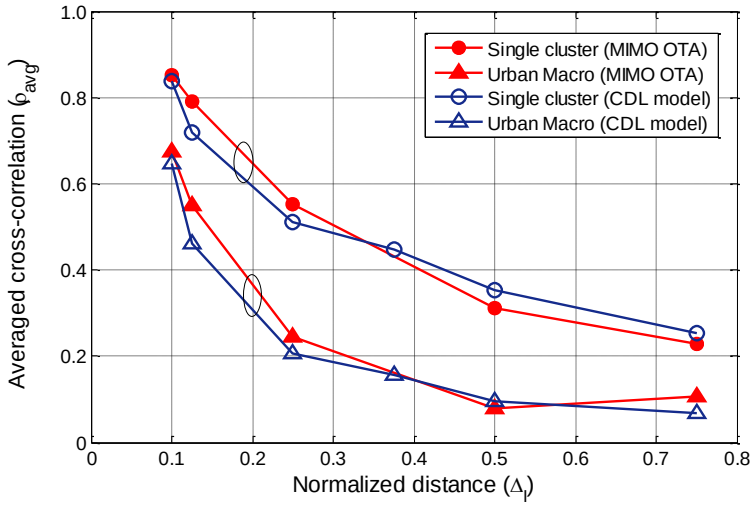

Figure 1.9 Comparison of the spatial correlation coefficients obtained from CDL channel model to the measurement results with MIMO OTA

1.6 Characterization of dual-polarized dipole antenna array in Ricean fading channels

As discussed in section 1.3, CDL based WINNER II channel model can be able to define the dual polarized channel both for NLOS and LOS paths. The polarization state is the result of Tx and Rx antenna radiation patterns as it is in the real world. In this chapter, ideal dipole antenna schemes B and C as defined in table 1.1 are analyzed by investigating the performance metrics discussed in section 1.3.

Antenna scheme B 2x2 MIMO links consist of dual polarized, co-located ideal dipole antennas for BS antennas, and co-polarized ideal dipole antenna array with 0.75λ of inter-element spacing for MS antennas. Antenna scheme C is a 2x2 MIMO link consist of the same BS antenna configuration as in B, and dual polarized ideal dipole antenna array on MS side with different inter-element tilt angles.

Each of realized channel transfer matrix by using the antenna radiation patterns are analyzed by investigating the performance metrics as a function of the Ricean K-factors from zero (NLOS) to 7.94 (or 9 dB). Geometrical scenario is Urban Micro channel model with fixed angles of arrival/departure as defined in table A.3.

1.6.1 XPD of dipole antenna array

It is important to understand the cross-polarization discrimination (XPD) properties of antenna under evaluation due to the fact that the polarization state of the radio channel in the WINNER II model is result of the antenna radiation patterns. XPD is defined by the ratio of H-pol gain to V-pol gain. In case of ideal dipole antenna, XPD is a function of its tilt angle from the zenith. Figure 1.10 and 1.11 show the gains and XPDs for two dipole antenna arrays defined in antenna scheme C as a function of tilt angles. In 7 different tilt angle combinations, the first dipole antenna remains $\vartheta_{1,} = 0°$ in most of the cases except for the last two cases; where $\vartheta_{1,} = 22.5$ and 45°. On the other hand, the second dipole antenna is tiled by $\vartheta_2 = \{0°, -22.5°, 45°, 67.5°, -90°, -22.5°, -45°\}$, where the maximum XPD is observed at -90°.

It is interesting to analyze the dipole antenna array with various tilt angles in Ricean fading channels to observe as to how the XPD of MS antennas would change the performance.

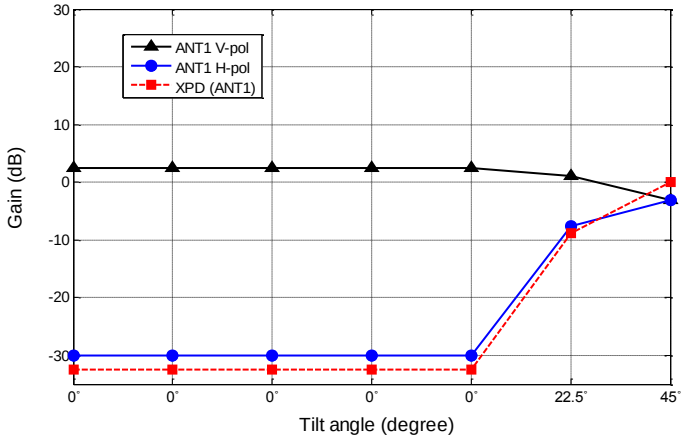

Figure 1.10 Polarization broken down antenna gains and XPD for antenna 1 as a function of tilt range

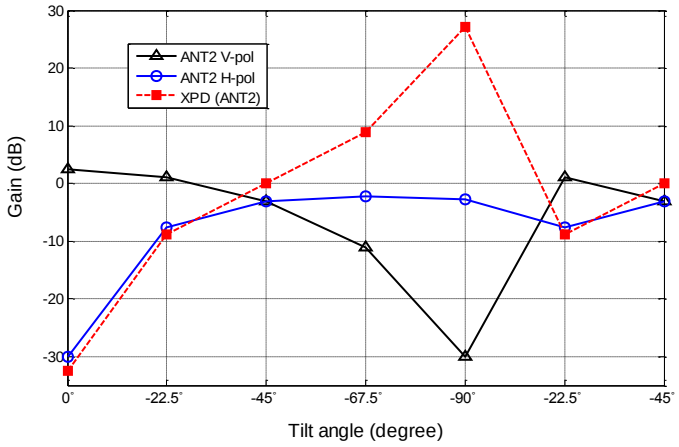

Figure 1.11 Polarization broken down antenna gains and XPD for antenna 2 as a function of tilt range

1.6.2 Diversity measure

As discussed in section 1.3.4, the diversity measure of MIMO radio channel is inversely proportional to the eigenvalue spread (or the variance of $\|H\|_F^2$) [17]. This means that the diversity measure will be infinite in AWGN channels ($K \rightarrow \infty$), which results in '0' spatial multiplexing gain.

Based on the generalized form in *Eq*. 1.13, the diversity measures for all antenna configurations are shown in figure 1.12. As K-factor in linear scale increases, the diversity measures show approximately monolithic increase for all antennas. It is observed that the diversity measure is also enhanced when the dipole antenna is spatially separated or the tilt angles are increased.

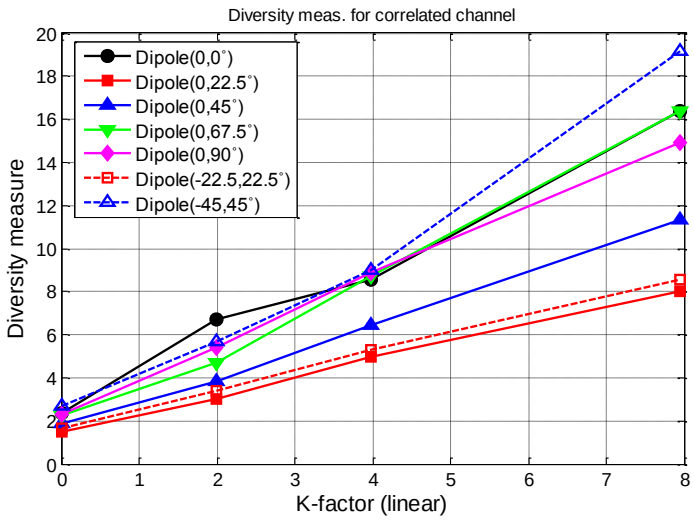

Figure 1.12 Diversity measure for dual-polarized dipole antennas with various tilt angles as a function of Ricean K-factor

1.6.3 Correlation properties

1.6.3.1 Co-variance matrix

From the co-variance matrix of the channel transfer matrix in *Eq*. 1.6, Tx and Rx spatial correlation coefficients can be obtained for Rayleigh fading channels. However, there are multiple correlation coefficients depending on which Tx and Rx branches are considered. i.e., Tx correlation coefficient either from vec[H(1,:)]vec[H(1,:)]' or vec[H(2,:)] vec[H(2,:)]' and Rx correlation coefficient either from vec[H(:,1)]vec[H(:,1)]' or vec[H(:,2)]vec[H(:,2)]'. In case of dual polarized antenna analysis, the

correlation coefficient obtained from this method may describe only a part of correlation properties of the channels.

Figure 1.13 shows Tx spatial correlation obtained from vec[H(1,:)]vec[H(1,:)]' as a function of K-factor. It should be noted from the results that the Tx correlation is low only when the polarization states between Tx and Rx antennas are the same. i.e., Dipole (45°,-45). Tx spatial correlation obtained from vec[H(1,:)]vec[H(1,:)]' as a function of K-factor.). Figure 1.14 shows Rx spatial correlation obtained from vec[H(:,1)]vec[H(:,1)]' as a function of K-factor. It is also observed that the antenna scheme having same polarization state as that of BS antenna showed low Rx correlation property as K-factor increases.

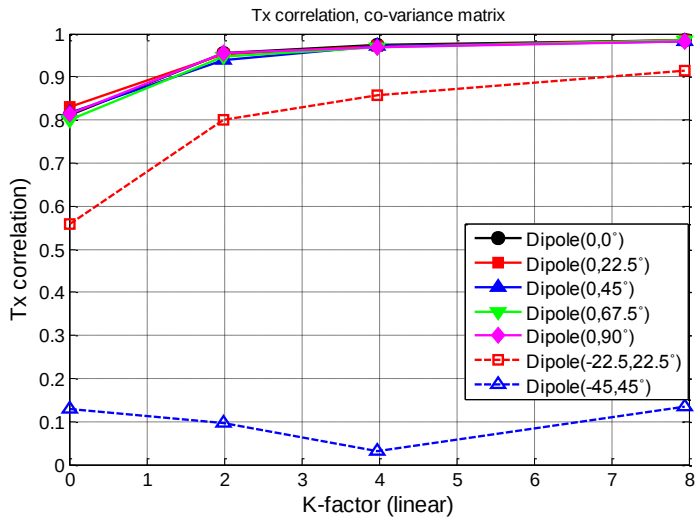

Figure 1.13 Tx spatial correlation coefficient obtained from vec[H(1,:)]vec[H(1,:)]'

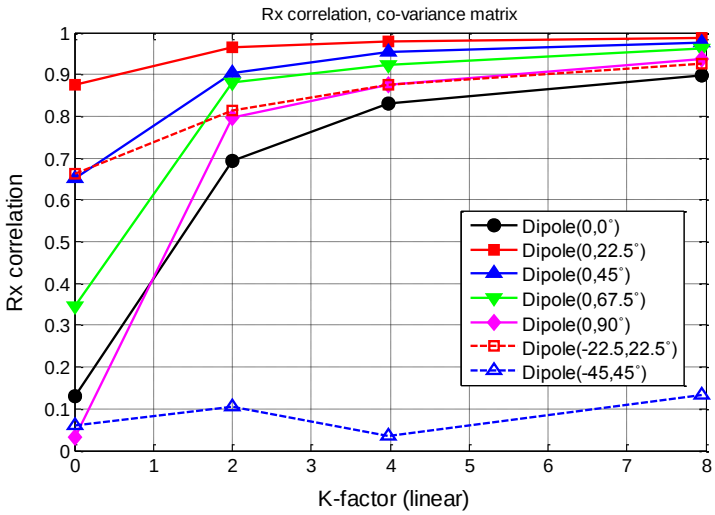

Figure 1.14 Rx spatial correlation coefficient obtained from vec[H(:,1)]vec[H(:,1)]'

1.6.3.2 Spatio-temporal correlation

In section 1.6.3.1, it is shown that the correlation matrix is only applicable to MIMO antennas with symmetric polarization states. To obtain the correlation properties of arbitrary polarized MS antenna, a spatio-temporal correlation in *Eq.* 1.8 and *Eq.* 1.9 can be used.

In contrast to the Tx correlation coefficients obtained from the co-variance matrix, temporal Tx correlation in Figure 1.15 shows clear tendencies against tilt angles of dipole antenna and Ricean K-factor. It is observed that the Tx correlation decreases as the two dipole antennas on MS become cross-polarized antenna. i.e., inter-element angle separation gets close to 90°. The reason for Tx correlation changes by the MS antenna is, that the spatial correlation in CDL model or geometrical channel is jointly defined due to Tx-Rx antenna inter-dependency of the model. It should be noted from the results that the Tx correlation of co-polarized dipole antenna is very high even in NLOS channel and approaches to ~1 as K-factor increases.

When co-polarized dipole antenna array is used at MS, dual polarized and co-located BS antenna creates very high Tx correlation because the vertical polarization components are dominated.

Figure 1.16 shows mean Rx correlation coefficients calculated from temporal correlation. Similarly, Rx correlation decreases as the angle between the dipoles increases. Thanks to the spatial separation of co-polarized dipole, the Rx correlation is very low in NLOS channel however, the Rx correlation increases dramatically even at K=2 (or 3 dB). The antenna schemes with smaller inter-element angle separation shows large Rx correlation properties even at NLOS channel because of 0.1λ of antenna separation. These results are consistent with the results that Rx correlation properties for the antenna schemes of which inter-element angle separations are the same showed the similar values. i.e., dipole (0°,45°) vs dipole(22.5°,-22.5°), and dipole (0°,90°) vs dipole (45°,-45°).

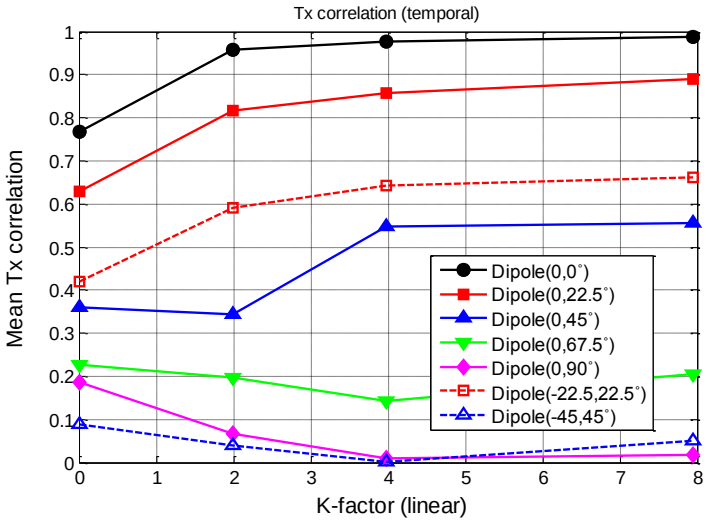

Figure 1.15 Mean Tx spatial correlation obtained from temporal correlation coefficient

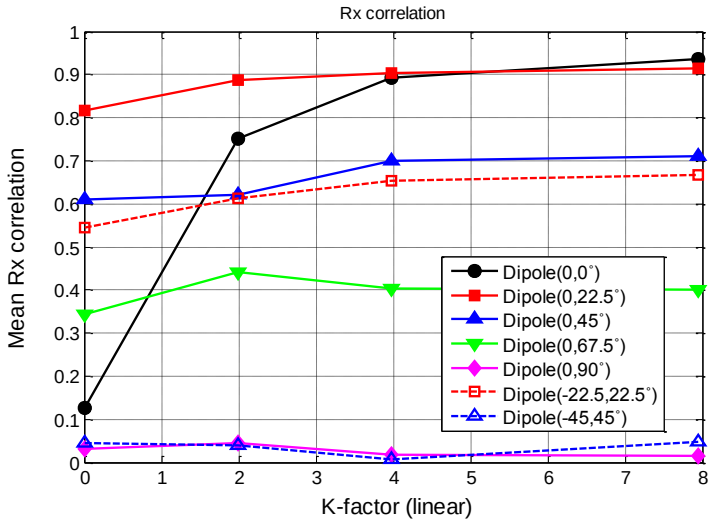

Figure 1.16 Mean Rx spatial correlation obtained from temporal correlation coefficient

1.6.4 Mutual information and LTE physical layer throughput

Finally, mutual information for antenna scheme B and C in table 1.1 are investigated for NLOS and LOS channels. The purpose of this study is to clarify the following questions.

- *How the Ricean K-factor differentiates the performance of co-polarized and dual-polarized antennas?*
- *What is the best performing MS antenna configuration both in NLOS and LOS channels?*

Figure 1.17 shows ergodic mutual information (MI) for dipole setups with respect to the Ricean K-factor. SNR is given as 30 dB in order to compare the performance in the high SNR range. It is clear from the results that the MI enhanced as the inter-element angle of the dipole array increased, which are consistent results with the Tx and Rx correlation properties in the previous section.

When K=0 (or NLOS channel), the largest MI can be sustainable with {dipole(45°,-45°), dipole(0°,-90°)}, and the smallest MI is experienced by dipole(0,-22.5°). The co-polarized dipole with 0.75λ separation shows better performance than dipole(0,-22.5°). Such small MI performance of dipole(0°,0°) even with substantially small Rx correlation can be explained by unacceptable high Tx correlation.

When K > 2 (or 3 dB), all antenna setups show a significant MI enhancement except for the co-polarized dipole, dipole(0°,0°) which shows large MI drop in Ricean fading channel, and this can be attributed to such a large increase in Tx and Rx correlation in Ricean fading channels. On the other hand, relatively smaller correlation enhancements in the dual polarized array with non zero tilt angle sates is observed as shown in figure 1.16. It is also important to note that the simulation results show that the impacts of Ricean channel are significant even from K=2 (or 3 dB)

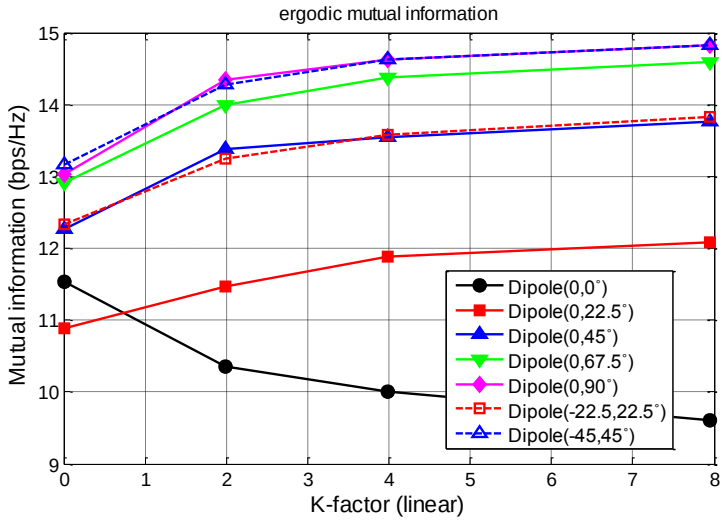

Figure 1.17 Ergodic mutual information for dual polarized dipole arrays as a function of Ricean K-factor

In contrast to co-polarized dipole, enhancement of MI for dual polarized dipole antenna configurations in Ricean fading channel are associated with following characteristics,

- *Polarization diversity prevails as K-factor increases whereas the spatial diversity is deteriorated*
- *Rx correlation properties for dual polarized antenna are not increased as much as in co-polarized antenna as K-factor increases*

After application of the effective bandwidth and correction factors summarized in section 1.3.6, LTE physical layer throughput can be estimated from Eq. 1.17. Figure 1.18 shows estimated throughput for dual polarized dipole array with respect to the Ricean K-factor. The MIMO decoder performance is not considered, and thus the estimated throughputs are the scaled version of MI. However, it is useful to compare the throughput measurement results with MIMO OTA system, which is discussed next.

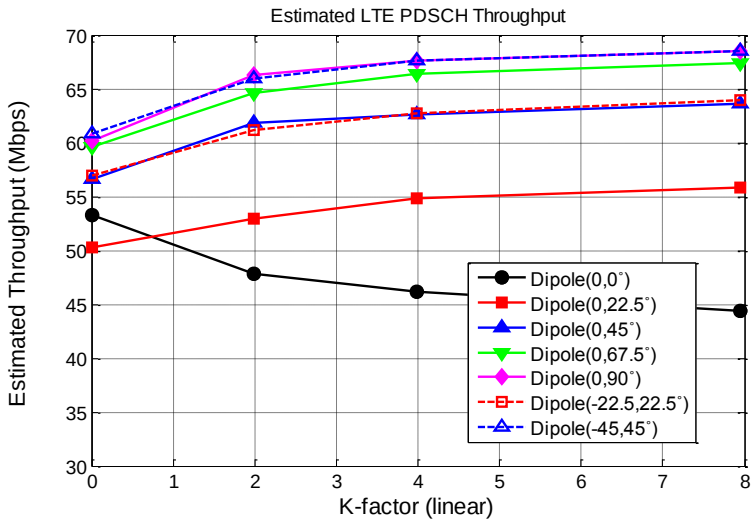

Figure 1.18 LTE physical layer throughput estimated from ergodic mutual information for dual polarized dipole array as a function of Ricean K-factor

1.6.5 LTE physical layer throughput measurement with MIMO OTA system

Figure 1.19 shows measurement results of LTE physical layer throughput for 2x2 MIMO spatial multiplexing mode by using the MIMO OTA setup in figure 1.1. The measurements are conducted with LTE mobile terminal operating at 700 MHz band over 10 MHz of system bandwidth. The dual polarized dipole array under evaluation is located at the center of the anechoic chamber, and connected to the mobile terminal via RF cables as in figure 1.1. For each channel model realization, gain of the channel model could be different, and needs to be calibrated by adjusting the channel output gain control so that the averaged total power measured at the center of the anechoic chamber is the same. SNR is kept at 27 dB during measurements.

As shown in the measurement results, co-polarized dipole antenna experiences large throughput drop as K-factor increases, which is consistent with the estimated throughputs in figure 1.18. Obviously, in case of dual polarized dipole, as the inter-element angle increases, from 22.5° to 90°, throughputs are significantly increased, and further enhancements are observed as the Ricean K-factor increases. It is important to note that the measured throughput results show exactly the same behavior with those observed in the simulation results obtained from the CDL model and ideal dipole antenna patterns. However, there are two differences.

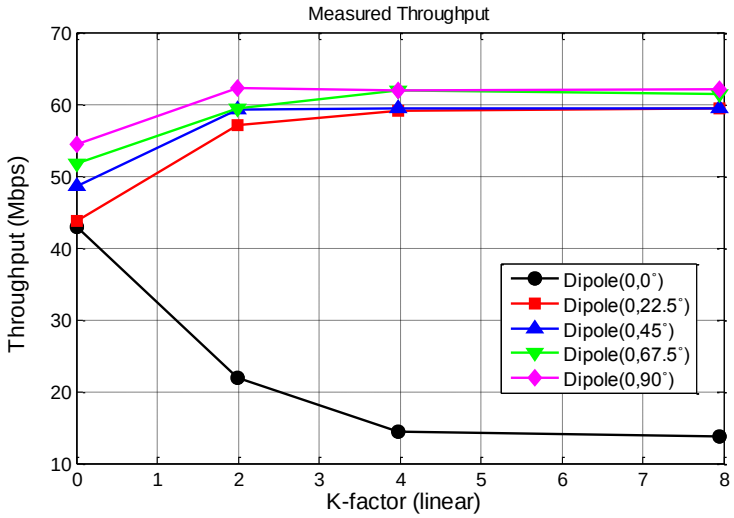

Figure 1.19 LTE physical layer throughput measurement results obtained from MIMO OTA system

1.7 Conclusion

In this chapter, it is demonstrated that the pattern correlation obtained from measured complex antenna patterns and PAS model can be a good approximation of correlation coefficient obtained by CDL model in cases where the PAS shape is uniform or with wide angular spreads. It is important to note that this simplified PAS model based approach may give underestimated values in cases where the angular spreads of the incident waves are narrow. The correlation error becomes significant especially when the angles of arrival are concentrated at the same direction. i.e., single spatial cluster model. These conclusions are verified by theoretically and experimentally through comparison studies on correlation properties obtained from the CDL based channel models and pattern correlation results. And finally, both simulation results are compared with the measured correlation coefficients with MIMO OTA system.

In addition to the co-polarized dipole studies, dual polarized dipole antenna arrays are comprehensively studied based on CDL channel model with dual polarized NLOS and Ricean fading channels. The performance of

dual polarized dipole arrays is investigated as a function of inter-element angle in order to see how the Ricean K-factor differentiates the performance of dual-polarized antennas with various polarization states. Through the study, it is found that the correlation coefficient obtained from the co-variance matrix of the channel transfer matrices cannot be used in case of asymmetric antenna radiation patterns, and found that the temporal correlation coefficients can correctly measure the correlation properties of asymmetrical antenna patterns both in NLOS and LOS channels.

It has been confirmed from the theoretical studies that the co-polarized dipole antenna experiences very high Tx correlation when co-located dual polarized BS antenna are used even under NLOS channels, and it is further increased as K-factor of the radio channel increases. It is also found that only a small inter-element angle between the dipole array significantly reduces the Tx and Rx correlation even under highly correlated Ricean channels.

Finally, LTE physical layer throughput performance is derived from the mutual information for dual polarized dipole antennas and compared to the measured throughput performance results at MIMO OTA system.

CHAPTER 2

Human hand effect on the MIMO OTA throughput performance

2.1 Background

In this chapter, the effects of human hand on the MIMO OTA performance are investigated for five different antennas types of LTE mobile terminals. Previous studies have concluded that the hand effects mainly degrade the SNR. However, some of those reports concluded that the MIMO reception performance is not deteriorated as much as SNR [26][27][28]. The previous studies were conducted by simulation works or the measurements in the live network. However, this work investigated the hand effects in the controlled lab environment to see how the human hand will change the LTE terminal's MIMO OTA performance through link level physical layer throughput measurements with MIMO OTA system.

For this study, five test devices operating at U.S upper 700 MHz band, or 3GPP Band 13, are selected. The antennas for these devices are properly tuned so that the test devices have various antenna correlation characteristics.

In the section 2.2, the descriptions on the antenna configurations of the selected DUTs (devices under test) and their antenna characteristics are summarized to facilitate the understanding of the scope of this study. In section 2.3, impact of hand grip on the correlation properties of the DUT is characterized based on the pattern correlation analysis with proper PAS model. In section 2.4, the hand grip effects on correlation characteristics are empirically investigated with MIMO OTA system. In section 2.5, the effects

of hand grip on the LTE physical layer performance are quantified by using the MIMO OTA system.

2.2 Antenna characteristics of LTE terminals

2.2.1 Description on the DUTs

In this section, the antenna schemes of selected DUTs are presented. The antenna schemes for DUTs in the Figure 2.1 are selected based on the idea that the pattern correlations of DUTs are evenly distributed between 0 to 1 in order to quantify the degree of correlation change caused by the hand grip.

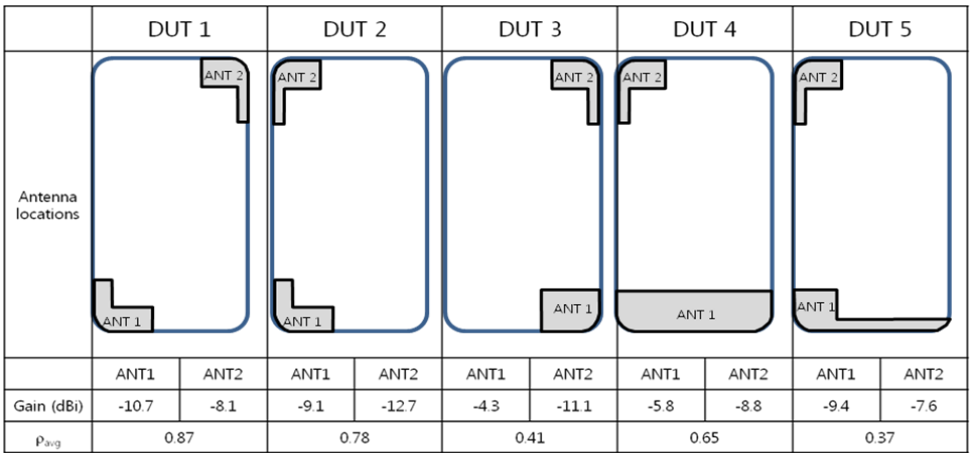

	DUT 1		DUT 2		DUT 3		DUT 4		DUT 5	
	ANT1	ANT2	ANT1	ANT2	ANT1	ANT2	ANT1	ANT2	ANT1	ANT2
Gain (dBi)	-10.7	-8.1	-9.1	-12.7	-4.3	-11.1	-5.8	-8.8	-9.4	-7.6
ρ_{avg}	0.87		0.78		0.41		0.65		0.37	

Figure 2. 1 Antenna configuration and placement information for DUT 1～5 and 2-Dimentional antenna gain characteristics

ANT1 denotes the main antenna branch, ANT2 denotes the secondary antenna. For all DUTs, ANT1 is located at the bottom of DUTs, and ANT2 is located at top. The antenna gains are measured in 2-D. The pattern

correlation values are derived by applying measured complex pattern for each DUT to *Eq*. 1.10.

2.2.2 Measurement conditions

Figure 2.2 shows, the measurement setup for a) test orientation, b) free space condition, and c) hand grip condition. The reference test orientation is tilted by 45° from the zenith for both conditions, which is chosen as typical position when the users are holding the devices for packet data communication such as web browsing or file downloading. The hand phantom used in this study is CTIA compliant PDA hand phantom [29].

In the following sections, the DUTs have been measured and analyzed based on the above assumptions and conditions unless mentioned otherwise.

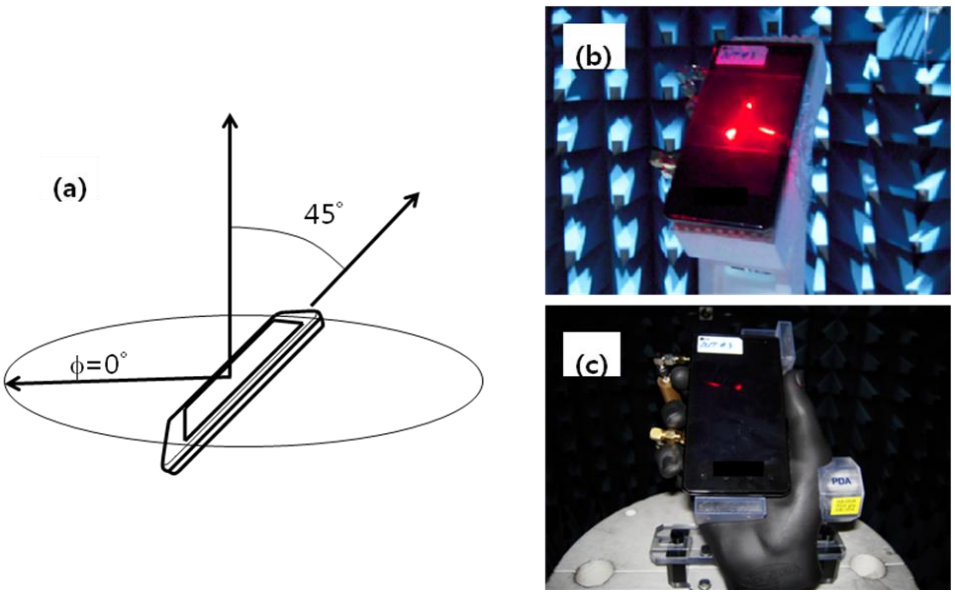

Figure 2. 2 UE test condition for antenna performance measurements (a) DUT orientation for 2D RFP measurement (b) mounted on a JIG for free space condition (c) mounted on a PDA hand phantom compliant with CTIA standards

2.3 Hand effects on correlation

2.3.1 Radiation patterns and hand effects

It is important to investigate the antenna patterns measured under free space condition and hand grip condition in order to understand how the hand grip would impact the antenna patterns and associated correlation characteristics.

Figure 2.3 ~ 2.5 show the radiation patterns of the DUTs for both test conditions. Each sub-figure shows the patterns for both antennas (ANT1 and ANT2) in the same polarization to show the impacted polarization component by the hand grip. The test orientation is tilted by 45° from the zenith for call cases. 'V' denotes vertical polarization or Θ polarization, 'H' denotes the horizontal polarization or Φ polarization.

Figure 2.3 shows the polarization broken down radiation patterns for DUT 1 and DUT 2 for both test conditions. In case of free space condition, both devices show Omni-directional antenna patterns in the V-polarization. By contrast, both devices show non Omni directional antenna patterns in the H-polarization. Depending on the angular directions of the peak positions in the horizontal polarization, the correlation between the two antennas will be affected. This is known as the pattern diversity [30]. The peak gain positions in the H-polarized antenna gains are marked with large triangles to visualize how the direction of the antenna directivity is rotated in 2-D space by the hand grip. In case of free space condition, the direction of the peak of each antenna in the H-polarization is in the similar direction. By hand grip, there are no significant deteriorations observed but the antenna patterns are slightly squeezed.

Figure 2.4 shows antenna patterns of DUT 3 and DUT 4 in the same manner. In contrast to the previous DUTs, DUT 3 and 4 experience large degree of pattern changes due to hand grip in both polarizations.

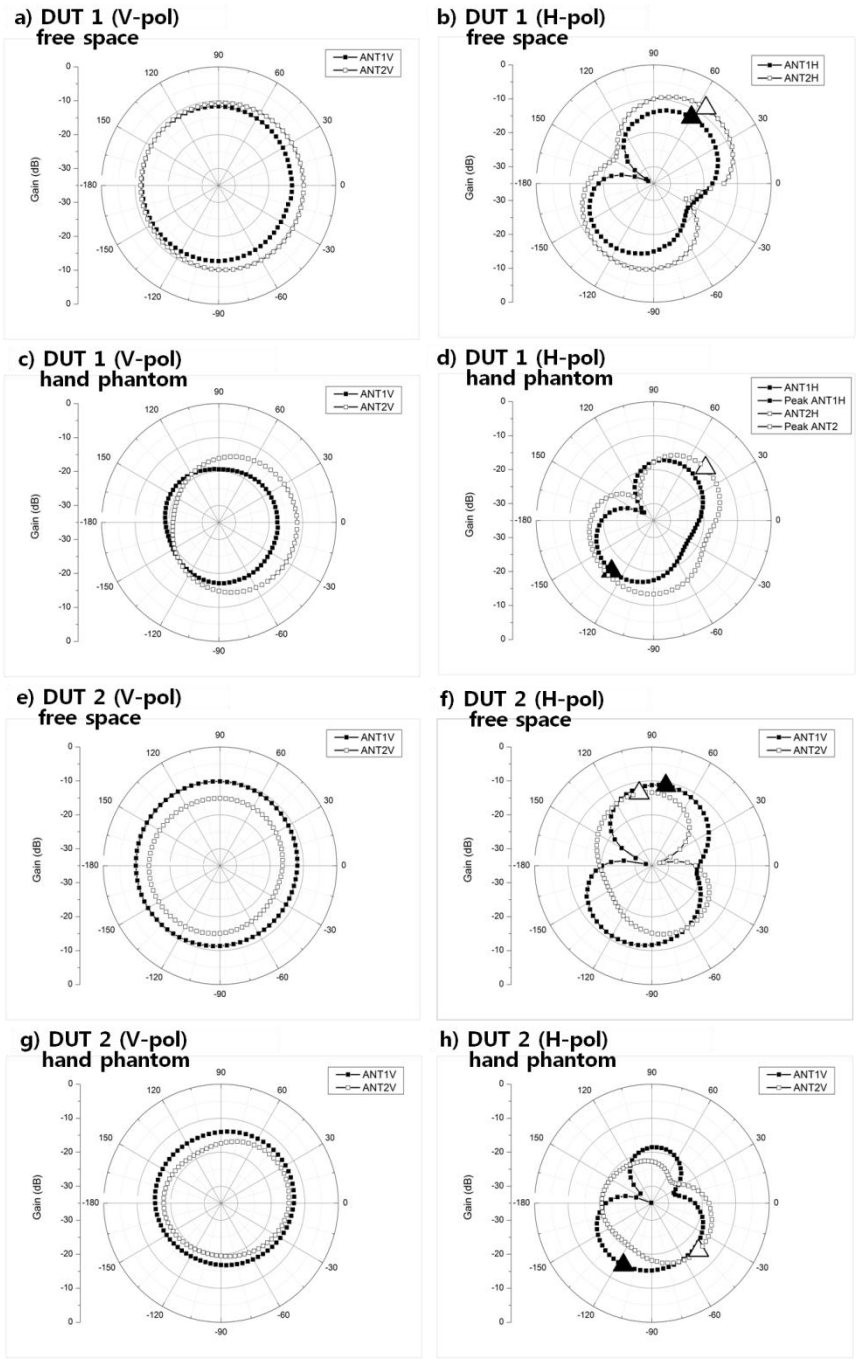

Figure 2.3 Antenna patterns for DUT 1 and DUT2 in a free space (a,b,e,f) condition and with hand grip (c,d,g,h). V-polarized gains are on the right column and H-polarized gains are on the left column.

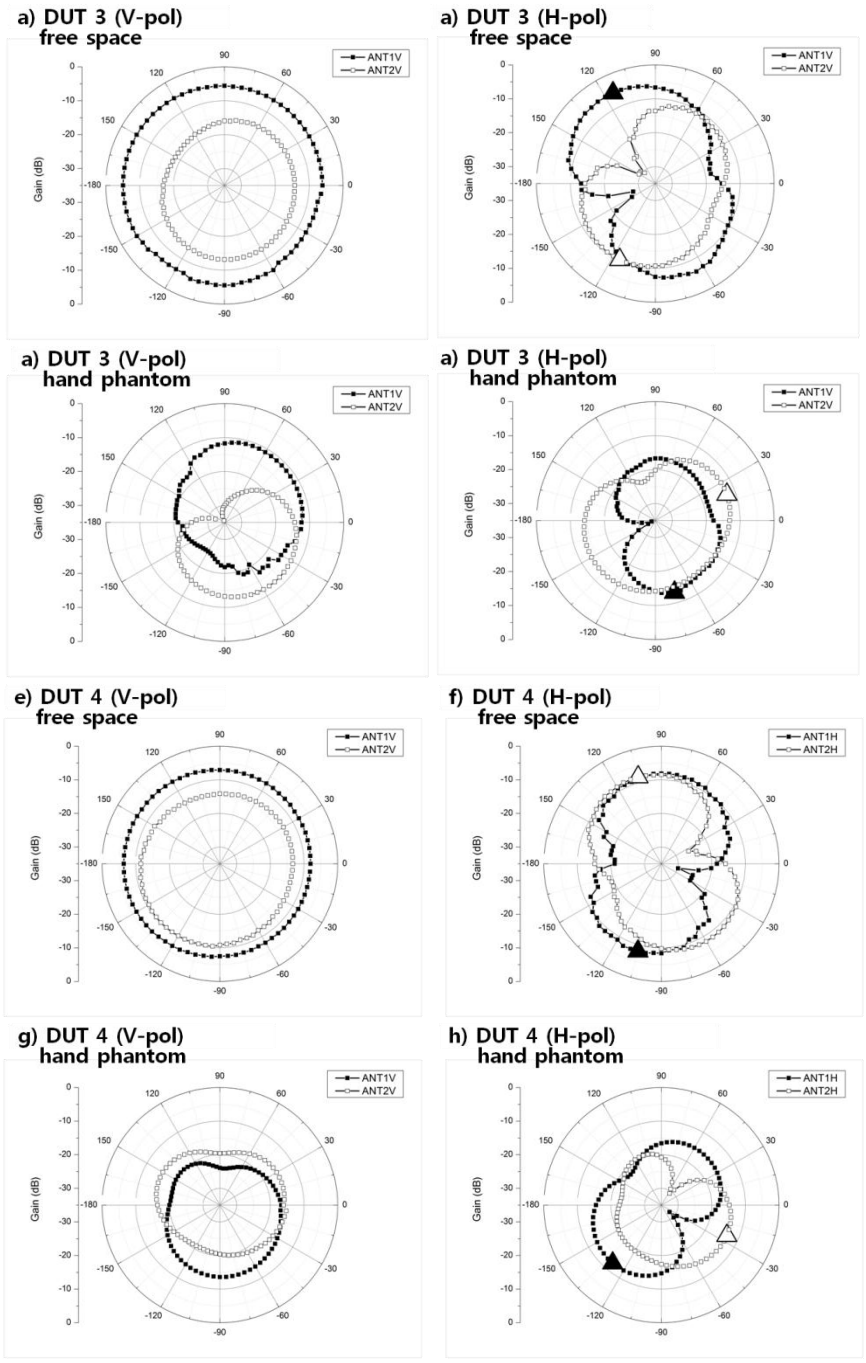

Figure 2.4 Antenna patterns for DUT3 and DUT4 in a free space (a,b,e,f) condition and with hand grip (c,d,g,h). V-polarized gains are on the right column and H-polarized gains are on the left column.

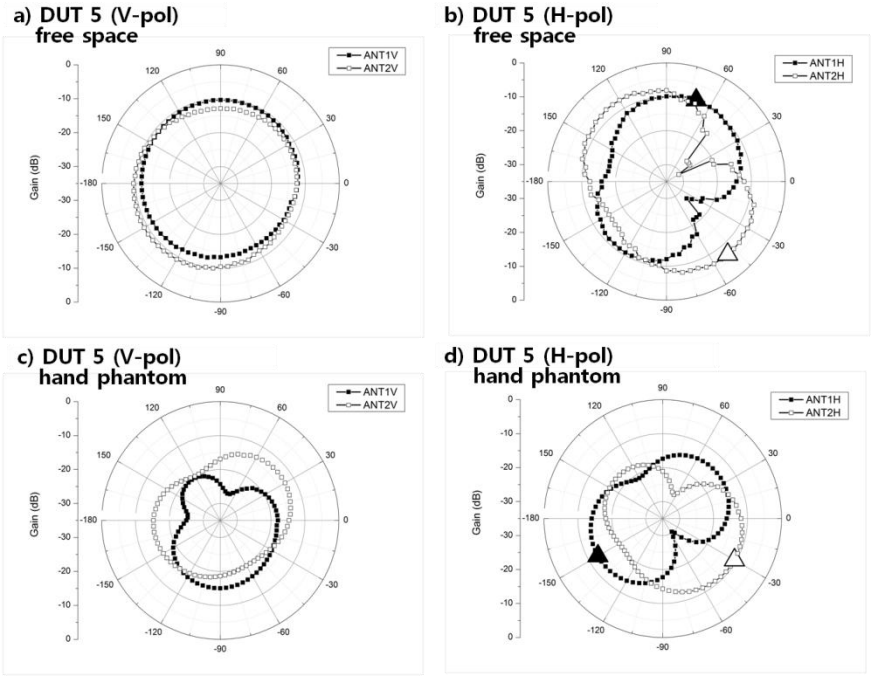

Figure 2.5 Antenna patterns for DUT 5 in a free space (a,b) condition and with hand phantom(c,d) in the vertical polarization (a,c) and in the horizontal polarization (b,d)

The main antennas for both devices are not Omni-directional, and the directions of the peaks of the secondary antennas are rotated by large angles. Similarly, figure 2.5 shows antenna patterns of DUT 5. It is observed that both antennas are squeezed and rotated in a great deal by the hand grip. It is interesting to see the changes in the radiation patterns and associated correlation properties for each device in the next section.

2.3.2 Pattern correlation properties

The pattern correlation coefficient; $\boldsymbol{\rho_F}$ can be derived by the *Eq.* 1.10 discussed in chapter 1, based on the measured antenna patterns of DUTs. The antenna patterns are measured taking into account the mutual coupling

effects with the measurement method discussed in chapter 1. For ρ_F calculation, Urban Macro PAS model is used as shown in figure 2.6.

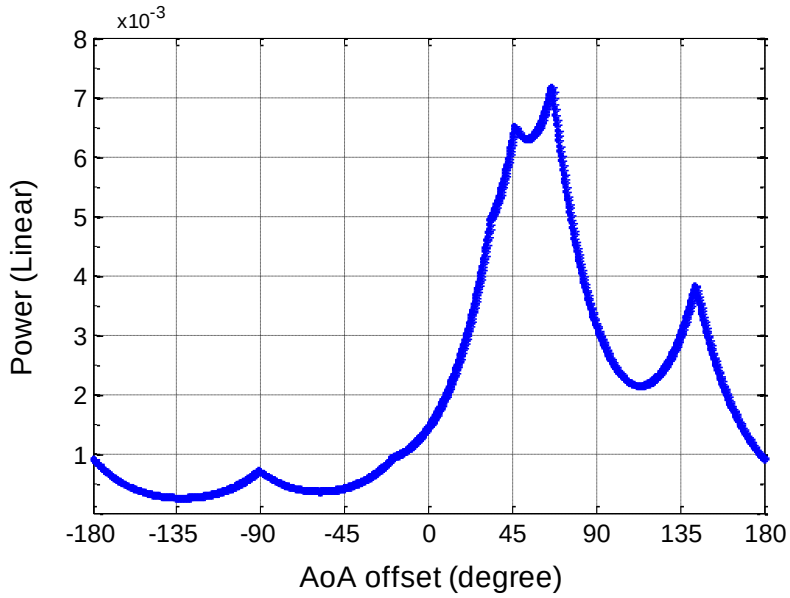

Figure 2.6 PAS model used for ρ_F calculation. The PAS is generated with Urban Macro-cell model

Figure 2.7 shows the pattern correlation for all DUTs as a function of Δ_{AoA} in free space condition. For reference, co-polarized dipole antenna with 1/4λ inter-element spacing is plotted. As the Δ_{AoA} increases from 0° → 180°, the AoAs of clusters shift from right to left. Depending on the angular positions of clusters, ρ_F is also varied. The periodicity of ρ_F is clearly observed in the case of the DUTs with lower ρ_F figures. The dipole antenna shows the largest amplitude variation over Δ_{AoA} change compared to the other DUTs. In this sense, the ρ_F needs to be averaged over the Δ_{AoA} as in chapter 1, and it will be compared to the power correlation measured by the MIMO OTA system.

It should be noted from the results in figure 2.7 that most of the DUTs show high correlation property near AoA offset is 20°~30°, where the AoAs of the clusters are moved to near 90°. This is the angle that high correlation is measured in the typical hand held terminals. Similarly, dipole array also experiences the high correlation when the AoAs of the clusters are near 90° (i.e., perpendicular to the broad side).

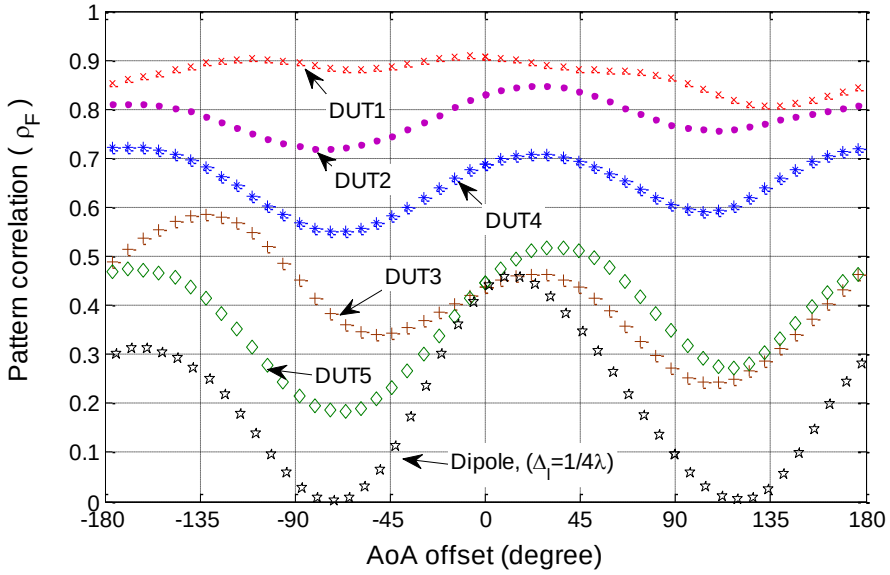

Figure 2.7 Pattern correlation characteristics as a function of Δ_{AoA} for all DUTs

2.3.3 Pattern and power correlation

Figure 2.8 depicts the pattern and power correlation in terms of averaged correlation over Δ_{AoA} for all DUTs. In principle, pattern correlation (or envelop correlation) derived from the PAS model and the power correlation obtained from the amplitudes of signal are different. However, as demonstrated in chapter 1, two methods are the same in case of clusters with wide ranges of AoAs. As the correlation coefficients are

averaged over AoAs, $\rho_{F,avg}$ denotes the average pattern correlation, $\rho_{pwr,avg}$ denotes the average power correlation, where Δ_{AoA}, $\Delta_{\mathrm{AoA}} \in \{0, 90, 180, 270\}$. It can be concluded from the results that there are no outstanding differences between the results from two methods.

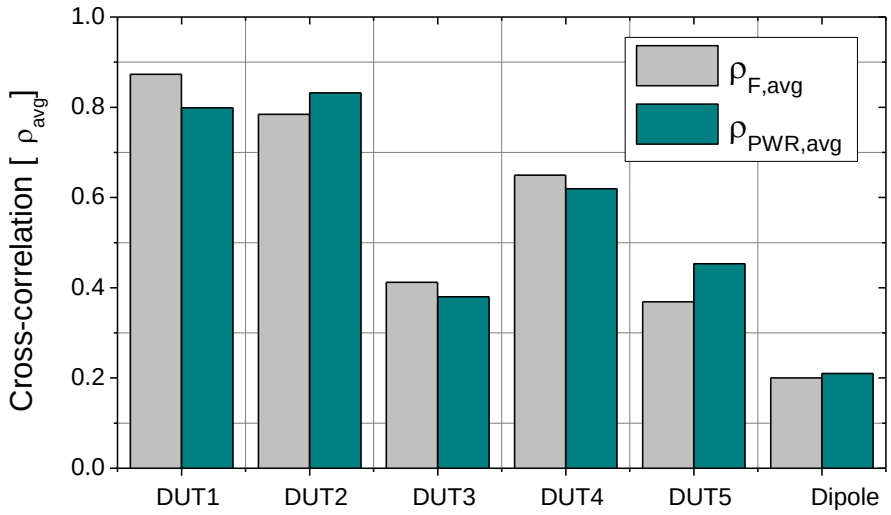

Figure 2.8 Comparison of $\rho_{F,avg}$ results obtained from the PAS model and the measured radiation patterns to the measured $\rho_{pwr,avg}$ with MIMO OTA system

2.3.4 Hand effects on antenna correlation

Figure 2.9 depicts the impact of hand grip on the antenna performance in terms of antenna gain and power correlation properties for all DUTs. The antenna gain and the power correlation for each DUT are compared in the presence of hand as well as free space condition. The antenna gain with hand grip is much lower than the gain obtained in free spec condition. The correlation with hand grip is also reduced compared to free space condition. This correlation reduction can be explained by the antenna pattern changes

by the hand grip observed in figure 2.3~2.5. Recall that DUT 1 and DUT 2 experience relatively smaller pattern changes compared to DUT 3~5. Thus, the impact of hand grip on antenna performance can be summarized as below.

- *Hand grip may decrease the antenna correlation when the antenna patterns are distorted severely in such a way that pattern diversity is increased between antennas*

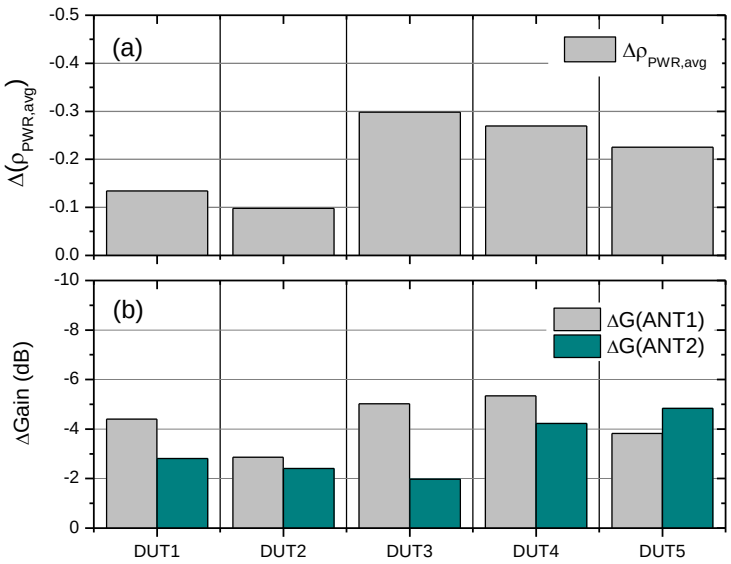

Figure 2.9 Measurement results for antenna performance change due to hand effect (a) Power correlation, (b) Antenna gain for ANT1 and ANT2

2.4 Numerical analysis of hand effects on device performance

Numerical analysis of hand effects are conducted based on CDL model and antenna patterns for all DUTs. Key parameters are summarized in table 2.1. The performance metrics are the diversity measure and LTE physical layer performance.

2.4.1 Diversity measure with hand effect

Diversity measure can be a good performance metric which can measure the diversity performance of antenna in the presence of hand effects. Diversity measure for each DUT is derived from the covariance matrix of channel coefficients realized based on CDL model and measured antenna patterns in figure 2.3~2.5. Applying the channel covariance matrix to *Eq*.1.12, diversity measure for each DUT in free space and in the presence of hand effects are obtained. Figure 2.10 shows diversity measure for each DUT. It is clear that the hand grip increases diversity measure of antenna. Theoretical upper bound of diversity measure is 4 in 2x2 MIMO Rayleigh fading channel

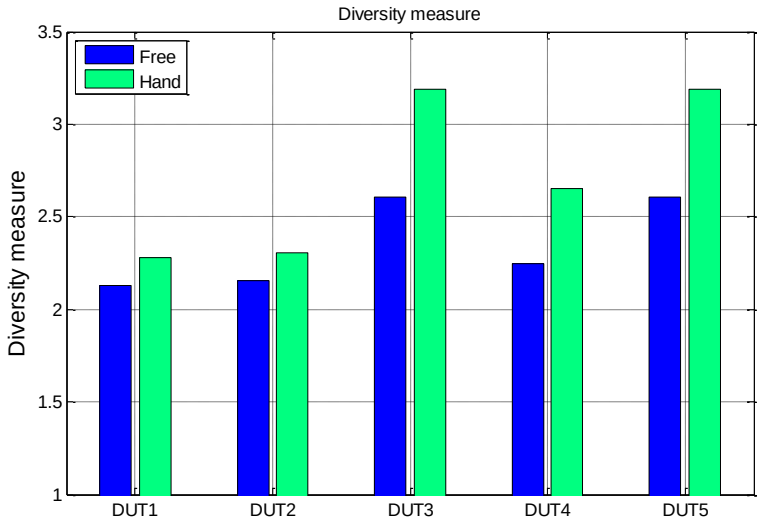

Figure 2.10 Diversity measure derive for antenna (a) Free space, (b) Hand grip

2.4.2 LTE physical layer performance estimation from CDL model

Diversity measure is favorable when the scattering richness is the only important parameter. However, analysis of hand effects should consider antenna gain degradation in order to provide fair comparison results. In physical layer performance estimation, device dependent SNR is introduced to the Shannon's channel capacity. P_{cell} denotes the signal power from the serving cell, P_{int} denotes the interfering power from adjacent cell, kTB denotes thermal noise over system bandwidth, NF denotes the noise figure of DUT.

$$\mathrm{SNR_{dev}} = \frac{\mathrm{E}\{\|\mathbf{H}\|_{\mathrm{F}}^2\} \cdot \mathrm{P_{cell}}}{\left(\mathrm{E}\{\|\mathbf{H}\|_{\mathrm{F}}^2\} \cdot \mathrm{P_{Int}} + \mathrm{kTB} \cdot \mathrm{NF}\right)} \qquad (Eq.\ 2.1)$$

In principle, $\|\mathbf{H}\|_{\mathbf{F}}^{\mathbf{2}}$ for the serving cell and adjacent cell are different. However, the same channel transfer matrices are assumed for simplicity in MIMO OTA system. In addition to the introduction of effective SNR, saturated SNR is also important to explain the behavior of realistic mobile terminals. SNR saturation observed in the typical terminals is caused by many factors. Thus, here I have selected required SNR for MCS 27, which is the practical limit on the maximum MCS level that the commercial devices can decode the based on the signals received. over the air. Finally the effective SNR is given by

$$\mathrm{SNR_{eff}} = \min\{\mathrm{SNR_{dev}}, \mathrm{SNR_{sat}}\} \qquad (\boldsymbol{Eq.\ 2.2})$$

Physical layer throughput is derived from *Eq.* 1.16 and *Eq.* 1.17 by applying system parameters in table 2.1. Figure 2.11 depicts spatial multiplexed PDSCH throughput for all DUTs. It is clear from the results

that hand grip decreases the physical layer performance of DUTs over the wide ranges of SNR. However, in high SNR ranges, performance is enhanced. Such improvements are attributed to increase of diversity measure results in the presence of hand.

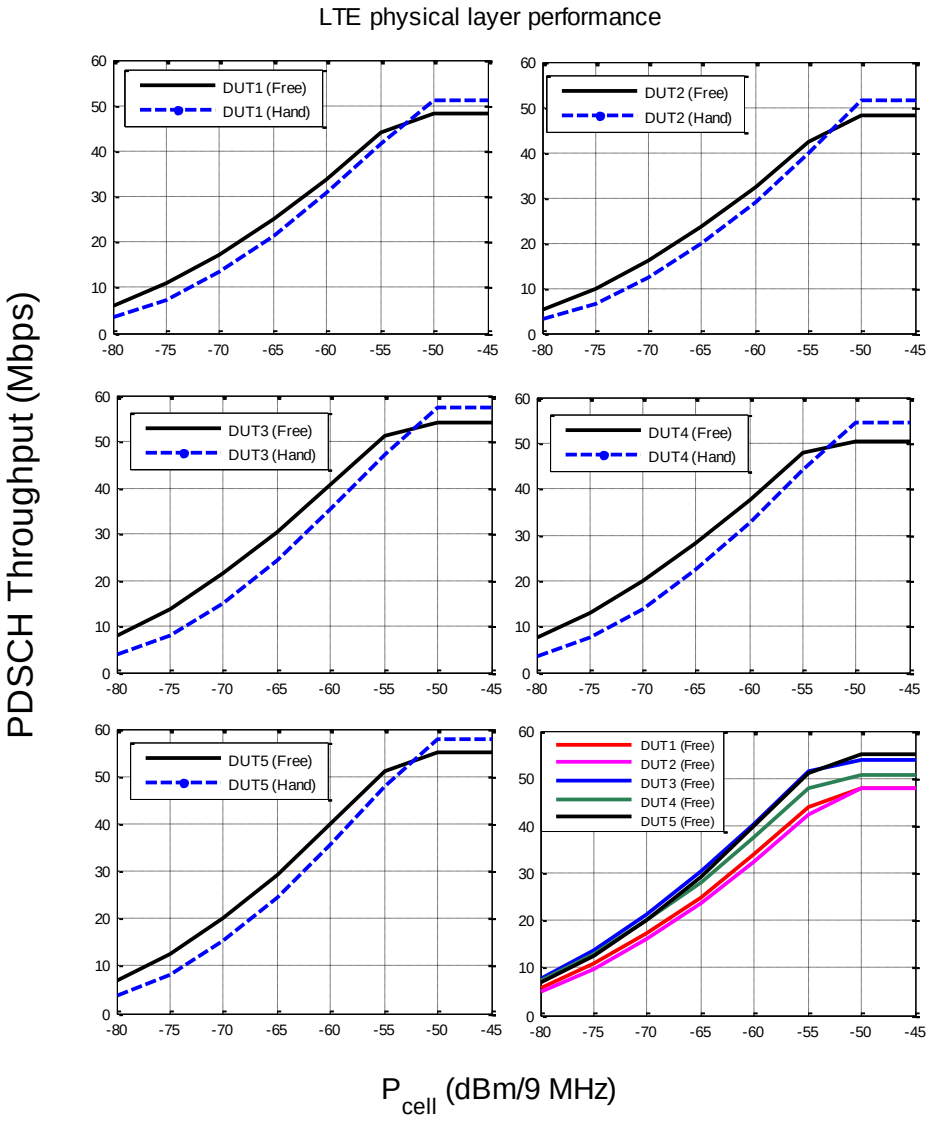

Figure 2.11 Numerical calculation results of LTE physical layer performance for the cases with hand grip and without hand. Bottom right shows the performance of all DUTs in the free space condition

2.5 Physical layer performance measurements

2.5.1 Physical parameters for measurements

Finally, the impact of hand grip on the LTE physical layer throughput performance is investigated by measuring the PDSCH (Physical downlink shared channel) throughput with MIMO OTA system. The measurements are conducted based on the parameters summarized in Table 2.1. The main goal of the measurements is to validate the assumptions built for numerical model for hand grip effects experimentally. In order to verify the hand effects in terms of antenna gain variations and correlation property changes, the LTE PDSCH throughput is measured over the power ranges of -45 ~ -80 dBm/9 MHz. During the measurements, MCS (Modulation coding scheme) is variable so that the maximum throughput can be achieved at a given $\Delta_{\mathbf{AoA}}$ and signal powers. The maximum MCS is determined while maintaining the BLER (Block Error Rate) counts from the CRC error of the MAC (Medium Access Control) PDU (Packet Data Unit) below 10%.

Table 2. 1 Parameter for MIMO OTA performance measurement

Parameters	Description
LTE frame structure	FDD with normal CP
System bandwidth	10 MHz
RB allocation	DL: 50 / UL: 12
Frequency	DL: 752 MHz, UL: 782 MHz
Total BS transmit power	-45 ～ -80 dBm/9 MHz
PDSCH Transmission mode	TM3 (Open loop spatial multiplexing)
PDSCH MCS	Variable (MCS Index= 0～28)
kTB·NF	-97.5 dBm/9 MHz
Channel model	Urban Macro, NLOS

At high channel power ranges, the performance is mainly dependent on the correlation properties of antennas as long as the power loss at the antenna does not affect the SNR. However, there are power ranges that start to degrade the effective SNR by the power loss at the antennas, which are modeled in the *Eq.* 2.1. Such power ranges are clearly observed in the numerical results in figure 2.11 in all DUTs.

Figure 2.12 shows the measurement results of LTE physical layer throughput performance as a function of channel power measured with MIMO OTA system. The channel power is defined as the total power transmitted by BS subtracted by free space loss between the OTA probe antenna and DUT, and RF cable losses between DUT inside of the chamber and the LTE terminal for throughput count. Note that the DUTs contain the antenna under test, and the active parts are in the LTE terminal outside of the chamber. Thus, -45 dBm/9 MHz channel power is incident power to the DUT at the center of the OTA chamber after compensation of all losses except for the antenna gain of DUT.

For comparison, the throughput without hand effects and those with hand effects are plotted in the same figure for each DUT. The results from figure 2.10 indicate that in the areas with high input signal strength, throughput performance with hand grip outperforms the results obtained from free space condition. This can be explained from the fact that the correlation properties are much reduced by hand grip. This holds true for all DUTs.

It should be noted that the throughput enhancement for DUT3 is not as much as expected because the amount of correlation drop due to the hand grip is the largest. This can be explained by the fact that the LTE terminal is already very close to its performance limit. Such performance limits can be caused by the presence of many non-ideal factors in the RF chains or in the channel decoder of the modem. In the numerical example presented in the previous section, this performance limit is considered by introducing the

saturated SNR. The advantages of reduced antenna correlation by the hand grip are more clearly observed in the DUTs with high antenna correlation. i.e., DUT1 and DUT2.

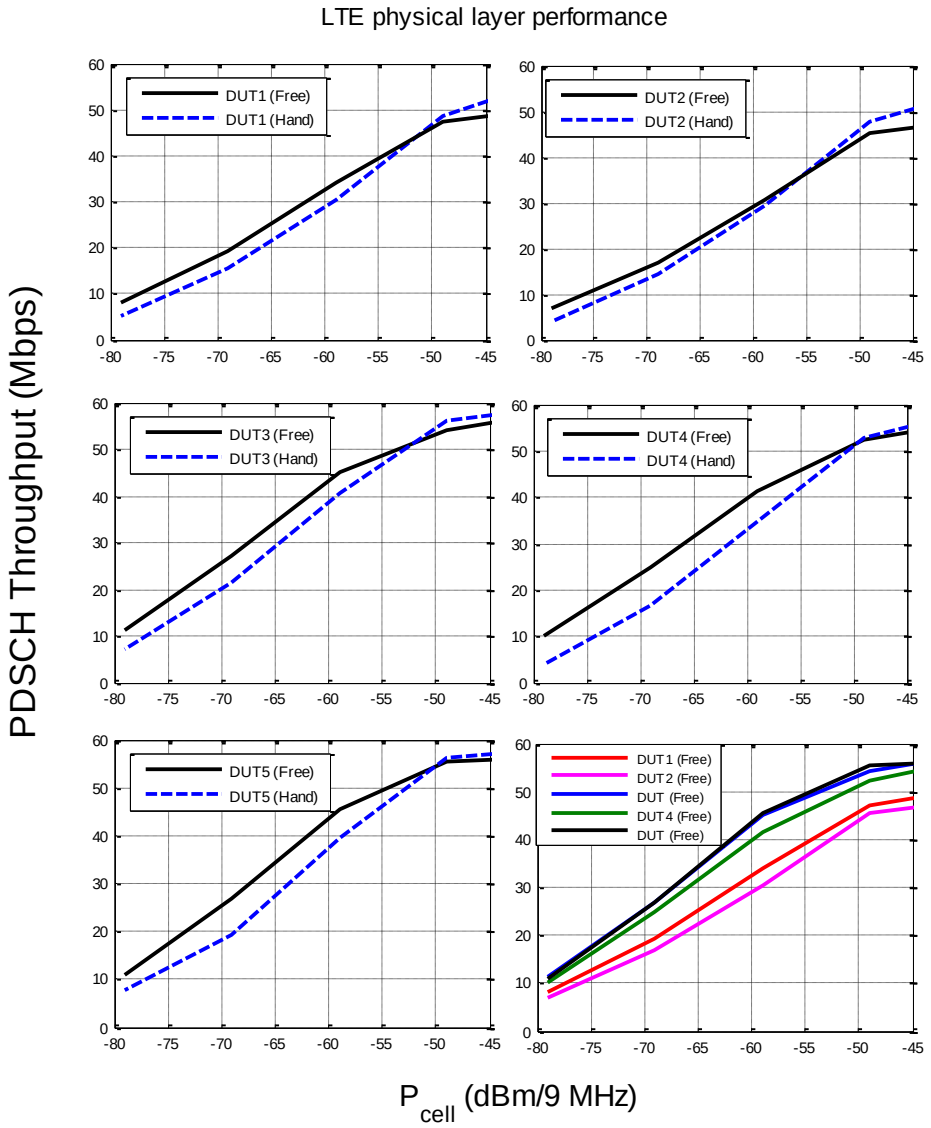

Figure 2. 12 Measurement results of PDSCH throughput performance as a function of channel power for the cases with hand grip and without hand. Bottom right shows the performance of all DUTs in the free space condition

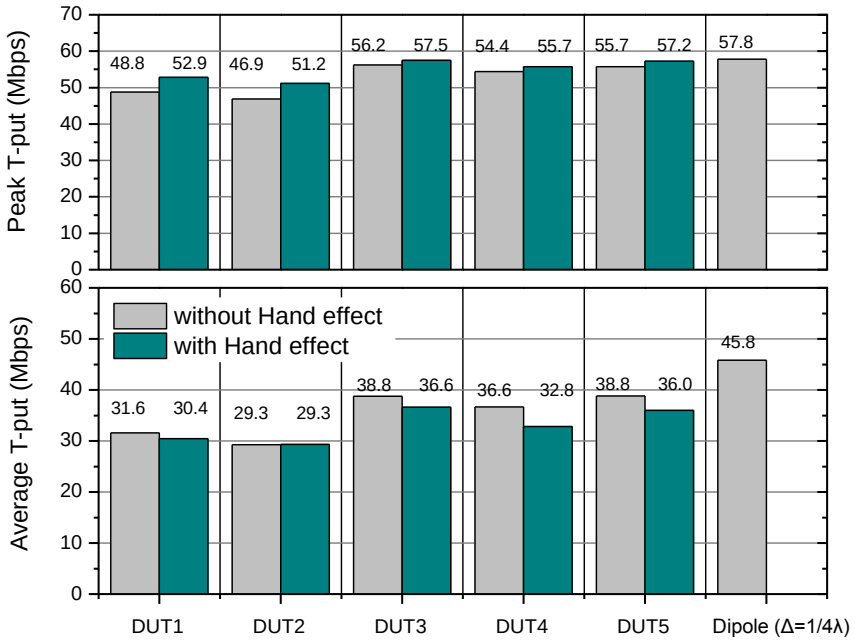

Figure 2. 13 Hand effect on PDSCH throughput performance in terms of peak throughput and average throughput for all DUTs

Figure 2.13 shows summarized results in terms of average throughput and peak throughput for each DUT. Throughputs are averaged over the number of points shown at figure 2.12 and peak throughput is the maximum throughput found from the results in figure 2.12. In case of DUT 1 and 2, there are no remarkable degradations observed in average throughput thanks to the improved throughput performance at high SNR ranges. However, the other DUT showed substantial throughput loss due to larger gain degradation by the hand grip.

2.4 Conclusion

In this chapter, it is found that, to some extent, hand effect can enhance the throughput performance at high SNR ranges. However, the average throughput results show that the hand effects have negative impact on the overall device performance. However, the negative impact is not as significant as in SISO system where there is no benefit of improved correlation. It is clear that in case of device with very high antenna correlation, the performance degradation could be minimized as demonstrated by DUT1 and DUT2.

Such conclusions are confirmed by developed system model and also by measurements conducted using MIMO OTA system.

CHAPTER 3

Analysis on spatial, polarization, and pattern diversities

3.1 Background

In this chapter, comprehensive performance evaluations on the MIMO antennas for the mobile terminals with different diversity schemes are conducted based on numerical analysis method presented in previous chapters. Three types of diversity schemes are investigated, which are spatial diversity, polarization diversity, and pattern diversity. The aim of this study is to investigate the effectiveness of the diversity techniques for mobile terminals by evaluating their link level performance in NLOS and LOS channel environments.

Spatial diversity has been extensively studied for exploiting the MIMO channel capacities for various inter-element spacing between dipole antennas - under different channel conditions - based on numerical methods and measurements [31][32]. As I discussed in chapter 1, section 1.4, spatial diversity requires antenna spacing in the order of 0.5λ in order to achieve low correlation property. Such wide spacing would not be accommodated in hand held mobile terminals.

Pattern diversity is also one of favorable technique that can reduce the antenna correlation. Practically, in mobile terminals, this can be achieved by placing both of antennas close together in such a way that the mutual coupling effects distort the radiation patterns of each other [33][34].

Polarization diversity became more attractive solution for MIMO antennas for BS than spatial diversity antennas because MIMO antenna

requires smaller space for antenna installation. As a result, the dual polarized MIMO antennas have been deployed by most of today's infrastructure vendors. Obviously, such is more attractive for 700 MHz band, which is a nation-wide LTE service band in North America.

In this study, 6 different types of antennas are prepared to exploit their performance both under NLOS and LOS channel environments. Co-polarized dipole array and cross-polarized dipole array are selected for references, and three types of UE antennas operating at 700 MHz band are prepared.

In the section 3.2, I provide introduction to the AUTs (Antenna Under Test) to be evaluated and summary on the characteristics of AUTs. In section 3.3, numerical analyses on the AUTs based on CDL model are discussed. In section 3.4, correlation properties of AUTs are investigated with MIMO OTA system. In the section 3.5, comparative analyses on the link level performance of AUTs with experimental data obtained from MIMO OTA system and compared against the numerical method.

3.2 Antenna performance

3.2.1 Antenna prototypes and diversity schemes

Figure 3.1 depicts the selected AUTs for investigation of discussed diversity schemes. The VV-0.7λ denotes co-polarized dipole antenna with inter element spacing of 0.7λ, the VH-0.1λ denotes cross-polarized dipole antenna with inter element spacing of 0.1λ. There are three types of prototype AUTs for mobile terminals which are designed for each diversity scheme in points. The physical dimensions of the mobile terminal for prototype design are 130 mm in length, and 70 mm in width.

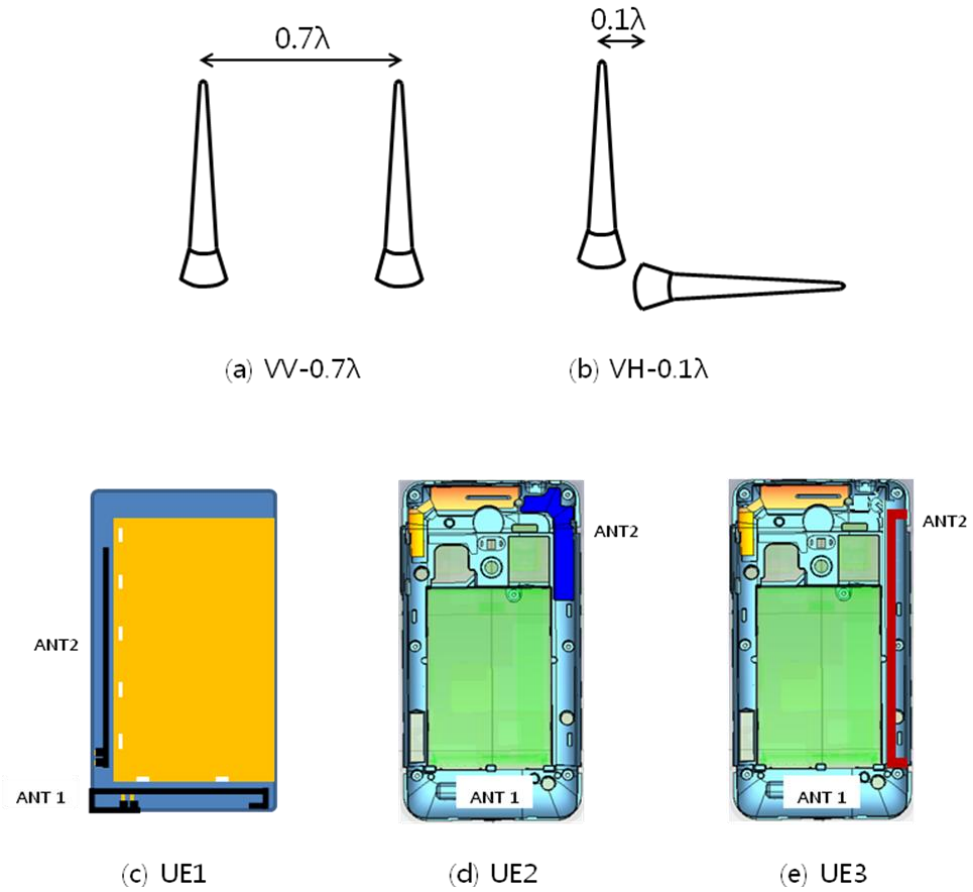

Figure 3.1 Antenna diversity schemes (a) co-polarized dipoles with Δ_l=0.7λ, (b) cross-polarized dipoles with Δ_l=0.1λ, (c) UE 1 with pattern diversity, (d) UE 2 with spatial diversity, (e) UE 3 with polarization diversity

3.2.2 Spatial diversity

Co-polarized dipole array with spatial separation can be a spatial diversity scheme. As discussed in chapter 1, section 1.5, when using a spacing of 0.25λ the averaged correlation coefficient is around 0.2 for Urban Macro-cell model - thanks to the mutual coupling effects. In order to achieve antenna spacing of 0.25λ in 700 MHz, the size of DUT should be slightly larger than 10 cm. In this sense, the mutual coupling effects always exist in mobile antenna characteristics. In addition, the antennas in a

handhelds share a printed circuit board (PCB) as ground plane and be affected by strong interferences between antenna elements. This would lead to a conclusion that the spatial diversity is difficult to be defined for mobile terminals. However, I define the AUT in figure 3.1 d) as spatial diversity antenna because the antennas are separated as much the device size allows.

3.2.3 Pattern diversity and mutual coupling effects

The closer the antenna spacing, the more patterns and the impedance changes due to the mutual coupling effects. It has been studied in the literatures about how the mutual coupling affects on the channel capacities of the radio channels [31][32]. As shown in figure 1.6 and 1.7, though the mutual information is not discussed, the mutual coupling effects reduce the correlation coefficients significantly and this would increase somehow the mutual information of the radio channels. However, it should be noted that the mutual information enhancement would not be significant as much as the reduction of the correlation due to the fact that mutual coupling effects always introduce gain degradation.

In [34] pattern diversity antenna was discussed with a switched parasitic antenna proposed by Vaughan [35] and others [36]. In their study, the radiation pattern of a dipole antenna was able to be modified by placing a second dipole antenna close to it and the degree of coupling between two dipole antennas were optimized by selecting proper load impedance to the second dipole antenna in such a way that the mutual coupling effects are maximized. The design concept of pattern diversity antenna for prototype UE 1 in figure 3.1 (c) is not actually motivated by the previous works. However, their theory of operation is the same in principle. Details on UE 1 will be followed in section 3.2.3.

3.2.4 Polarization diversity

The dual-polarized dipole antenna configuration has been widely used for comparative studies on the performance of polarization diversity and spatial diversity schemes [32][37][38]. Implementation of polarization diversity antenna for handhelds is challenging due to physical size limitations. In case of prototype UE 3 antenna design in figure 3.1 (e), polarization diversity is supported with unacceptable large gain difference between two antenna branches. The vertical polarization is mainly supported by ANT1 where as the horizontal polarization is supported by ANT2. Vertical polarized gain of ANT2 is intentionally suppressed to implement horizontal polarized antenna as purely as possible and this results in 13 dB of gain imbalance between two antenna branches.

3.3 Antenna prototypes

Table 3.1 summarizes antenna properties of the AUTs in figure 3.1. There are antenna gains, directivity [39], XPD (polarization discrimination ratio) [40], gain imbalance and antenna pattern coefficient as derived for all antennas.

Table 3.1 shows dipole antenna configurations for both spatial and polarization diversity schemes that represents low correlation properties and good antenna gains. On the other hand, UE form factor antennas shows clearly smaller gains, especially for ANT2. This is associated to the limitation of physical dimensions of the UE design. This problem is often cited as common problem encountered in MIMO antenna design for handhelds.

Table 3. 1 Antenna parameters

Antenna			Gain (dBi)	Directivity (dB)	XPD (dB)	Imbalance (dB)	Pattern correlation
Dipole	V-V 0.75l	ANT1	-1.5	NA	-19	< 0.5	0.05
		ANT2			-19		
	V-H 0.1l	ANT1			-19		0.02
		ANT2			19		
UE1(Z1)		ANT1	-5.4	3.1	-0.2	0.1	0.25
		ANT2	-5.5	2.7	1.3		
UE (Z2)		ANT1	-3.3	2.2	-1.2	3.4	0.59
		ANT2	-6.7	2.7	0.6		
UE 2		ANT1	-5.7	1.3	-3.9	3.0	0.62
		ANT2	-8.7	2.0	1.0		
UE 3		ANT1	-2.9	1.4	-2.5	12.8	0.10
		ANT2	-15.8	2.6	6.8		

3.3.1 Prototype UE antenna with pattern diversity

Figure 3.2 shows the diagram of impedance tuning network for pattern diversity implementation for prototype UE 1. There are two different optimized impedance values; Z_1=j85 and Z_2=-j42. The value of Z_1 represents the maximum degree of mutual coupling between ANT1 and ANT2 while Z_2 is defined to minimize the coupling by detuning the matching of ANT2 toward higher frequency range. The impedance value switch is controlled by the baseband part of prototype through GPO (General Purpose Output) pin as shown in the figure 3.2. The size of prototype is 125x65 mm^2, which conforms the typical size of handheld devices. In order to maximize the antenna coupling effects, the feed ports of both antennas are spaced closely on the right upper edge of PCB, and the type of antenna is PIFA (Planar Inverted F Antenna) operating at 700 MHz band.

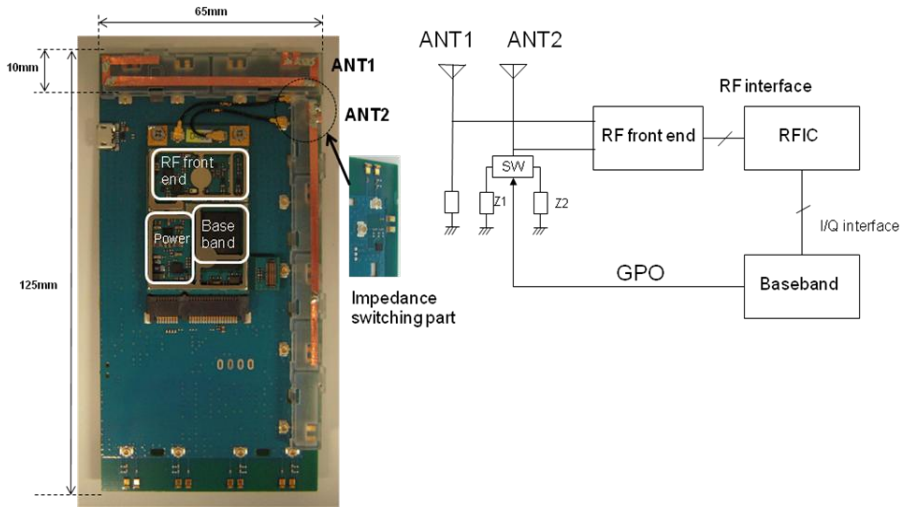

Figure 3.2 Prototype antenna design for pattern diversity scheme (UE1). Size of PCB is 125x65 mm^2, where ANT1 is mounted on the top and ANT2 is mounted on the right side.

Sub-figures in figure 3.3 show the measured scattering parameters antenna system with respect to the different impedance matching values for ANT2. S_{11} is measured at the port of ANT1, S_{22} is measured at the port of ANT2, and S_{21} is measured from the port of ANT1 to the port of ANT2. The range of matching values to ANT2 are Z = {-j424, -j177, -j64, -j42, -j31, j85} while the matching value for ANT1 is unchanged. The measurements are conducted as Z is changed from –j424 to j85 in {Z}. Figure 3.3 (a) shows measured S_{22}, which shows that the resonance frequency of ANT2 is close to 746~756MHz (Marked with 'U' shape in the figure). It is observed that the resonance point of ANT2 is shifted by about 65MHz when the matching impedance value is changed over values in {Z}.

Figure 3.3 (b) shows measured S_{11} with respect to {Z}. Even there are no matching value changes for ANT1, it is clearly observed that the resonance point of ANT1 is shifted from 750 MHz to 738 MHz due to the impedance variation at ANT2 because the mutual coupling effects change the impedances of the coupled antennas of each other.

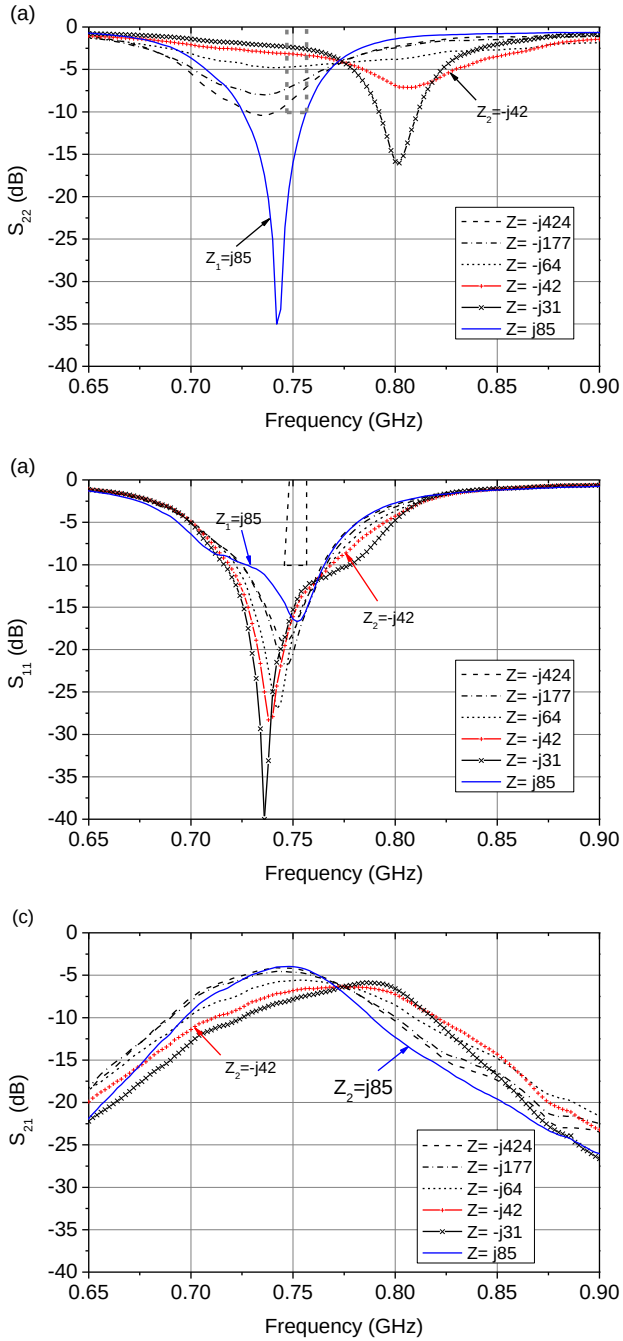

Figure 3.3 Measured scattering parameters of antennas with respect to the matching impedance values for ANT2. (a) S_{11} is measured at the port of ANT1, (b) S_{22} is measured at the port of ANT2, (c) S_{21} is measured between the port of ANT1 and ANT2

The range of resonance frequency shift observed in ANT1 is 16 MHz which is around 25% of that range of ANT2.

Figure 3.3 (c) shows S_{21} between two antennas. It should be noted that the frequency ranges of the peak of S_{21} is shifted from 750 MHz to 790 MHz as Z is changed from –j424 to j85. It is clear that the isolation between two antennas become smallest at 750 MHz (Rx band) when Z_1=j85.

Figure 3.4 shows the pattern correlation and antenna gain for each antenna path as a function of {Z}. The pattern correlation and the gain of ANT1 have similar tendencies against {Z}. This would mean that the pattern correlation is mainly determined by the ANT1. It is note that the maximum correlation is occurred when the mutual coupling is the smallest (Z_2= -j42), and minimum correlation is achieved when the mutual coupling is the largest (Z_1=j85).

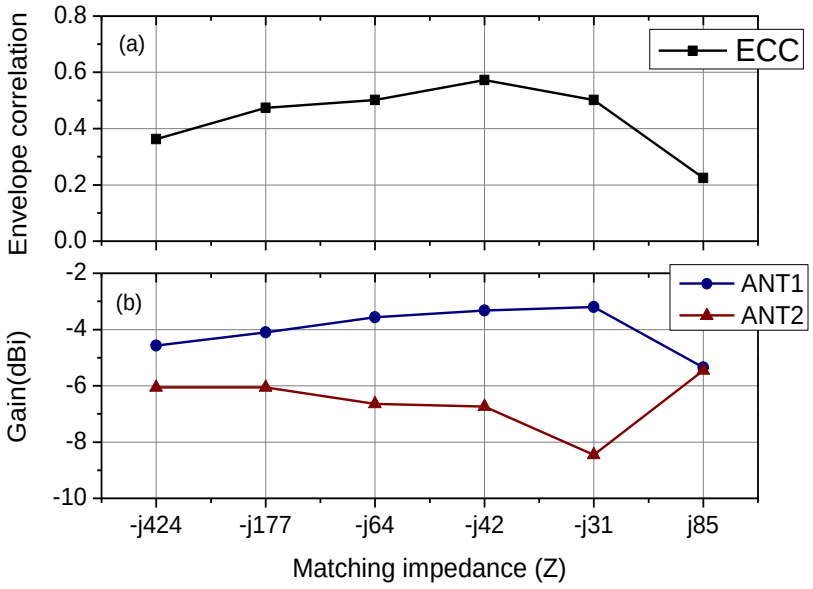

Figure 3.4 Measured antenna gain and pattern correlation as a function of matching value for ANT2 of prototype UE 1. (a) pattern correlation, (b) antenna gain for ANT1 (solid line), and ANT2 (dashed line)

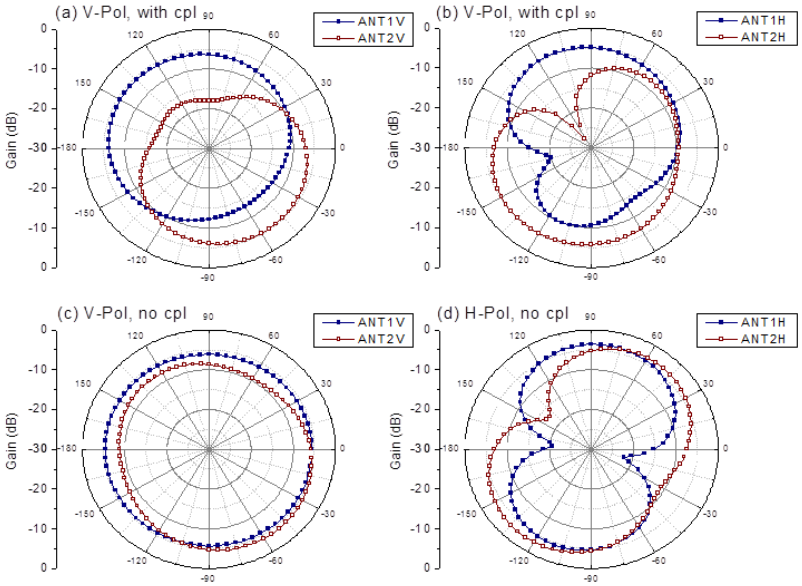

Figure 3.5 Antenna pattern changes observed in UE1 (Z_1) due to mutual coupling effects. a) and b) show gains in the presence of mutual coupling, c) and d) show gains without mutual coupling

In order to show how the mutual coupling effects change the antenna patterns of UE1(Z_1), antenna patterns for the cases in the presence and absence of mutual coupling effects are depicted in figure 3.5. The measurement method is presented in chapter 1.section 1.4 for how to measure the antenna patterns can be measured in the presence of mutual coupling effects or without the mutual coupling effects.

Figure 3.5 a) and b) show the antenna patterns measured under "with mutual coupling" condition whereas c) and d) show the patterns which are measured under "without mutual coupling" condition. It is shown that the antenna gains for both polarizations are distorted by mutual coupling effects in such a way that the directivities for each antenna increase in the opposite directions. These results are achieved when the impedance value of ANT2 is Z_1=j85. When we compare with "without mutual coupling" case, directivities of ANT1 and ANT2 of "with mutual coupling" case are

increased in opposite directions. It is also note that efficiencies near the angles where two antennas are facing are much lowered. The degree of distortion is larger for ANT2 especially in V-pol. From *Eq*. 1.10, the pattern correlation coefficient of "with mutual coupling" condition is 0.25 and that of "without mutual coupling" condition is 0.77.

Figure 3.6 shows the changes in the radiation patterns for prototype UE 1 when ANT2 is switched between Z_1 and Z_2. It is interesting to note that only patterns of ANT1 experience large degree of distortions by switching the matching impudence of ANT2 from Z_2 to Z_1. This is consistent with the results observed in the figure 3.4, where the correlation properties are mainly determined by ANT1. However, it is important to note that the ANT2 is under large degree of pattern distortions in both impedance values because of the presence of ANT1 for which matching impedance is well optimized.

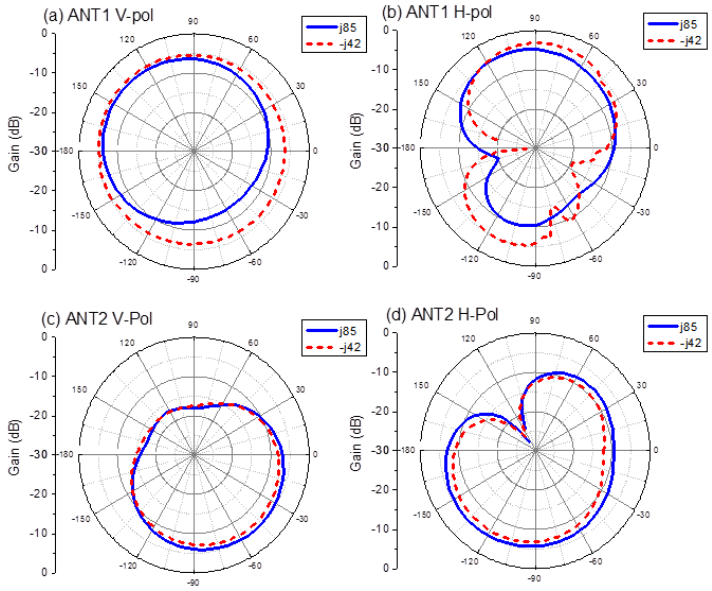

Figure 3.6 Antenna pattern distortions observed in UE1 by switching the matching impedance for ANT2, a) and b) show gains of ANT1 while c) and d) show gains of ANT2.

3.3.2 UE antenna with space diversity

Prototype antennas for UE 2 are designed in a way that the antennas are separated as further away in order to avoid any antenna interferences or mutual coupling effects. It should be note that the complete elimination of the antenna coupling effects is not possible because the antenna separation is not sufficient in hand held devices. This somehow would impact on antenna efficiencies and correlation properties. Figure 3.7 shows measured antenna patterns for UE 2 in 2-D space. V-pol gain of ANT2 is much smaller than that of ANT1 while H-pol gains for both antennas are similar. It should be noted that the H-pol gain for ANT2 in typical UE antenna design is higher than V-pol gain. This confirms the results of XPD value of ANT2 for UE 2 to be 2 dB in table 3.1.

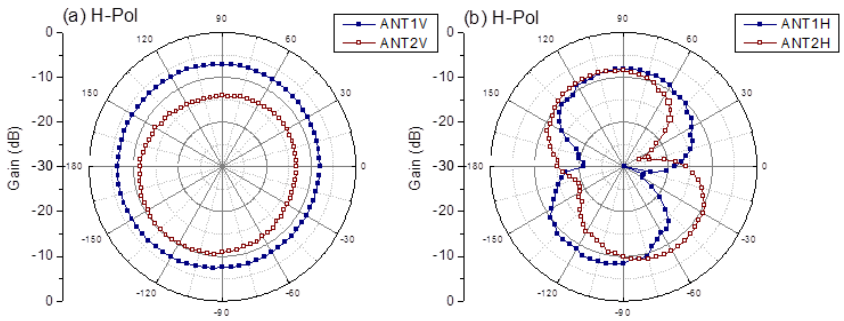

Figure 3.7 Antenna patterns of UE2, a) V-pol and b) H-pol. UE's front side is at ϕ=0°

3.3.3 UE antenna with polarization diversity

Figure 3.8 depicts antenna patterns for UE 3. It is clearly observed that V-pol gain of ANT2 is negligible compared to that of UE 2. It can be explained that the extended antenna element for ANT2 of UE 3 make the effective ground length short in the longitude direction of the phone and therefore, the radiation efficiency is reduced in vertical direction. In addition

the angle of ANT2 of UE3 is rotated in 2-D space by around 60° from the original design (ANT2 of UE2). As a result, the relative angle between the H-pol gain of ANT1 and ANT2 of UE3 become around 60°. This would also significantly reduce the correlation coefficient at the cost of too low efficiency to be used in commercial devices.

With such low antenna efficiency of ANT2 of UE3 results in 12.5 dB of gain imbalance between two antenna branches. This can be regarded as an extreme case that shows very low antenna correlation at the cost of such a large gain imbalance. Because of the large gain imbalacne, there would be a substantial drop in SNR in the second branch of receiver, which will be a limiting factor in operating at a high MCS especially in open-loop spatial multiplexing mode. It would be interesting to see the performance of this extreme case, UE 3, both in MIMO OTA system and in the live network.

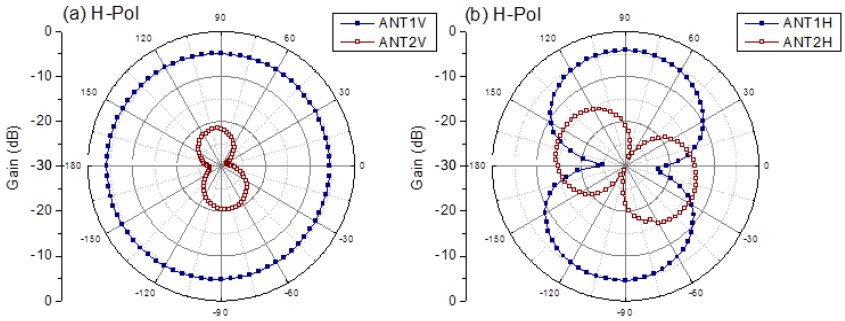

Figure 3.8 Antenna patterns of UE3, a) V-pol and b) H-pol. UE's front side is at ϕ=0°.

3.4 Numerical analysis on the performance of AUTs in Rayleigh and Ricean fading channels

Numerical analysis of AUT's performance under Rayleigh and Ricean fading channels are conducted based on CDL model discussed in section

1.2.2.2 of chapter 1. Channel transfer matrices are generated incorporating measured complex antenna patterns for each AUT in order to compare to the measurement results in section 3.5. Geometrical scenario used is Urban Micro Channel Model as shown in table A.2. Figure 1.4, in chapter 1, depicts the equivalent PAS shape of the Urban Micro Channel Model. It should be noted that the six different AoAs of Urban Micro channel model are near ϕ=0°.

BS antenna patterns are the same as for scheme B and C of table 1.1 (co-located slanted dipole). Channels are realized for four different Δ_{AoA}, which are {0°, 90°, 180°, 270°}, and the link level performance of AUTs are analyzed for the four channel realizations defined by new AoA for nth cluster with,

$$\delta'_{\mathrm{n,AoA}} = \delta_{\mathrm{n,AoA}} + \Delta_{\mathrm{AoA}} \qquad (Eq.3.1)$$

3.4.1 Diversity measure

The 2x2 MIMO radio channel transfer matrices derived with CDL model and complex antenna patterns of AUTs, The co-variance matrix is obtained from *E*q. 1.6 whereas diversity measure for Rayleigh channel is obtained from *E*q. 1.12.

Figure 3.9 shows calculated diversity measure for all AUTs. It is found that the UE1 (Z1), the pattern diversity antenna shows the largest diversity. In contrast to UE1 (Z1), impedance detuned antenna for higher antenna efficiency, UE1 (Z2) shows smaller diversity measure. It is also interesting to note that both of the co-polarized and dual-polarized dipole array shows similar diversity performance compared with the other AUTs.

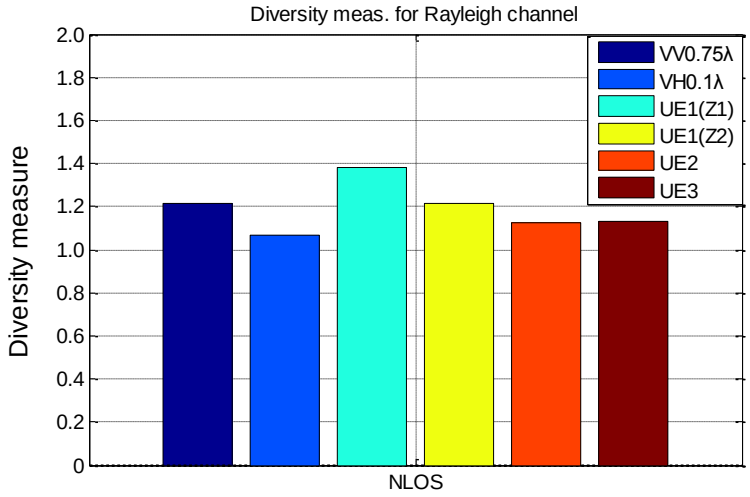

Figure 3.9 Diversity measure of all AUTs under NLOS channel averaged over $\Delta_{\mathbf{AoA}} \in \{0°, 90°, 180°, 270°\}$

3.4.2 Correlation properties

For arbitrary polarized antenna patterns, spatio-temporal correlation coefficients are needed to be used as the correlation metric. Tx and Rx correlation coefficients for all AUTs of NLOS and LOS channels are obtained from *Eq.* 1.8 and *Eq.* 1.9. Figure 3.10 depicts the numerical correlation coefficients averaged over four Δ_{AoA}. Recalling the dual-polarized dipole as discussed in section 1.6.3 of chapter 1, it is observed that the correlation coefficients of co-polarized dipole array are dramatically increased as K-factor increases whereas those of dual-polarized dipole are not incased as much as co-polarized dipole. The same correlation enhancements is observed for co-polarized dipole in LOS channel while other AUTs show a slight increase of correlation properties. This would mean that the other AUTs with UE form factor have, in some extent, dual-polarized antenna characteristics. It is interesting to note that the Rx correlation of UE3 decease in LOS channel condition.

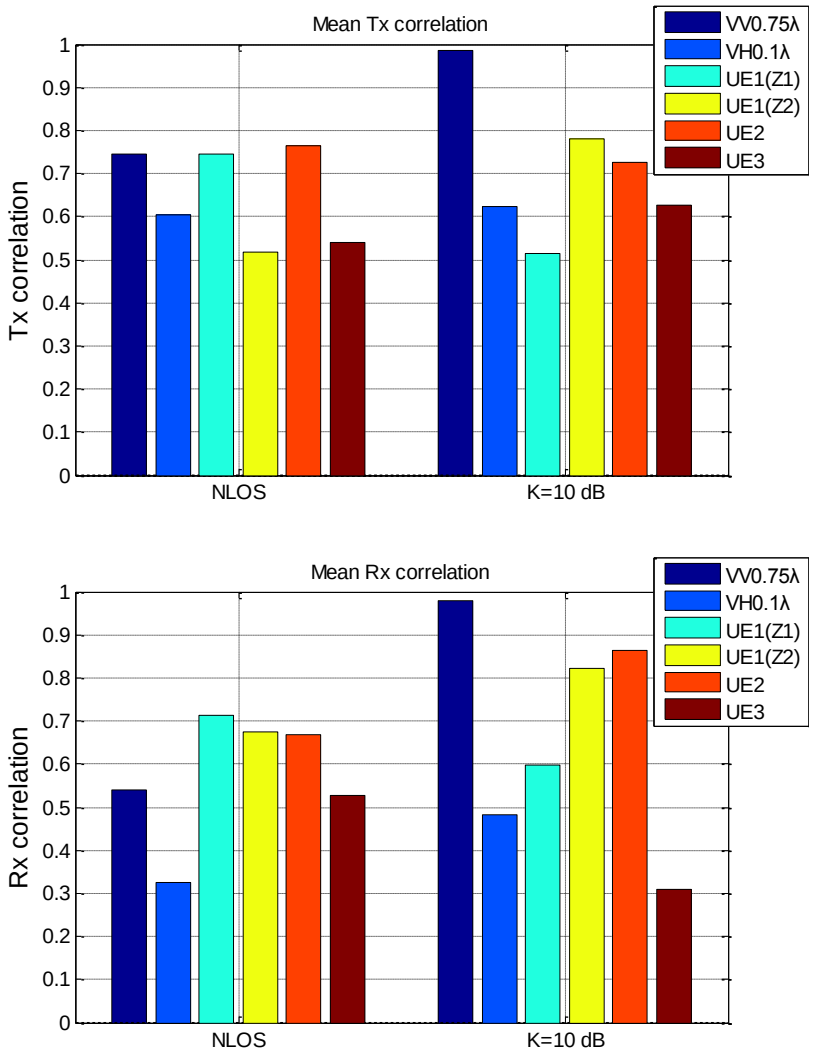

Figure 3.10 Spatio-temporal correlation coefficients for all AUTs for NLOS (Upper figure) and LOS (Bottom figure, K-factor = 10 dB) channels.

3.4.3 LTE physical layer performance

In order to consider the antenna gain effects for performance estimation, effective SNR is defined in Eq. 2.1. LTE physical layer throughput performance for AUTs are calculated from the ergodic mutual information of the channel with given effective SNR and system parameters defined in table 2.1.

Figure 3.11 depicts the results of estimated average throughput performance for each AUT in NLOS and LOS channels. As expected, co-polarized dipole antenna experiences significant degradation of throughputs in the Ricean channel. Similar throughput performance decrease is observed in the results of UE1 (Z_2). Interestingly, the UE1 (Z_1) outperforms the other UE form factor antennas both in NLOS and LOS channels. This can be attributed to large diversity performance of UE1 (Z_1) in NLOS channel and reduced correlation in LOS channel experienced. The UE3 shows the smallest throughput in NLOS, however, remarkable throughput performance enhancements are observed in LOS channel in high SNR range.

It should be note that the throughput performance differences between AUTs in NLOS are larger than in LOS condition under low SNR ranges. This can be explained by the fact that the throughput performance in NLOS is less dependent on correlation than in LOS channel.

Further, it should be noted that the actual throughput performance of real mobile terminals are largely dependent on the decoder performance of the communication modem that chipset has adopted. Thus, the throughput estimation can be a performance metric which can estimate the linkf performance of AUTs purely based on the radio channel and antenna patterns.

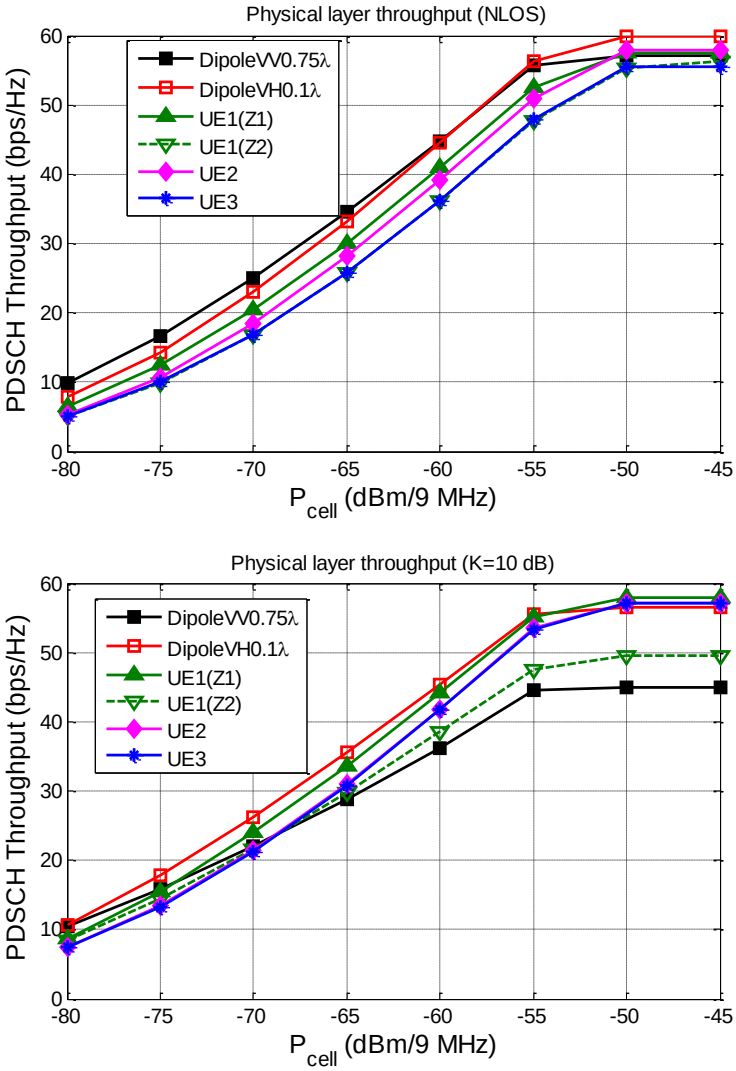

Figure 3. 11 Ergodic mutual information as a function of incident power for all AUTs under NLOS(Upper figure) and LOS (Bottom figure, K-factor=10 dB) channels.

3.5 MIMO OTA performance

In this section, we will discuss about the correlation characteristics, and PDSCH throughput performance of AUTs based on the experimental data obtained from the MIMO OTA system. The system setup shown in figure 1.1 on section 1.2 of chapter 1 is used for measurements. For comparative study between the numerical correlation and throughput performance discussed in section 3.4, the Urban Micro channel model is used for channel model for the measurements in the MIMO OTA system.

3.5.1 Comparison of the correlation properties in MIMO OTA system

Figure 3.12 (a), (b) represents measured power correlations for all antennas measured under Urban Micro-NLOS and LOS channel conditions, respectively. The power correlations are measured at four different Δ_{AoA} defined by *Eq*. 3.1. In the MIMO OTA system, the direction of ϕ=0° is aligned to the broad side of dipole antenna arrays and the front side of the UE form factors.. During the measurements, the average power at the center of the anechoic chamber is maintained at -35 dBm/ 9MHz. When we take into account the cable loss, the actual power would be -50 dBm/9 MHz per antenna port. The measured power correlations are varied with respect to Δ_{AoA} changes. Such dependencies of correlation on Δ_{AoA} are become more significant in LOS model because of the coherency of the LOS path.

The VV-0.7λ shows fairly low correlation of 0.12 in NLOS channel whereas that in LOS channel is increased to 0.93. Such high correlation in LOS channel is attributed to the fact that co-polarized dipole antennas have little gain in the horizontal polarization, and the power correlation are determined mostly by coherent, vertical polarization components of LOS path.

The VH-0.1λ shows the smallest correlation properties in NLOS channel and it also experience a substantial increase of correlation characteristics in LOS channel but still maintain much lower correlation than VV-0.7λ.

The UE form factors show very different correlation properties of each other. Interestingly, most of them show very high correlation at Δ_{AoA}= {90°, 270°}. Such symptom is clearer in LOS than in NLOS channel. This is because there is little H-pol gain on the sideward of the UE factors and then the correlation properties are determined by the V-pol gain which results in high correlation.

UE1 (Z_1) shows 0.27 in NLOS thanks to the mutual coupling effects whereas UE1 (Z_2) shows 0.56 in NLOS. However, both of them show very high correlation properties in LOS channel. This is due to the fact that the devices have different gains and polarization ratios depending on the angle in Azimuth plane. There can be a certain angles where the antenna gains are single polarized for both of antennas. In such cases, the correlation characteristic would be very high. For example, UE 1 shows power correlation greater than 0.9 at Δ_{AoA}=90° and 270° and UE 2 experiences such high correlation at Δ_{AoA}= 270°. At all of these angels, both antenna gains are almost single polarized; either V-polarized or H-polarized.

It is clear that all antennas show dramatic increase in power correlation in LOS model due to the coherency of the Ricean components and this would impact the device's throughput performance as discussed in the next section.

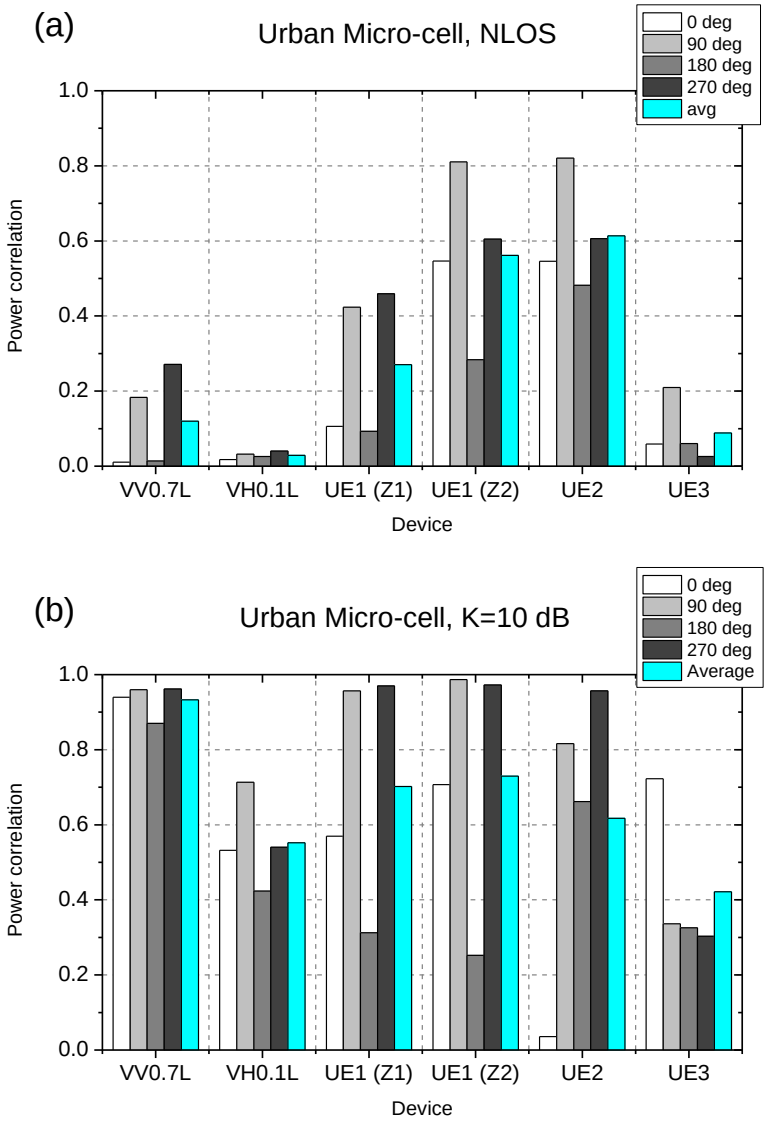

Figure 3.12 Measured power correlation properties of all AUTs with respect to four different $\Delta_{\mathbf{AoA}}$ under NLOS (a) and LOS (b) channels.

3.5.2 SNR performance in MIMO OTA system

In our measurement setup, measurements are conducted while locating the AUTs inside of anechoic chamber, which are connected to the LTE UE located outside the anechoic chamber through the RF cables. while the LTE

UE is located outside the chamber through RF cables. Then the SNR is given by,

$$\text{SNR} = P_{Cell} - (G_{ANT} + L_{Cable} + Noise) \qquad (Eq.3.5)$$

$$\text{Noise} = \text{kTB} + \text{NF} + \text{IM} \qquad (Eq.3.6)$$

where P_{Cell}, is averaged channel power measured at the center of the chamber under spatial fading emulation. G_{ANT} is antenna gain, L_{Cable} is cable loss used for connecting the antennas in the chamber to the UE's antenna ports. The *kTB* is thermal noise power at the antenna port of the UE over system bandwidth. The NF is noise figure of the UE's receive chains. The IM is implementation margin including RF impairments. Assuming that P_{Cell}= -35 dBm/9 MHz, G_{ANT}= -5 dBi, L_{Cable}=15 dB, and Noise=-95.5 dBm/9 MHz, then the expected SNR would be 40 dB. However, under the fading channel, the accuracy of SNR measured by the UE gets dropped due to RF impairments and noise estimation error. Thus the actual SNR reported by the UE can be much lower than 40 dB. In our UE design the SNR is saturated at around 30 dB.

Figure 3.13 shows the measured SNR for all AUTs. The SNR is reported by LTE UE which is connected to the AUTs from outside of the chamber. The SNR performance includes the antenna gain of antenna under test, and impairments in the RF chain as well as the Minimum Mean Squired Error (MMSE) channel estimator of the UE. Thus, the SNR curve is a function of averaged channel power which can give a faire comparison data for each antenna under test. Note that VV-0.7λ, co-polarized dipole shows the best SNR performance and VH-0.1λ is the second rank. UE1 (Z1) and UE2 are ranked in the middle, and UE1(Z2) and UE3 shows the worst due to large antenna gain imbalance. In particular, UE1(Z2) has very low gain for ANT2 near ϕ=90° as shown in figure 3.4 (c) and (d).

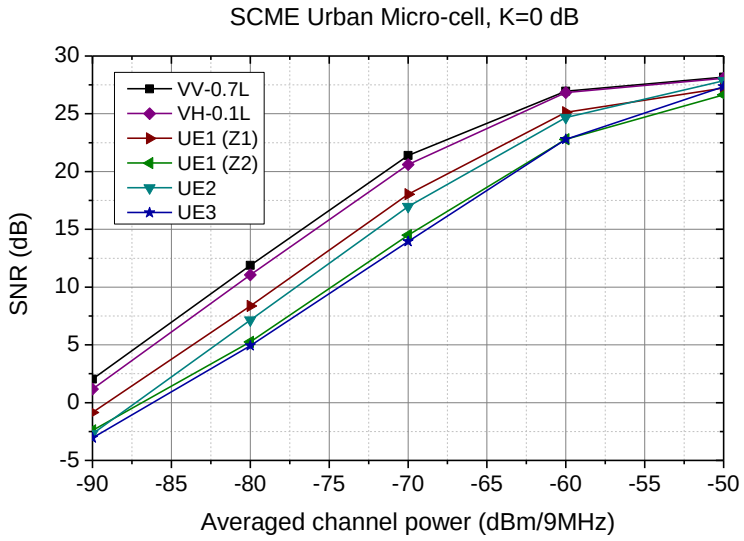

Figure 3.13 SNR performance of all AUTs with respect to the averaged channel power at the center of MIMO OTA system.

3.5.3 PDSCH throughput comparison in MIMO OTA system

As discussed in chapter 1, there are a number of parameters that impact on the downlink throughput performance of LTE UE. In this section, the set of parameters for MIMO OTA system are summarized in Table 2.1. The channel model is changed from Urban Macro-cell model to Urban Micro-cell model as explained in section 3.3.1. The throughput performance of all antennas in figure 3.1 is evaluated under NLOS and LOS channel models.

3.5.3.1 Throughput in a high SNR range

PDSCH throughput measurements are conducted at -50 dBm /9MHz averaged channel power at the center of the chamber. At this power, the SNR is almost saturated and the SNR performance gaps become smaller between antennas as shown in figure 3.13. Therefore, the antenna performance benchmark tests are conducted in a condition that the

throughput performance are mainly determined by the antenna correlation property rather than efficiency or gain imbalances.

The PDSCH transmission mode is set to TM3. At a given Δ_{AoA}, the automated test agent running on the test computer searches the maximum throughput by searching the maximum MCS where the CRC (Cyclic Redundancy Check) error can be maintained below 10%.

Figure 3.14 (a) shows the PDSCH throughput measurement results in NLOS channel model for all antennas. It is observed that the antennas with polarization diversity, VH-0.1λ and UE 3 outperform the VV-0.7λ and other UEs due to significantly low power correlation properties as shown in figure 3.12 (a). In the case of antenna with pattern diversity, UE 1 with Z1 performs slightly better than UE 1 with Z2 even there are substantial reduction of correlation in NLOS channel. On the other hand, antenna with spatial diversity, VV-0.7λ shows much lower throughput than other antennas.

In figure 3.14 (b), there are the throughput measurement results under the LOS channel model. It is expected that there are significant performance drops for all antennas associated with high correlation properties of antennas under LOS channel model. However, again the antennas with polarization diversity, VH-0.1λ and UE 3 throughput results are higher than in NLOS channel model even there are substantial increase in the power correlation in LOS channel. It is also remarkable that the throughput of UE 2 become quite closer to that of UE 3 that is not the case under NLOS channel. On comparison between the throughput measurement results under NLOS and LOS conditions, the following observations can be made:

- Co-polarized dipole shows unacceptable throughput performance drop in LOS channel condition due to high Tx and Rx correlation characteristics. Such throughput performance drop due to high correlation characteristics is also observed in the UE form factor

antennas when the signals are impinging on the sideward of the UE form factors.

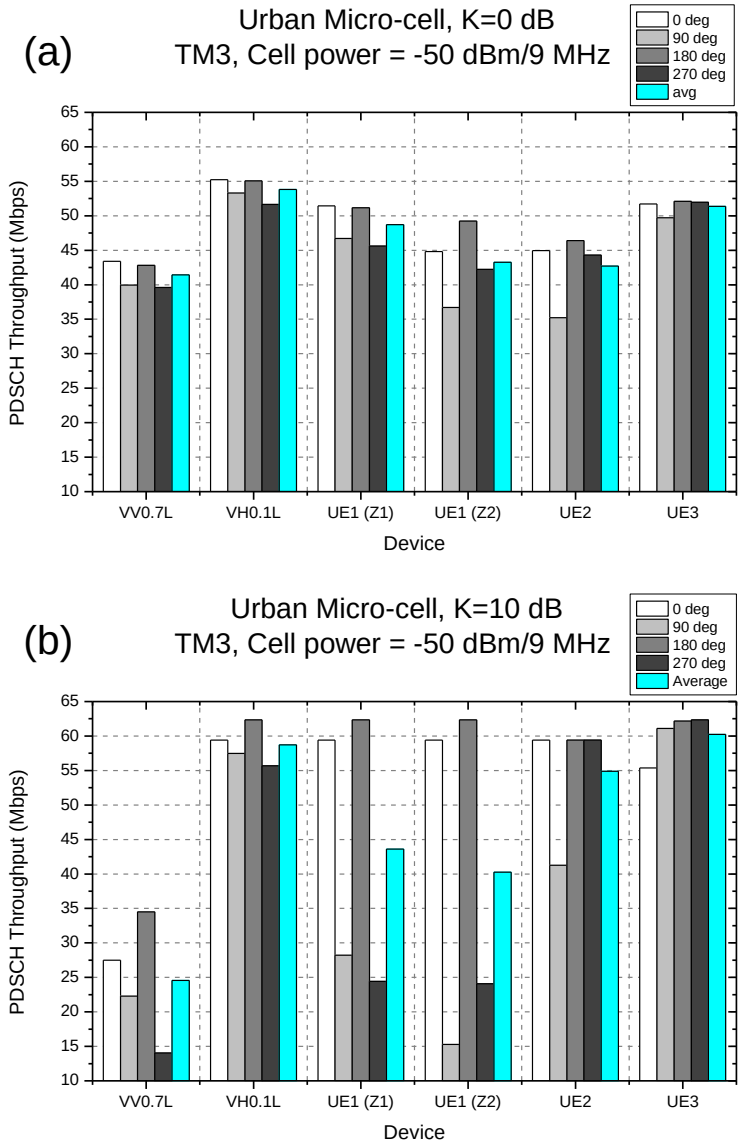

Figure 3.14 Measured PDSCH throughput at high SNR range (a) NLOS and (b) LOS (K-factor=10 dB) channels

- In LOS channel condition, dual-polarized dipole and UE 3 with polarization diversity antenna also experience substantial increase in correlation properties. However, the throughput performance are much

improved as compared to NLOS channel condition. This is because orgorgorality between codeword streams transmitted from the BS is well maintained in LOS condition and this improves channel estimation performance at the UE and therefore better throughput performance.

3.5.3.2 Throughput performance in a wide SNR range

Figure 3.15 (a) and (b) show, respectively, TM3 PDSCH and TM2 PDSCH throughput under NLOS channel model, over $\{\Delta_{\mathrm{AoA}}\}$ for antennas under evaluation with respect to the channel power. Note that the channel powers include attenuation due to cables. For TM3, open-loop spatial multiplexing mode, the channel powers are varied from -50 dBm/9 MHz to -80 dBm/9 MHz and associated SNR ranges are from 30 dB to around 5 dB as shown in figure 3.13. For TM2, transmit diversity mode, the channel powers ranges are from -70 dBm/9 MHz to -90 dBm/9 MHz and the corresponding SNR ranges are from 23 dB to -3 dB depending on the antenna under test.

Fair comparison works can be made by the following way.

- *Antenna correlation properties with respect to the AoA of the PAS*
- *Antenna efficiencies with respect to the AoA of PAS and associated SNR performance*
- *Antenna gain imbalances between branches with respect to the AoA of PAS and associated SNR performance*

In a low SNR range, around 10 dB for example, the antenna efficiencies may be more important than the correlation properties because the PDSCH is scheduled in such low SNR range that the BS normally selects the transmit diversity scheduling according to the CQI and RI feedbacks in order to improve receiver performance robustness [41].

It is clear from the throughput in figure 3.15 (a) that the VH-0.1λ outperforms the other antennas under test over the entire power ranges. On

the other hand, UE3 with dual polarized antenna shows high throughput results only between -50 ~ -55 dBm/9 MHz of cell power and shows significant throughput drop below -55 dBm/9 MHz due to deteriorated SNR. UE1(Z1) with pattern diversity antenna performs well in a wide range of channel power compared to UE1(Z2), suggesting that the pattern diversity provides more spatial multiplexing gain in NLOS channel model.

When comparing throughputs in figure 3.15 (b), spatial diversity and polarization diversity dipoles clearly outperform in the transmit diversity mode. It should be note that UE1 (Z1), UE1 (Z2) show better performance among the prototype UE antennas. This further emphasizes the pattern diversity scheme works well in NLOS channel model.

Figure 3.16 (a), (b) show throughput against channel power under LOS channel condition. In case of TM3 throughput, it is interesting to note that the UE3 with dual polarized antenna outperforms the other UE antennas over almost all of channel power ranges. It should be noted that UE1(Z1) and UE1(Z2) with pattern diversity antennas show lower throughput under LOS channel. In case of co-polarized dipole, it shows even worse throughput than in NLOS.

In case of TM2 throughput, all AUTs perform similarly for LOS and NLOS channels except for dual-polarized dipole due to the fact that the dual-polarized dipole experience smaller signal reception from the antenna branch tilted by 90 degrees in LOS channel. Figure 3.17 (a), (b) show Cumulative Distribution Functions (CDFs) for throughput over two channel conditions. The measurement conditions are the same as presented in figure 3.15 and 3.16. The CDFs are derived from the set of the maximum throughput measured data at each given range of channel power and Δ_{AoA} defined previously. Depending on given channel power, throughputs are measured in TM2 or TM3 modes. The purpose of this CDFs plots is to compare the tendencies of throughput results for each antenna under test between in MIMO OTA system and in the live network.

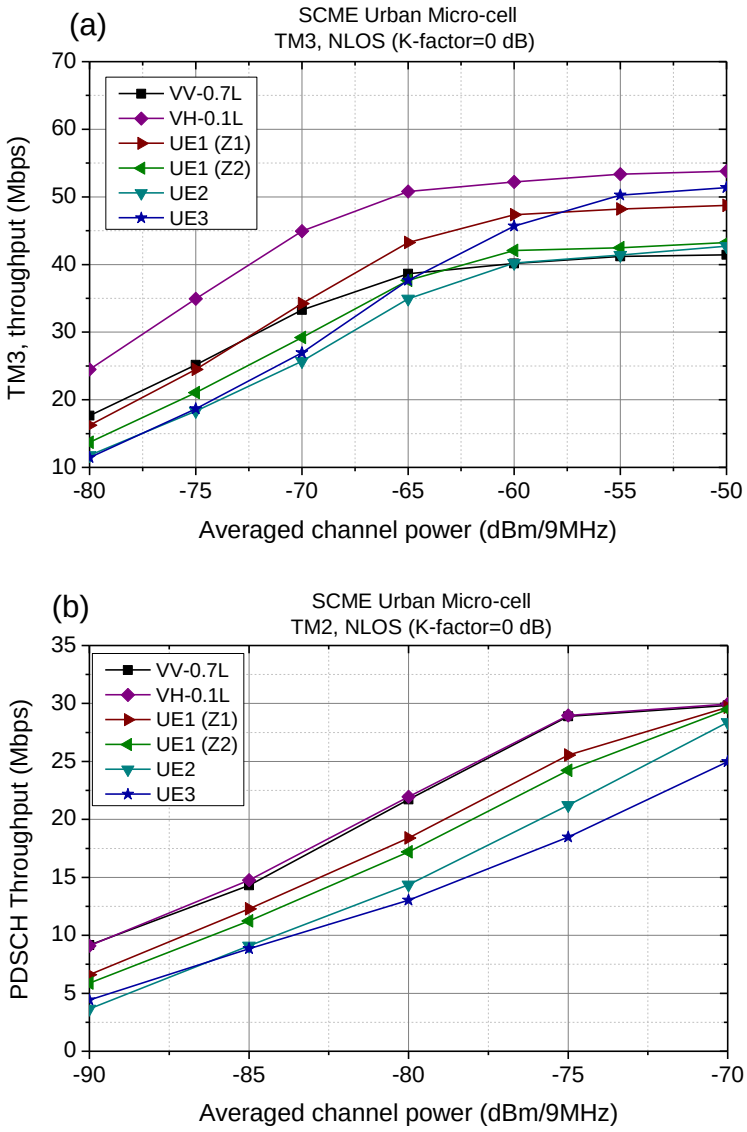

Figure 3. 15 Measured (a) TM3 and (b) TM2 PDSCH throughput for all AUTs over wide SNR ranges under NLOS channel

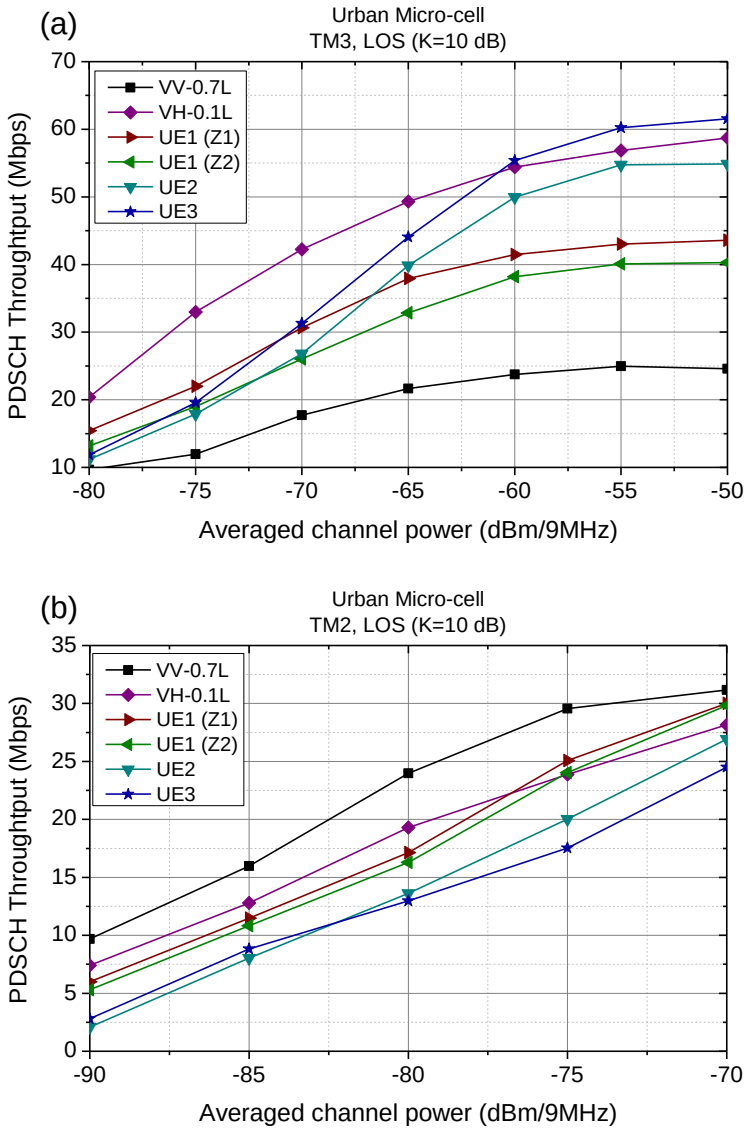

Figure 3.16 Measured (a) TM3 and (b) TM2 PDSCH throughput for all AUTs over wide SNR ranges under LOS (K-factor=10 dB) channel

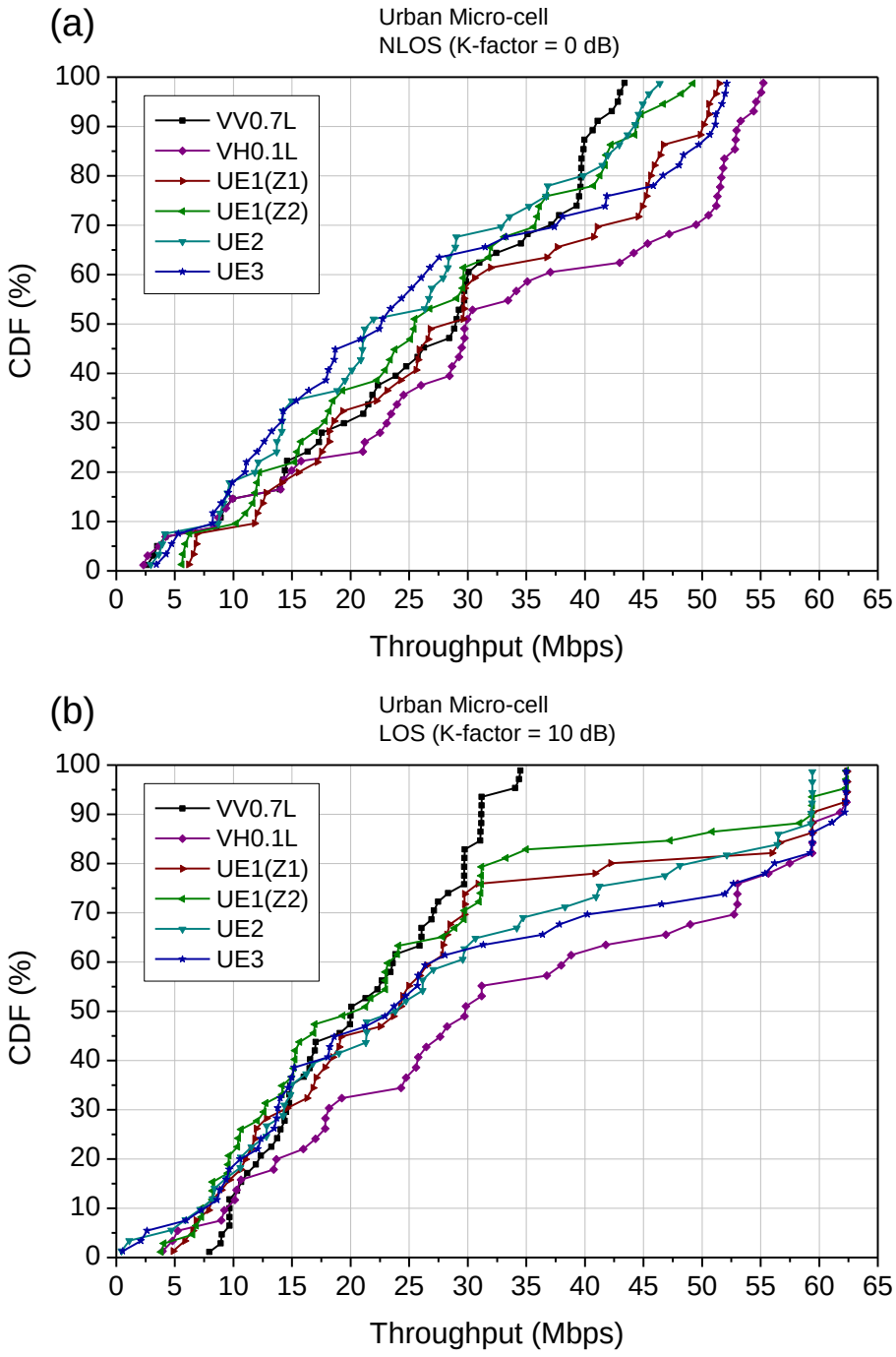

Figure 3.17 CDFs for all AUTs with respect to PDSCH throughput for (a) NLOS and (b) LOS channels

3.6 Conclusions

Comparing between the throughput measurement results in NLOS and LOS conditions, the following observations can be made:

Antenna correlation properties are more important than antenna efficiency or imbalance between branches in high SNR ranges. This is particularly true in LOS channel condition.

Gain imbalance between branches is more important parameter in NLOS channel than in LOS channel condition.

Spatial diversity scheme shows low spatial multiplexing gain than other diversity schemes especially in LOS channel. However, co-polarized dipole antenna showed good performance in the transmission diversity mode.

Pattern diversity scheme performs well in NLOS channel. However, significant throughput drop is observed in LOS channel condition because of its AoA dependencies of correlation properties and gain characteristics.

Polarization diversity scheme shows the highest spatial multiplexing gain both in NLOS and LOS channels. However the transmit diversity gain is slightly lower than spatial diversity scheme.

CHAPTER 4

Spatial, polarization diversity and UE form factor antenna performance in a trial live network

4.1 Background

In this work, an evaluation is discussed on the device performance with spatial, polarization diversity and form factor antennas in LOS, NLOS, and Indoor NLOS radio channels. The performance measurements are conducted in a LTE trial network in Ottawa, Canada for the end-to-end system throughput performance evaluation on the co-polarized dipole antenna, dual-polarized dipole antenna, and prototype form factor antennas for mobile handsets. The operating bands of antenna under test are AWS (Advanced wireless service) band or 3GPP E-UTRAN band 4 [43].

Previous studies have concluded that the MIMO channel capacities in LOS indoor channels deteriorate the channel capacity due to increased channel correlation in case of uniform linear array (ULA) antennas [44]and dual polarized antenna [45]. These studies focused on characterizing the channel properties of indoor channels and channel capacity estimations based on the channel impulse response measurements. It has been shown that the polarization diversity incurs a loss in SNR and diversity gain when compared to spatial diversity in an indoor environment with low-K-factors [32]. On the other hand, several outdoor field measurement reports concluded that the performance of polarization diversity was comparable to that of spatial diversity in case of vertically polarized transmit antenna [46].

Another field measurement study has shown that cross-polarized antenna showed better performance than co-polarized antenna at 64QAM whereas co-polarized antenna showed slightly better performance in 16QAM using a LTE test bed [47]. It has also been addressed that cross-polarized antenna experienced SNR degradation in case where the transmitter antenna at BS was vertically polarized antenna array. Such properties of dual polarized antennas also have been observed in the extensive comparison works in the previous chapter.

To our best knowledge not many studies have been carried out on the performance verification for the various diversity schemes by comparing the throughput performance under LOS and NLOS channels.

The aim of the field measurements and comparison works are to investigate the best antenna configuration both in a LOS and NLOS radio channel conditions in a trial field network and compare the conclusion from the trial with the conclusion of chapter 3.

4.2 Antenna performance

4.2.1 Antenna prototypes for diversity schemes

Figure 4.1 shows AUTs for field trials against LTE live network. The trials are performed for 3 different types of dipole antenna configurations- VV-0.25λ, VV-1.0λ, VH-0.1λ and 3 types of UE antennas, which are PIFA type. The UE antennas depicted in figure 4.1 (d)~(f) are designed in such a way that the isolation between ANT1 and ANT2 can be adjusted by changing the antenna spacing, which are D1, D2, and D3. The intention of differentiating the antenna isolations was to change the degree of mutual coupling between antennas and intended to achieve the pattern diversity.

A summary of the antenna parameters is shown in Table 4.1. The isolation between ANT1 and ANT2 of UE antennas is a function of antenna

separation. Note that the antenna spacing D ∈ {6mm, 12 mm, 18 mm}, and resultant isolation (S_{21}) are shown in table 4.1. It is observed that as D of UE antenna increases, S21 as well as the polarization ratio increase. This would mean that as the degree of mutual coupling between antennas is decreased, H-pol gain components are more enhanced than V-Pol gain components. The Gain imbalance of the dual antenna was maintained within 1 dB to minimize the impact of the gain imbalance on the performance.

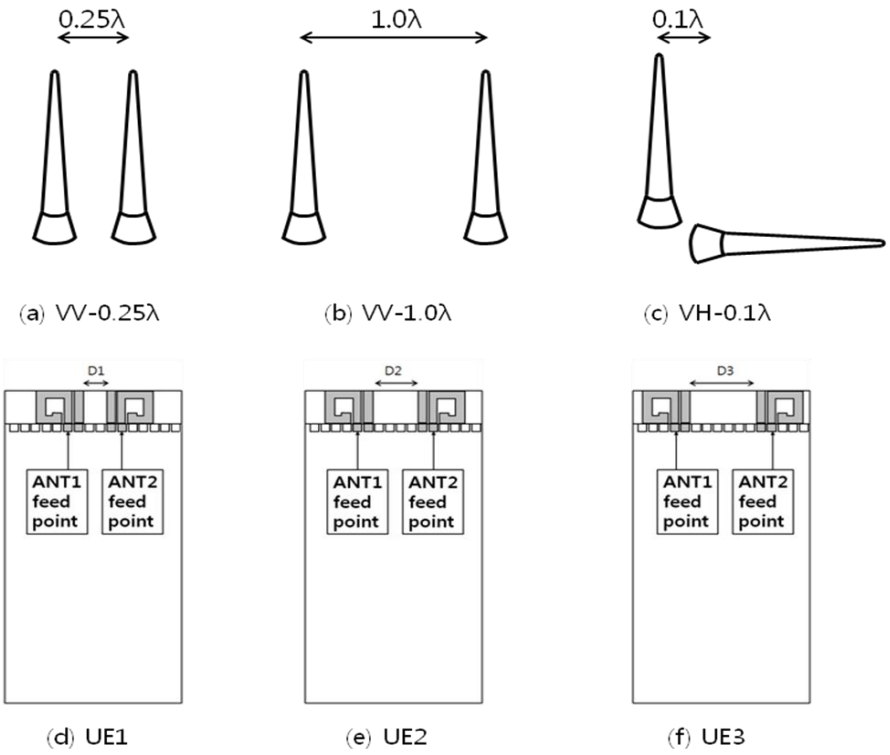

Figure 4.1 Antenna configurations for field trial (a) co-polarized dipoles (Δ_l=0.25λ), (b) co-polarized dipoles (Δ_l=1.0λ), (c) cross-polarized dipoles (Δ_l=0.1λ), (d) UE1 (D1=6 mm), (d) UE2 (D2=12 mm), (e) UE3 (D3=18 mm)

Table 4. 1 Antenna parameters

Antenna			Gain (dBi)	Directivity (dB)	XPD (dB)	S21 (dB)	Imbal (dB)	ρ
Dipole	VV-0.25λ	ANT1	-1.5	Omni-directional	N/A	N/A	<0.5	0.21
		ANT2						
	VV-1.0λ	ANT1						0.01
		ANT2						
	VH-0.1λ	ANT1						0.01
		ANT2						
UE1 (D1=6 mm)		ANT1	-5.6	2.4	-1.3	-4	0.53	0.19
		ANT2	-6.2	2.8	-2.0			
UE2 (D2=12 mm)		ANT1	-2.6	2.3	2.8	-10	0.13	0.04
		ANT2	-2.8	2.5	1.9			
UE3 (D3=18 mm)		ANT1	-2.0	2.1	2.1	-16	-0.60	0.07
		ANT2	-1.4	2.1	2.1			

4.2.2 Radiation patterns and correlation properties of UE form factor prototypes

Figure 4.2 shows the antenna patterns of UE antennas. It is observed that the antenna patterns of UE1 are distorted severely both in V-polarization and H-polarization. This explains the larger directivity of UE1 than that of other prototypes as in the table 4.1. When we compare all UE antennas, it is clear that the H-polarized gain components are much improved as the isolation between two antennas are reduced. It is interesting to note that the directivity of H-polarized gains are rotated by 90° in 2-D space suggesting reduced pattern correlation property.

Figure 4.3 shows the pattern correlation of three types of UE antennas with respect to the Δ_{AoA} ={-180:1:180} and XPR of the PAS. When we compare the correlation for each UE antenna under XPR=30 dB, UE1 shows the highest correlation with large dependency of Δ_{AoA} than the other UE antennas. However, when XPR = -30 dB, UE1 shows the smallest

correlation due to a large degree of mutual coupling between ANT1 and ANT2 in H-polarization.

Interestingly, all UE antenna show high correlation around Δ_{AoA} = ±90° when XPR=30 dB. This can be explained by the fact that the ANT1 and ANT2 have peak gains near ϕ= ±90° in the V-polarization suggesting high correlation properties near around these directions. On the other hand, it is found that the H-pol gains of ANT1 and ANT2 are more affected by the mutual coupling effect. As shown in the figure 4.3, the pattern distortion in H-pol gains of the UE antennas are significantly reduced when the isolation between two antennas increase. This explains the high correlation of UE3 when XPR=-30 dB.

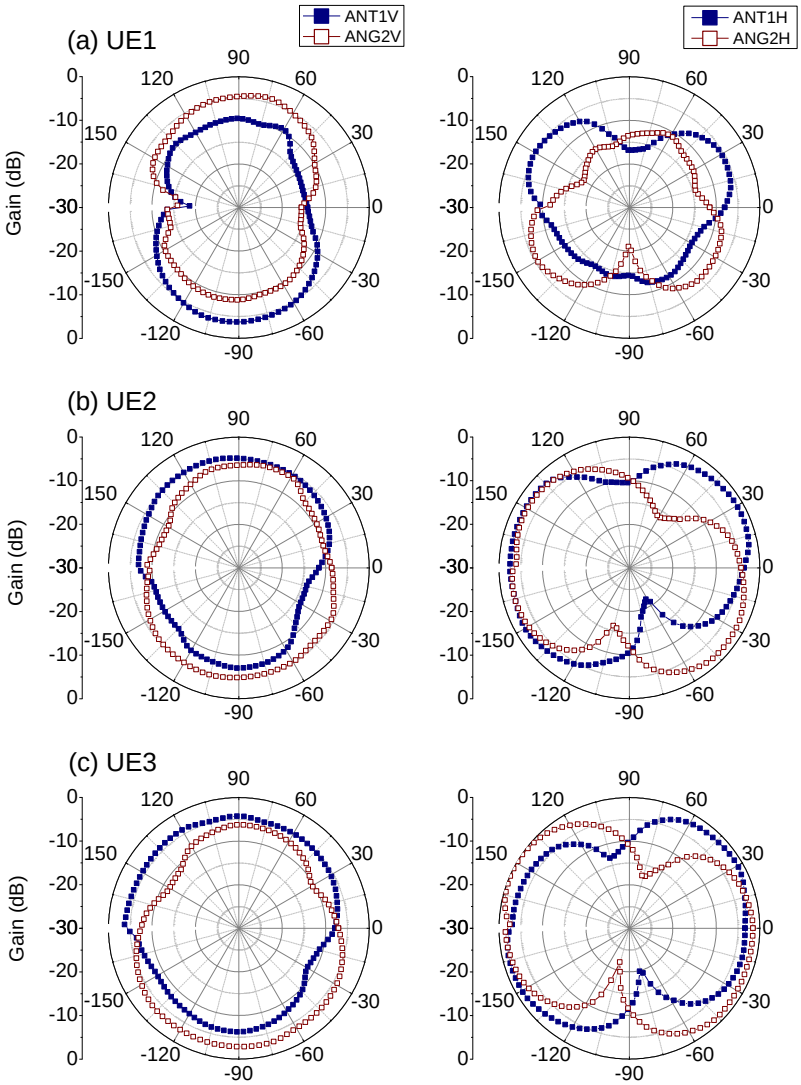

Figure 4.2 Antenna patterns for prototype UE antennas. (a) UE1 (S_{21} = - 4 dB), (b) UE2 (S_{21} = - 10 dB), (c) UE3 (S_{21} = - 16 dB)

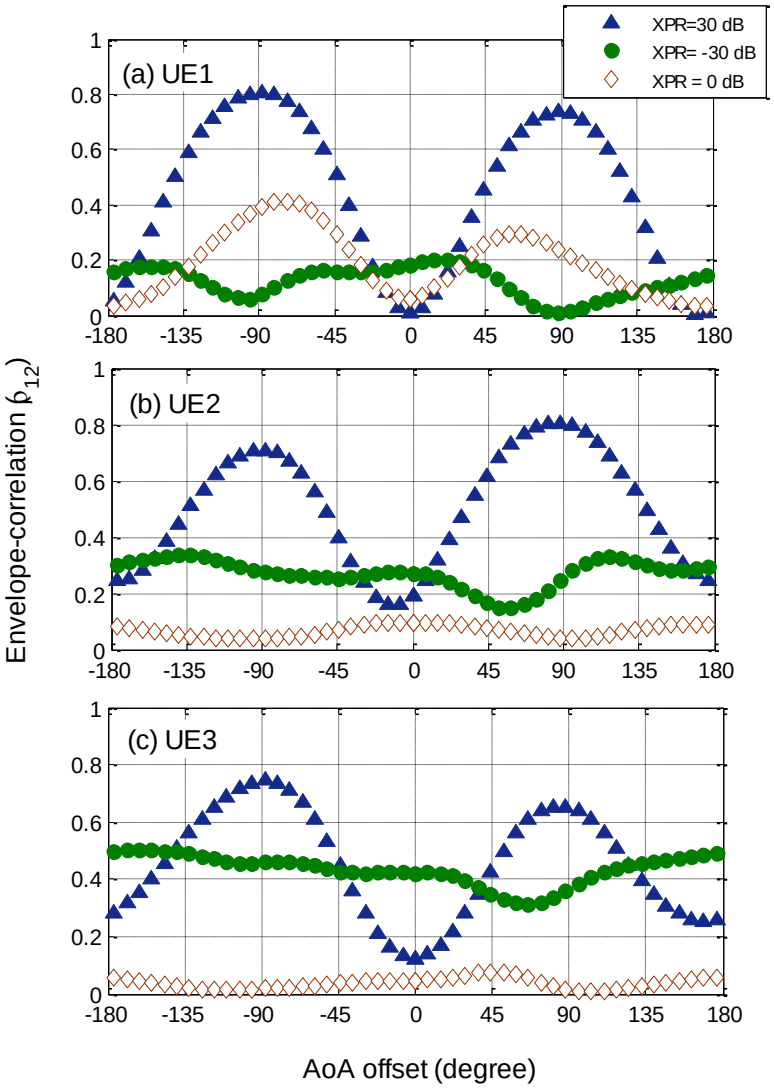

Figure 4.3 Pattern correlations with respect to Δ_{AoA}={-180:180} and XPR for (a) UE1 (S21 = - 4 dB), (b) UE2 (S21 = - 10 dB), (c) UE3 (S21 = - 16 dB)

4.3 Measurement campaign in live network

4.3.1 Live network environments

The field trials are conducted in two different areas in the city of Ottawa, Canada where the former Nortel Networks is located. This work is the part of LTE interoperability development test activities between the former Nortel Networks and LG Electronics. Figure 4.4 shows test routes of LOS and NLOS channels in Ottawa. LOS route is a local drive way crossing a highway in the middle. It has a typical suburb landscape. The LOS component of the channel is the strongest on the hill side, where the route is crossing the highway. Note that NLOS route in Aspan area is a typical residential area with a few high storied buildings.

Figure 4.5 shows network coverage simulation results for both areas when all the cells in the area are activated. The simulation results were provided by former Nortel Networks. This shows the impacted carrier to noise ratios at each location in space. The LOS route is in the direction of the 2nd sector of L6. NLOS route is in the coverage of the sector facing the East. The coverage map suggests that the LOS and NLOS routes are chosen correctly.

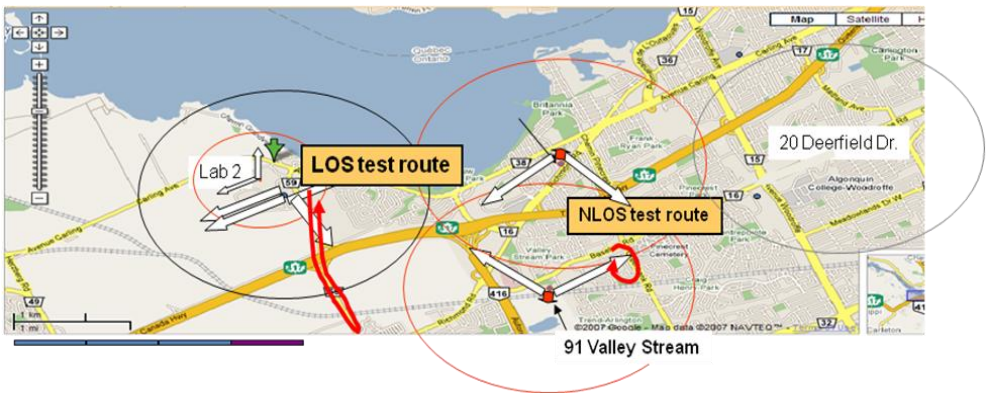

Figure 4.4 Field test routes of LOS and NLOS radio channel environments. LOS route is the long red arrow on the left, and NLOS route is the red circled route on the bottom right

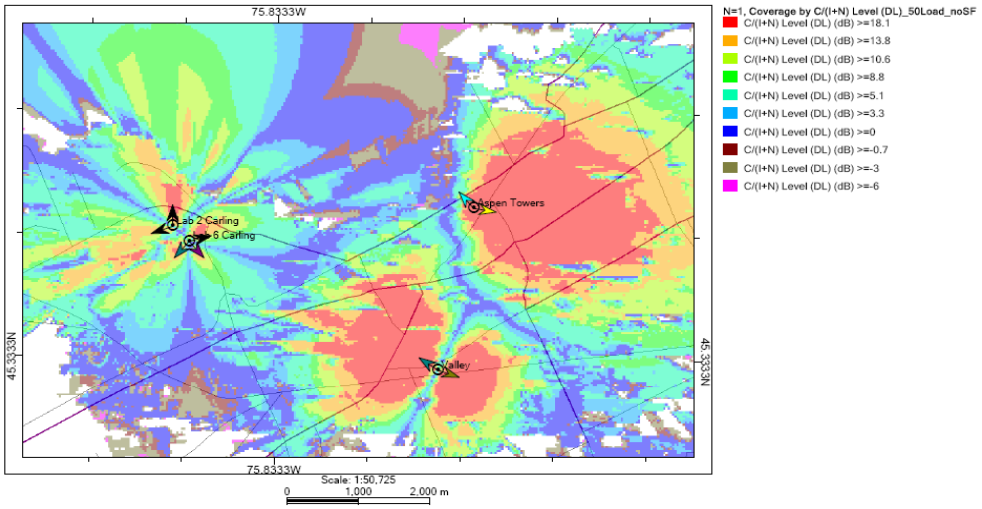

Figure 4.5 Network coverage simulation results of areas for NLOS and LOS routes.

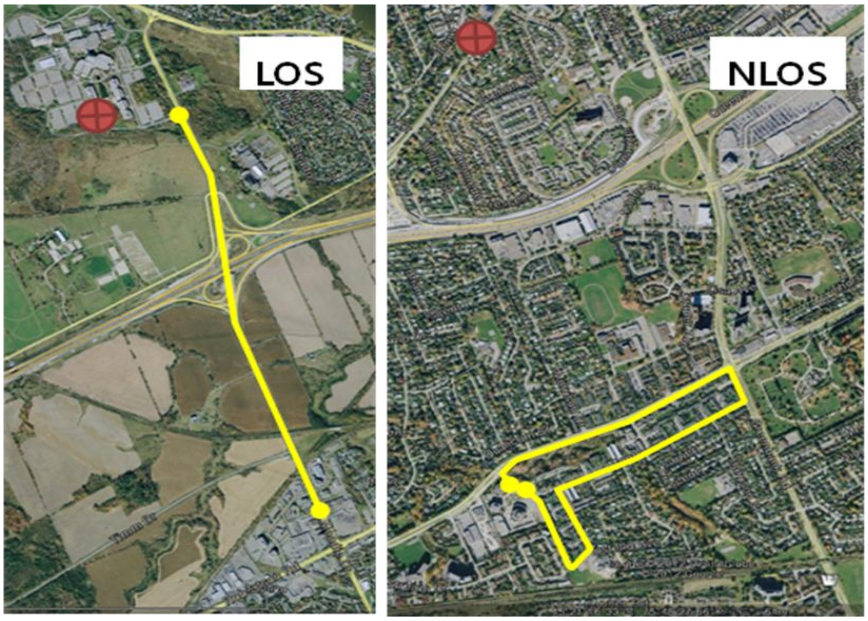

Figure 4.6 Test drive routes for LOS (left) and NLOS (right) in Ottawa, Canada.

It is observed that the field distribution for the 2nd sector of L6 in LOS route is highly directive suggesting the LOS route is properly chosen. In addition, the field distribution created by the east sector of Aspen tower was very uniform, where rich scattering environments were expected.

Figure 4.6 shows the satellite view of test routes for LOS and NLOS environments captured from the Google Earth. The location of BS on each route is marked with red circles on the pictures, and the test routes are visualized with yellow lines. During drive tests, the network is forced to schedule only TM3, the open-loop spatial multiplexing, and rank2 performance, whereas single UE scenario is considered by the network. The environments are noise limited because only single cell is turned-on, which eliminate any impacts from interferences and any throughput disruptions caused by inter-cell handovers. A dedicated file server was used for transferring UDP packets in the downlink to isolate additional network delays in TCP/IP packets.

Table 4.2 shows a summary of LTE link parameters used for the tests. During the driving test, dipole antennas and prototype antennas were mounted on the roof of van, and were connected to a LTE trial UE platform via RF cables. The driving speed was mostly kept around 60 kmh in LOS route and 30 kmh in NLOS route.

4.3.2 Channel statistics of live networks

Figure 4.7 shows cumulative distribution function (CDF) for measured Reference Signal Received Power (RSRP) reported by the UE with each of antenna under evaluation. RSRP is defined for cell specific signal strength, and separately defined to rank the cells mainly for handover purpose. The power of RSRP is defined per reference carrier and it should be compensated by multiplying the number of subcarriers over the system bandwidth. The conversion can be done easily by adding 10log(600) or 27.8

dB to the measured RSRP - that gives us Received Signal Strength Indicator (RSSI). However, the RSSI is not available from the diagnostics monitoring program used for the measurements; therefore we compare the antenna performance with RSRP.

In case of LOS route, all of dipole antennas and UE1 are tested and under NLOS route, all antennas including UE2 and UE3 are evaluated From the RSRP measurement results in LOS route, we can have information on the power loss or the effective gain for each antenna under test at given signal conditions. As expected, the largest power loss is observed for UE1 and VV-0.25λ due to the gain degradation caused by the mutual coupling effects. The RSRP results observed in NLOS route clearly show the difference of antenna gains between AUTs because AoAs are more diverse than in LOS route. However, the signal strength in NLOS route is around 15 dB smaller than in LOS route when compared at 0.8 of CDF.

Table 4. 2 Link parameters for field measurements

	LOS	NLOS
System bandwidth	10 MHz (Band 4)	
Number of subcarriers	600 (15 kHz sub-carrier separation)	
BS antenna configuration	Slanted dual polarized antenna (+45/-45 degrees)	
PDSCH spatial transmission mode	Forced to TM3	
Number of Tx/Rx antennas	2, 2	
UE speed	60 kmh	30 kmh
Route length	5.4 km	4.8 km

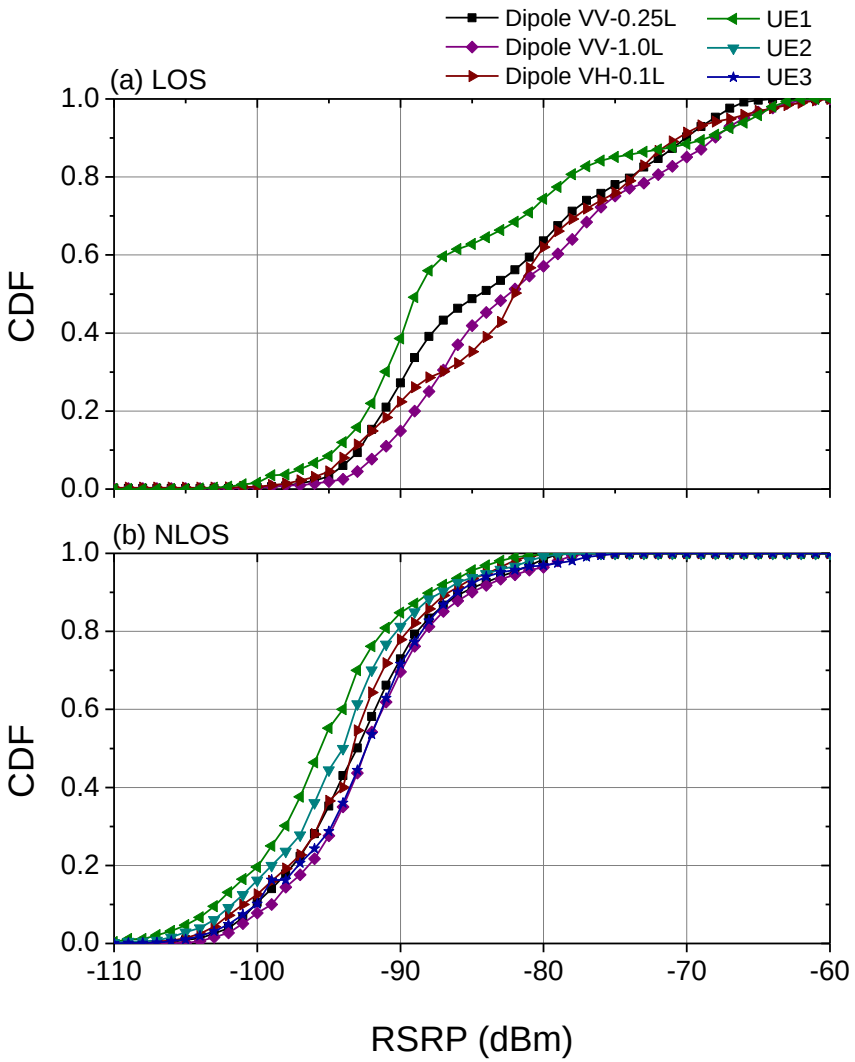

Figure 4.7 CDFs as a function of RSRP measured by each AUT for (a) LOS route, and (b) NLOS route.

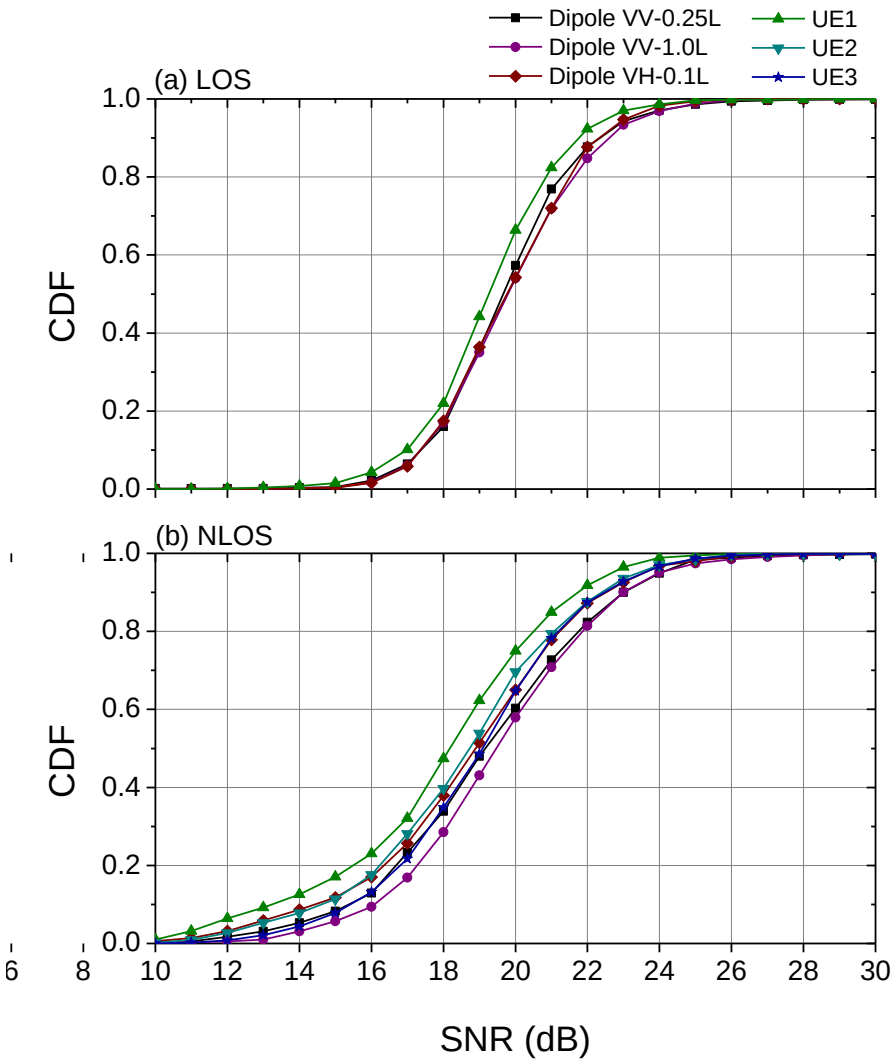

Figure 4.8 CDFs as a function of SNR measured by each antenna under test for (a) LOS route, and (b) NLOS route

Figure 4.8 shows CDFs as a function of SNR for LOS and NLOS routes. There are no significant differences in SNR performance between antennas in LOS route except for UE1. This would mean that the signal strength in LOS route is sufficient so that the UE experienced only a small SNR drops due to the power loss at the antenna. Only the UE1 experiences noticeable SNR degradation due to the power loss at the antenna. On the

other hand, in NLOS route, substantial differences in SNR performance between antennas are observed. This would mean that the power loss in the antennas started to impact on SNR in NLOS route. In the mid SNR range, the prototype UE1 and UE2 experience 1~1.5 dB of SNR degradation compared to the best performing antenna, VV-1.0λ. This confirms that the environment is noise limited system.

Figure 4.9 shows CDFs as a function of the channel correlation measured by the UE based on *Eq*.1.8 and *Eq*.1.9. In LOS route, antennas show correlation properties under the typical LOS channel condition as seen in the figure 3.12 in section 3.5.1, which shows measured power correlation properties of AUTs under LOS channel by using MIMO OTA system. i.e., co-polarized dipole array show extremely high correlation regardless of the inter-element spacing, and the dual polarized dipole array showed substantially low correlation even at highly coherent channel characteristics. It is observed that at least 80% of the correlations are measured below 0.2. On the other hand, the co-polarized dipole antennas showed 80% of measured correlation below 95% of CDF. It should be noted that the UE1 shows similar correlation performance as the dual polarized dipole antenna, which is consistent results observed in section 3.5.1 in a sense that the UE antenna has dual-polarized characteristics. These correlation properties in LOS channel are similar to the results obtained from MIMO OTA system discussed in section 3.5.1.

For NLOS route, the correlation figures for co-polarized antennas are reduced particularly for VV-1.0λ due to the enriched scattering in the radio channels. However, it still shows fairly high correlation figures than it supposed to show under NLOS channel condition. Recall that the co-polarized dipole array shows around 0.1 of correlation at an inter-element spacing of 0.7λ as shown in the figure 3.12 in section 3.51. This means that

there exist substantial amount of LOS component in the radio channel even I name the route as NLOS.

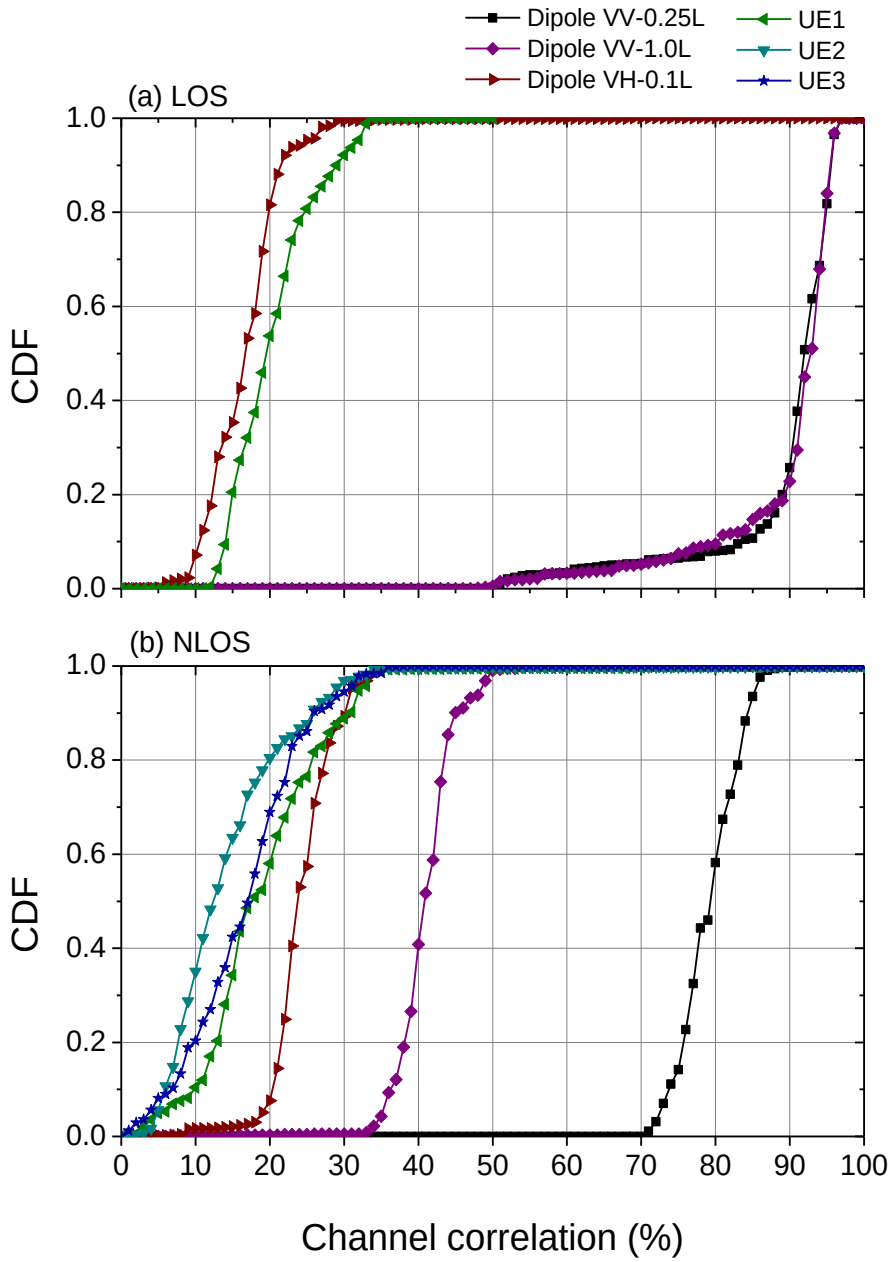

Figure 4. 9 CDFs as a function of channel correlation measured by each antenna under test for (a) LOS route

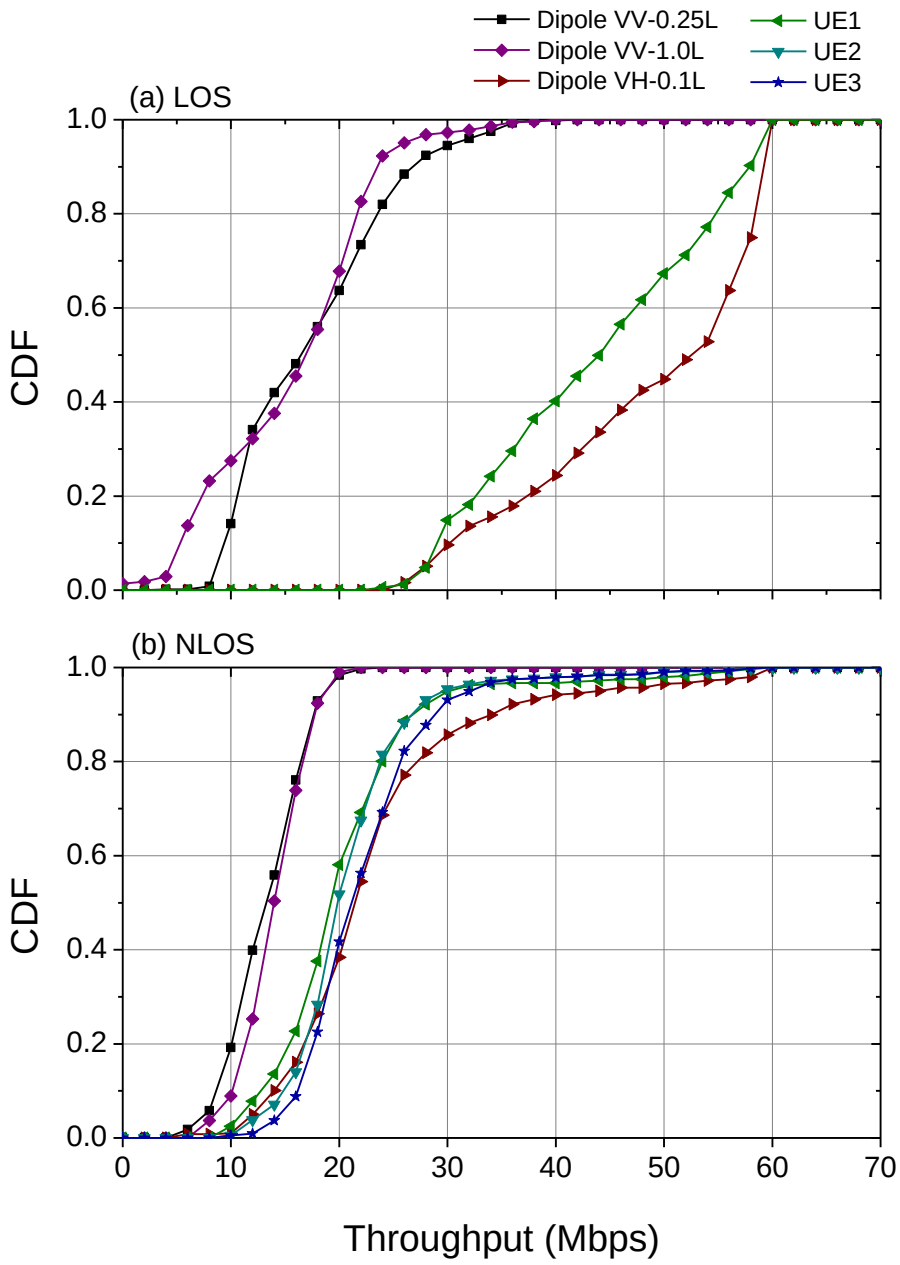

Figure 4. 10 CDFs as a function of PDSCH throughput measured by each antenna under test for (a) LOS route, and (b) NLOS route

Figure 4.10 shows CDFs of measured throughput for AUTs in both routes. As expected, the co-polarized dipole antennas showed lower throughput performance in both areas, especially in LOS route. It is found from the downlink scheduling information that the co-polarized dipole antenna array is mostly scheduled with the TM2 due to unacceptable high correlation. It is clear from the throughput results in both routes that co-polarized dipole array experience more throughput degradation as LOS components are enhanced. However, the dual-polarized dipole array and UE antenna show significant throughput enhancement in LOS channel.

When we compare the performance of UE antennas to that of dual-polarized dipole array, there is no such a large throughput performance gap in both areas. This would mean that the UE antennas have the dual-polarization characteristics.

4.3.3 Summary of the measurement results in live network

Figure 4.11 shows averaged throughput and correlation over the LOS route for the AUTs. Comparing the prototype UE antennas with the VH-0.1λ dipole antenna, the UE antennas show around 20% smaller throughput. Such differences are caused by higher correlation of UE antennas; VH-0.1λ showed at least 30% smaller correlation properties than the UE antennas. It is clear from figure 4.11 that the throughput performance of AUTs in LOS channel has a large dependency on the correlation between antennas. Such dependency becomes smaller in NLOS channel and the antenna gain involves in the throughput performance when we compare the dual-polarized dipole array and the UE antennas in figure 4.12.

It should be noted that the co-polarized dipole antenna array shows similar Rx correlation regardless of the inter-element spacing in both areas indicating the channel properties in NLOS route is also coherent.

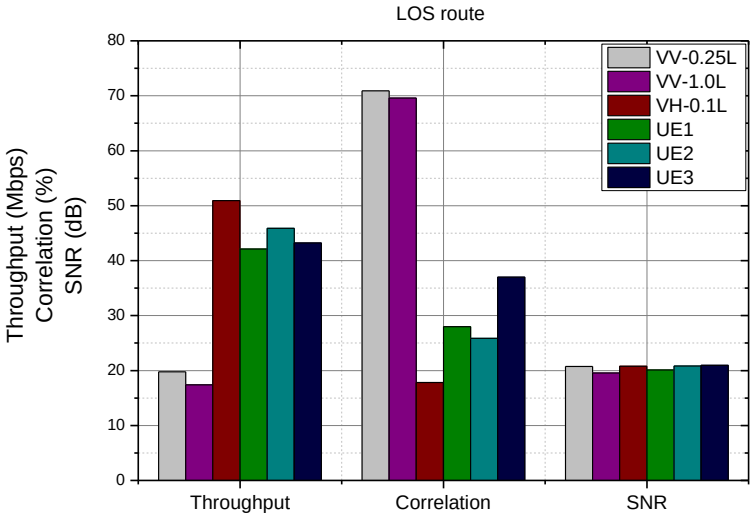

Figure 4.11 Averaged throughput, correlations, and SNR measured in LOS route

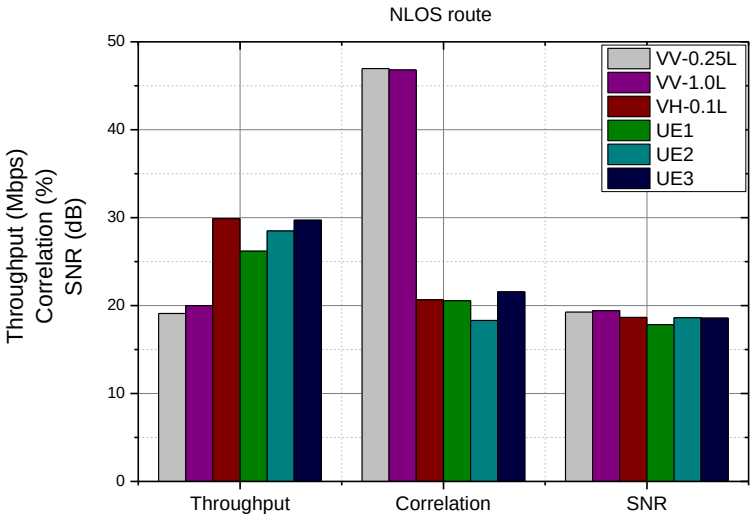

Figure 4.12 Averaged throughput, correlations, and SNR measured in NLOS route

4.4 Measurement campaign in an Indoor environment

The conclusion achieved from the two measurement campaigns in NLOS and LOS routes in the live network showed LOS channel characteristics. Thus, it is important to compare each AUT under indoor NLOS indoor channel environment in order to understand the best diversity scheme under real NLOS channel.

4.4.1 Indoor environment

Throughput performance measurements are conducted in an indoor channel environment to evaluate all antennas under discussion.

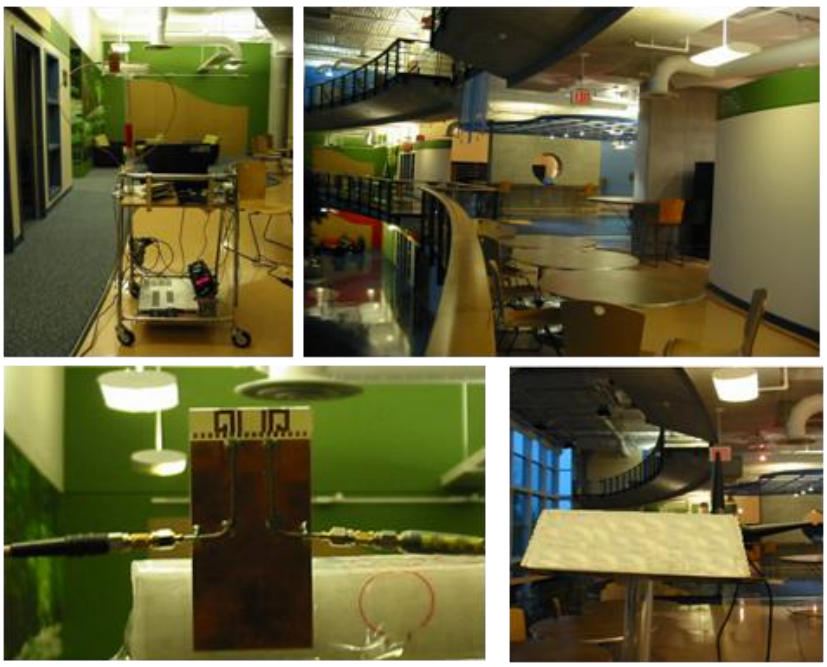

Figure 4.13 Indoor test environment (Top right picture), LTE UE prototype modem platform (Top left picture), Prototype UE form factor antenna (Bottom left picture), VH-0.1λ Dipole antenna (Bottom right picture)

The test location is 2nd floor of a 3 storied building with a large open foyer in each floor. There is a large glass wall on the side of the building and there are BS antennas on the roof of the adjacent building. The measurement route is chosen in such a way that the AUTs experience rich scattering channel conditions as visualized in figure 4.14.

The length of route is around 50 meters and it took around 2 minutes by walk to complete a round trip. Each AUT is measured three times over the test route and then the results are averaged in order to collect more reliable data. Measurements are conducted while the antennas under tests are mounted on a cart using an electromagnetically neutral pole as shown in the figure 4.13.

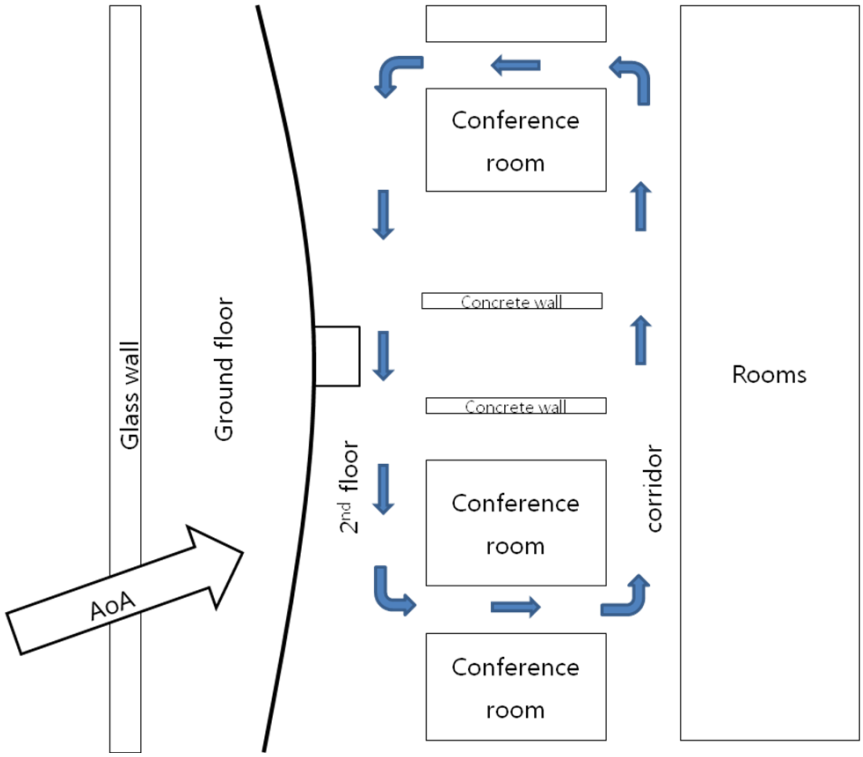

Figure 4.14 Sketched test plan for indoor measurements

4.4.1 Summary of the measurement results in an indoor environment

Figure 4.15 shows average throughputs and Rx correlation properties for all AUTs. Comparing with the results obtained from the live network, following observations can be made:

- *It can be concluded that the performance of spatial diversity scheme became evident in case of indoor environment from the fact that the correlation properties of co-polarized dipole array, VV-0.25λ and VV-0.1λ dropped significantly.*
- *The performance gap between good antennas and bad antennas are reduced due to the rich scattered channel characteristics.*
- *UE1 showed around 10% lower throughput than UE3 even the correlation properties are slightly lower than UE3 indicating that that the power loss in the antenna become more important in the indoor NLOS environments.*

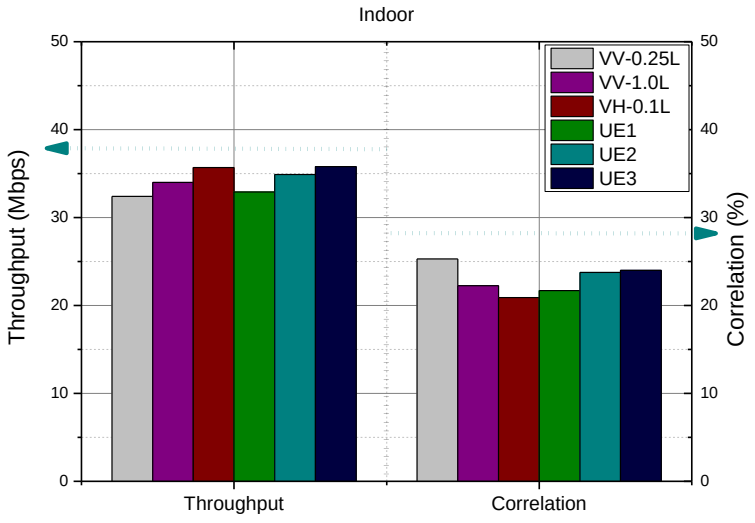

Figure 4.15 Average throughputs, correlation properties for all AUTs under an indoor environment

4.5 Conclusions

In this chapter, spatial, polarization diversity and form factor antennas are verified in LOS, NLOS, and indoor NLOS radio channel conditions. Based on the results achieved the measurement campaigns, following conclusions can be reached.

- *LOS channel conditions should be considered when designing antenna for MIMO capable handsets. The best performing diversity scheme in LOS channel condition is the polarization diversity.*
- *UE antennas have dual-polarization characteristics in a sense that there are substantial H-pol gains as well as V-pol.*
- *UE antennas performed better than co-polarized dipole array at all times, and also showed comparable throughput performance with dual-polarized dipole array.*
- *Measurement results through field trials proved that throughput performance ranks and correlation properties of AUTs measured in MIMO OTA system are well matched to those observed in the live network.*

CHAPTER 5

Performance comparison of diversity schemes in a commercial live network

5.1 Background

In chapter 4, performance comparisons are conducted for spatial, polarization diversity and form factor antennas are verified in a LTE trial network,-single cell/single UE scenario, a noise limited system, and the network is forced to schedule only the TM3. In such a trial network, the comparison works are relatively straight forward because less non-ideal factors exist. However, in the commercial networks, there are a number of factors limiting the throughput performance of the DUTs, which are co-channel interferences from the adjacent cells, inter-cell hand over, rank adaptation between transmission modes.

In this study, evaluation of the MIMO throughput performance of AUTs in a LTE commercial network is conducted through field measurements. The selected measurement routes for this study are in two different cities in U.S with strong LOS characteristics. Similar as in chapter 4, three types of AUTs are tested, co-polarized dipole antenna with different inter-element spacing, and three types of UE antennas are designed for a selected LTE smart phone operating in 700 MHz band where the antenna design has been always challenging due to long wavelength compared to phone size. Two of UE's antennas are identical which was evaluated in chapter 3.

The measurement campaigns in the live network are designed to investigate how the antenna diversity schemes may impact the MIMO

throughput performance under NLOS and LOS channel conditions. It is also discussed that the comparison between the results from the field measurement campaigns and experiments results in the MIMO OTA system.

5.2 Antenna performance

In table 5.1, antenna characteristics of AUTs are summarized. There are three kinds of dipole antenna arrays and three types of UE antennas in the table. As mentioned, UE2 and UE3 are the same AUTs evaluated in chapter 3. UE1 is a new antenna design with very high pattern correlation. Note that the XPD of ANT1 for UE1 is much smaller compared to the other UEs, which means that the ANT1 is strongly V-polarized antenna. ANT2 of UE1 is also a V-polarized antenna with small H-polarization characteristics. Antennas of UE2 have similar gains in both polarizations showing enhanced H-polarization gain for both antenna branches. UE3 show more enhanced H-polarization gain especially for the ANT2 at the cost of the total gain.

Table 5. 1 Antenna parameters

Antenna			Gain (dBi)	Directivity (dB)	XPD (dB)	Imbalance (dB)	Envelope correlation
Dipole	VV-0.1λ	ANT1	-1.5	NA	-19	< 0.5	0.59
		ANT2					
	VV-0.7λ	ANT1					0.05
		ANT2					
	V-H 0.1λ	ANT1					0.02
		ANT2			19		
UE1		ANT1	-7.2	1.2	-14.7	2.1	0.7
		ANT2	-9.3	2.1	-6.8		
UE 2		ANT1	-5.7	1.3	-3.9	3.0	0.62
		ANT2	-8.7	2.0	1.0		
UE 3		ANT1	-2.9	1.4	-2.5	12.8	0.10
		ANT2	-15.8	2.6	6.8		

5.3 Live network environments

The field tests are carried out in two different cities in North America. The test routes are local freeways in suburban areas, where there are one or two storied houses and business buildings besides on the freeway as exampled in Figure 5.1. Area-A is a local freeway crossing a typical residential areas near Irvine, U.S. There are around 3 meters height sound barriers on both sides of freeway almost all the way between the start and the return point of the test drives. These sound barriers could increase the degree of scattering of the radio channels. The test route in area-B is also a freeway near Dallas, U.S. There are no such sound barriers on either side of the freeway. There are a few high storied business buildings along the route but the density was low. There are also a few large open spaces without any buildings or large parking lots with no buildings around in the middle of the route, and this might increase LOS component in the radio channel.

As shown in picture 5.1, the terrines of both test routes are mostly flat with smooth up/down hills along the routes. In the bottom figures, there are dots along the freeways showing the GPS trances logged during the driving tests. Area-A is rather a typical sub-urban area with many buildings whereas area-B has less buildings or other scattering objects than in area-A.

The networks deployed in two areas have different BS scheduler behaviors which determine the transmission mode of the UE depending on CQI (Channel Quality Index), RI (Rank Indicator), and PMI (Preferred Matrix Indicator) reports by the UEs. Table 5.2 shows summary of key parameters of in the test areas where the measurements have conducted.

Figure 5.1 Pictures on freeways in the test route in Area-A (Left) and in Area-B (Right). Terrine was mostly flat along the route.

Table 5.2 Table 5.2 Link parameters for field measurements

	Area-A	Area-B
System bandwidth	10 MHz	
Number of subcarriers	600 (15 kHz sub-carrier separation)	
PDSCH MCS index range	0-28	
HARQ	Enabled	
BS antenna configuration	Slanted dual polarized antenna (+45/-45 degrees)	
PDSCH spatial transmission mode	TM2, TM3 Adaptive rank adaptation	TM2, TM4 adaptive rank adaptation
Number of Tx/Rx antennas	2, 2	2, 2
Channel characteristics	Near LOS	Mixed LOS and NLOS
UE speed	100 kmh	100 kmh
Route length	50 km	30 km

In the commercial networks with multi-cell, there is large degree of interference due to the neighbor cells. Hand over between cells is enabled during the driving tests. The downlink data transferred with FTP (File Transfer Protocol) from a dedicated FTP server.

AMC, HARQ, and rank adaptation are enabled by the networks in the test routes. The most prominent difference between the networks in the two test areas is that the MIMO selection schemes supported by the networks. In area-A, the BS support the adaptive rank adaptation only between transmission mode 2 (TM2) and TM3 whereas the BS in Area-B select between TM2 and TM4. In other words, network in area-A the network never selects the closed-loop spatial multiplexing mode and the network in area-B never selects the open-loop spatial multiplexing mode. Such difference of behaviors of schedulers in each area impacted on the test results. Table 4.3 is description for each transmission mode [49].

Table 5. 3 Transmission mode supported by the network [49]

TM node	Description
Transmission Mode 2	Transmit diversity
Transmission Mode 3	Open-loop spatial multiplexing
Transmission Mode 4	Closed-loop spatial multiplexing

During the driving test, dipole antennas were mounted on the roof and the UEs were inside of van as shown in Figure 5.2. The dipole antennas were connected to a LTE smart phone via RF cables, and UE1~3 were mounted on the window inside van. Potentially, UE might experience more scattering than the dipole antenna as well as slight signal strength degradation due to the effect of placing inside van. This could be verified from the measurement results.

The driving speed is mostly kept around 100 kmph (~60 mph) for all tests and the length of the route is approximately 50 km for Area-A and 30 km for Area-B.

The measurement reports at the UE were logged through a USB cable for post-processing purpose in case of any disruptions occurred due to unexpected situations encountered such as traffic.

Figure 5.3 shows the test route in each area where the field tests are carried out. Measured RSRP and SINR (Signal-to-Interference plus Noise Ratio) are plotted on the map in order to compare the radio signal conditions in the test routes. As shown in the figure 5.3, the signal conditions in both areas are strong signal strength areas where the probability for SINR > 20 dB are 43% for area-A and 38% for area-B, respectively. It should be note that there are only 16% probability for SINR <10 dB in area-A, and 23% for area-B. This means that the signal qualities of both areas are sufficient for performance tests.

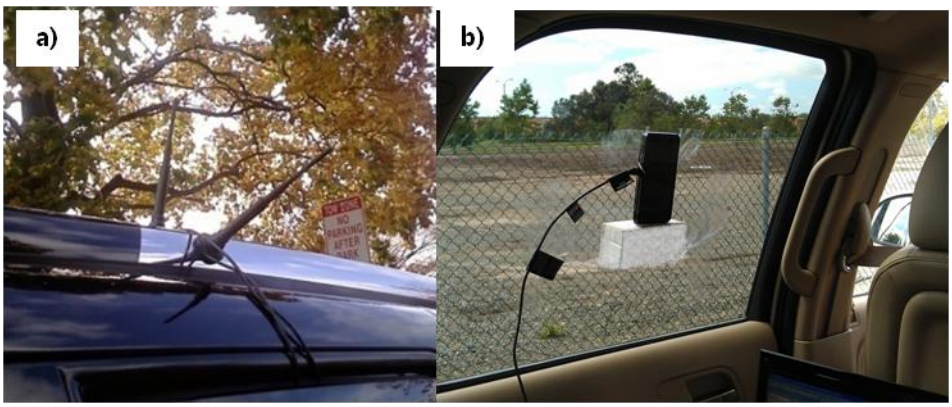

Figure 5.2 a) Dipole antenna mounting setup on roof of van by using magnetic stone on the bottom of dipole antennas. Dipole antennas are connected through a LTE DUT by using a pair of RF cables. b) LTE DUT mounted on the window inside of van

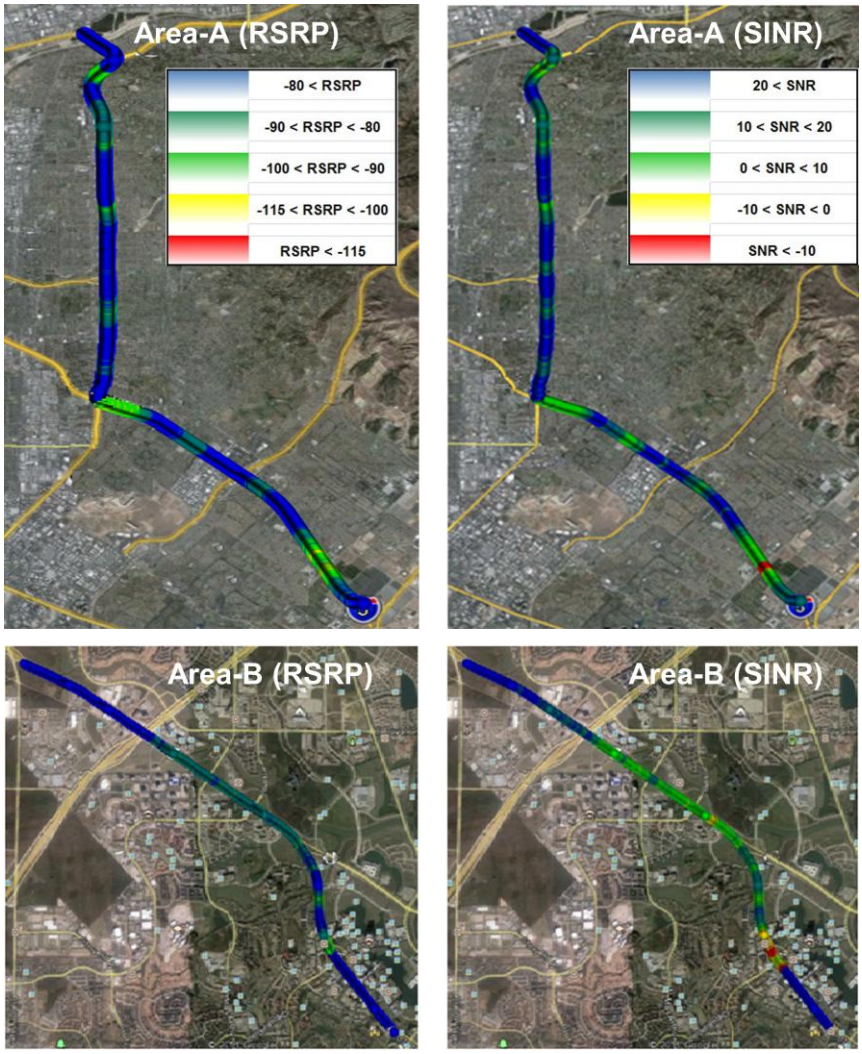

Figure 5. 3 Field test routes showing measured RSRP and SINR along the test routes. Top left/right: RSRP/SINR for Area-A, Bottom left/right: RSRP/SINR for Area-B.

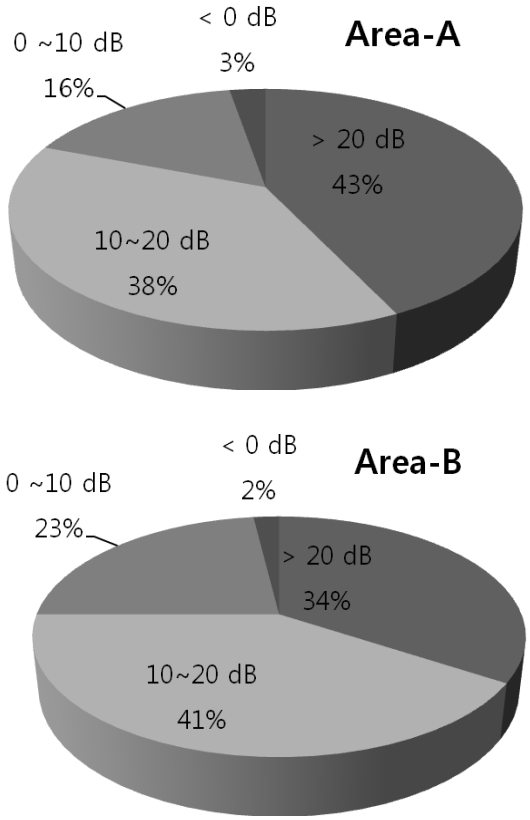

Figure 5. 4 SINR ratios for test route in each area collected by dipole antennas. Top: area-A, Bottom: area-B

5.3 Channel statistics

In all measurements all antennas are tested except for VH-0.1λ in area-B. Figure 5.5 shows CDF as a function of measured RSRP for all AUTs over both test routes. RSRP values for dipole array include 1.5 meter-RF cable loss, which is around 1.4 dB. The received power from VV-0.1λ is relatively lower than the other dipole configurations due to the mutual coupling effects. Note that UE1 and 2 receive around 4~5 dB less power than VV-0.1λ dipole. As shown in the Figure 5.5, the RSRP measurement results followed the primary antenna gain of UE. This means that the gain imbalance do not affect the RSRP reported by the UEs. This explains UE3

show better RSRP than other UEs even it has 13 dB of gain imbalance. UE1 showed the lowest distribution of RSRP compared to the UE antennas by around 3 dB due to smaller primary antenna gain. It should be note that VV-0.7λ showed the highest RSRP distributions than other antennas in both areas.

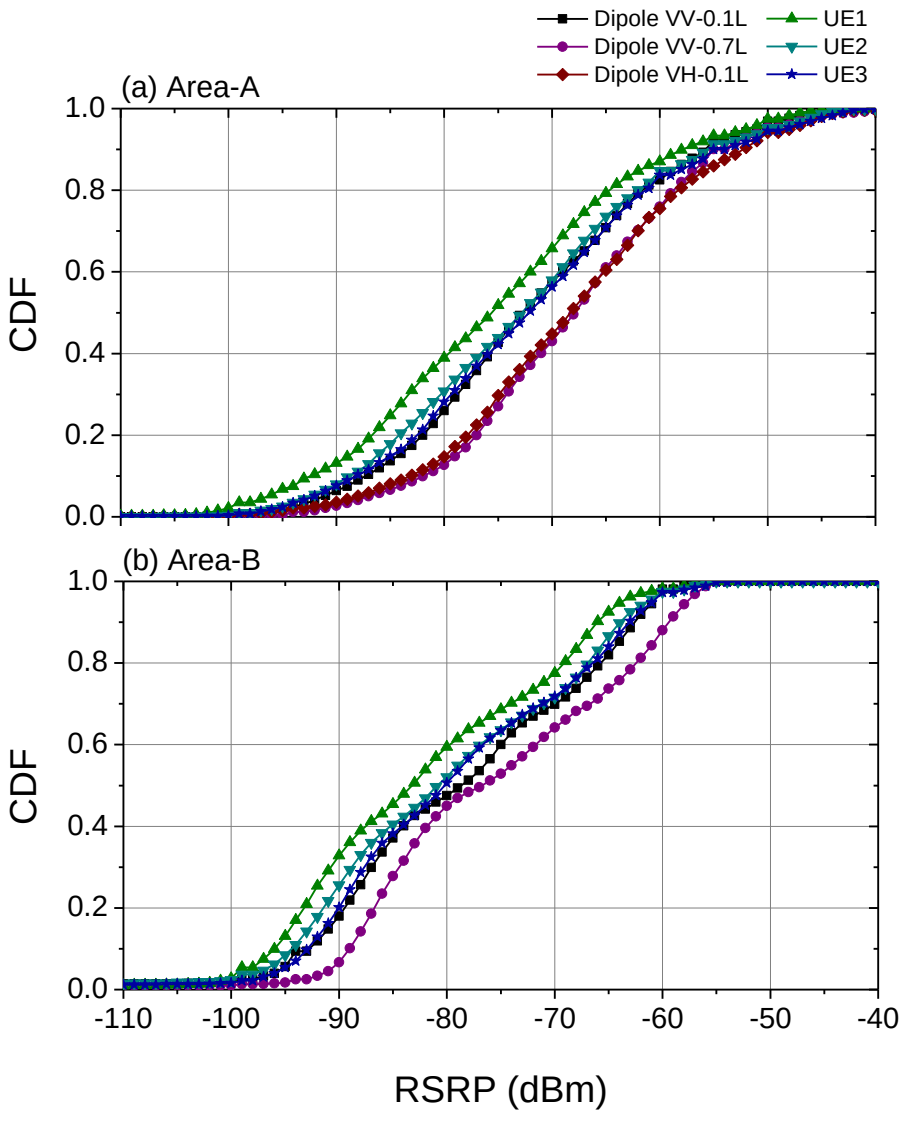

Figure 5. 5 CDFs with respect to measured RSRP for a): area-A and, b): Area-B obtained with each antenna

When we compare the signal distribution properties of the two test routes, area-A showed wider distributions at signal strength higher than -60 dBm and this is consistent with figure 5.4, where the ratio at SINR > 20 dB was 9% larger in area-A than in area-B. On the other hand, area-B show larger distribution in the lower signal strength ranges compared with area-A.

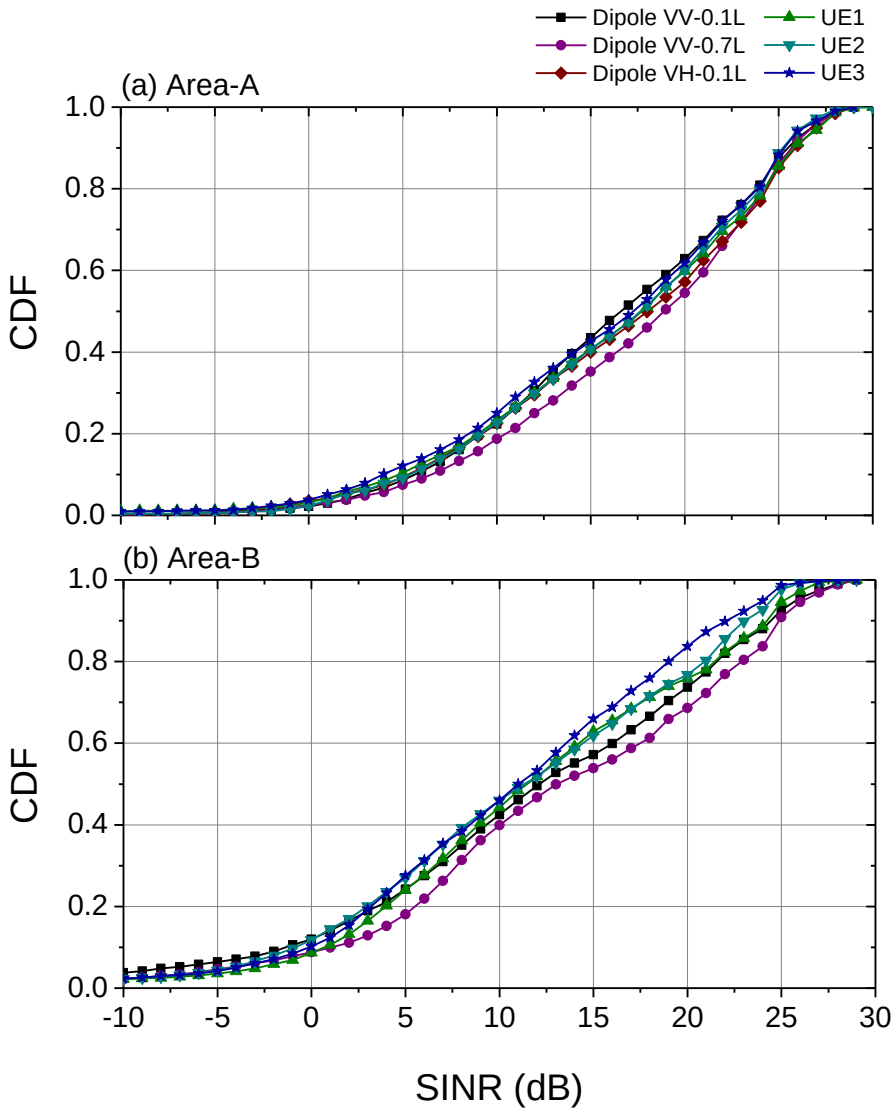

Figure 5.6 CDFs as a function of measured SINR for a): area-A and, b): Area-B obtained with each antenna

In Figure 5.6, SINR distributions over two test routes are presented. The gap between antennas observed in RSRP results is much reduced in SINR distributions. In interference limited system, the impact of antenna gain on SINR can be reduced depending on the degree of interference levels. When we compare the SINR distributions in both areas, the SINR performance differences between antennas are more clearly observed in area-B than in area-A. It can be explained from the fact that the degree of interference level in area-A is larger than in area-B. This can be further explained by comparing SINR distributions at SINR=0 point for both areas, of which point can be regarded as the cell edge. The cumulative probability at SINR=0 is at least 3.5% in area-A, and 12% in area-B meaning that the interference level in area-A is higher than that in area-B. It is also clear that UE3 showed substantial SINR drop due to the large gain imbalance between two antenna branches. In case of dipole antenna, it is noticeable that VV-0.7λ showed best SINR performance in both areas.

In Figure 4.8, the relation of RSRP and SINR over two test routes is further investigated in order to clarify level of interferences in each area. In a lab environment when there are no noise sources, the SINR is defined as *Eq*. 5.1.

$$\mathrm{SINR} = \mathrm{RSRP}_{Serv} + (I + N) \qquad (Eq.5.1)$$

$$\mathrm{I} = \sum_{k} \mathrm{RSRP}_{Neigh}, \quad N = \frac{kTB}{B_C} + NF \qquad (Eq.5.2)$$

Where, $RSRP_{serv}$ is measured RSRP associated with the serving cell, $RSRP_{Neigh}$ is measured RSRP associated that the neighbor cell. *K* is the number of neighboring cells in the cell search list, *kTB* is thermal noise of the UE over system bandwidth, B_C is bandwidth calibration factor between power over system bandwidth and RSRP which is 27.8 dB. *NF* is noise figure of UE. All of the parameters are mostly constant except for $RSRP_{servin}$

and $RSRP_{Neigh}$ in *Eq*. 5.1. Based on *Eq*. 5.1, we can define a lower bound for RSRP as a function of SINR as in Figure 5.7.

The gap between linear fitted line and lower bound defined by *Eq*. 5.1 is SINR degradation due to interferences in test routes. The range of SINR degradation is 18~27 dB indicating interference limited radio environment. In such interference limited radio channel, impact of antenna efficiency on the SINR may not be significant. Similarly the gain imbalance between to antenna branches also would not be significant than in the noise limited system.

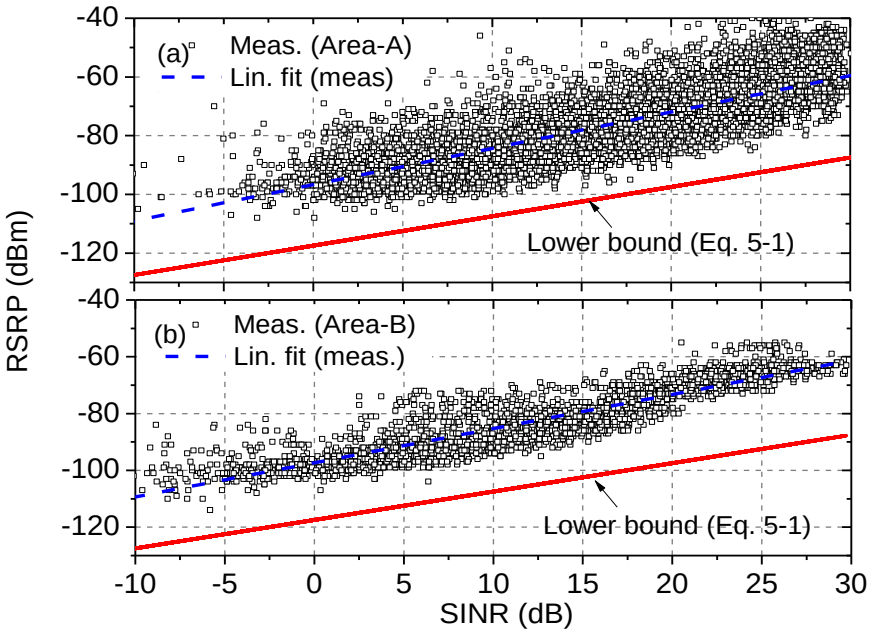

Figure 5. 7 RSRP as a function of SINR for (a) Area-A, for (b) Area-B. Dashed line is linear fit of measurements and solid line is the lower bound by *Eq*. 5.1.

Figure 5.8 shows CDF as a function of Rx correlation measured over both test routes for the AUTs. It is clearly observed in area-A that the correlation of co-polarized dipole antennas showed at least 85% of measured correlations are less than 59% in case of VV-0.1λ of which

pattern correlation coefficient is 59%. 90% of measured correlations were less than 28% in case of VV-0.7λ of which pattern correlation coefficient is 0.05. This explains that there are certain amounts of LOS components over the test route in area-A.

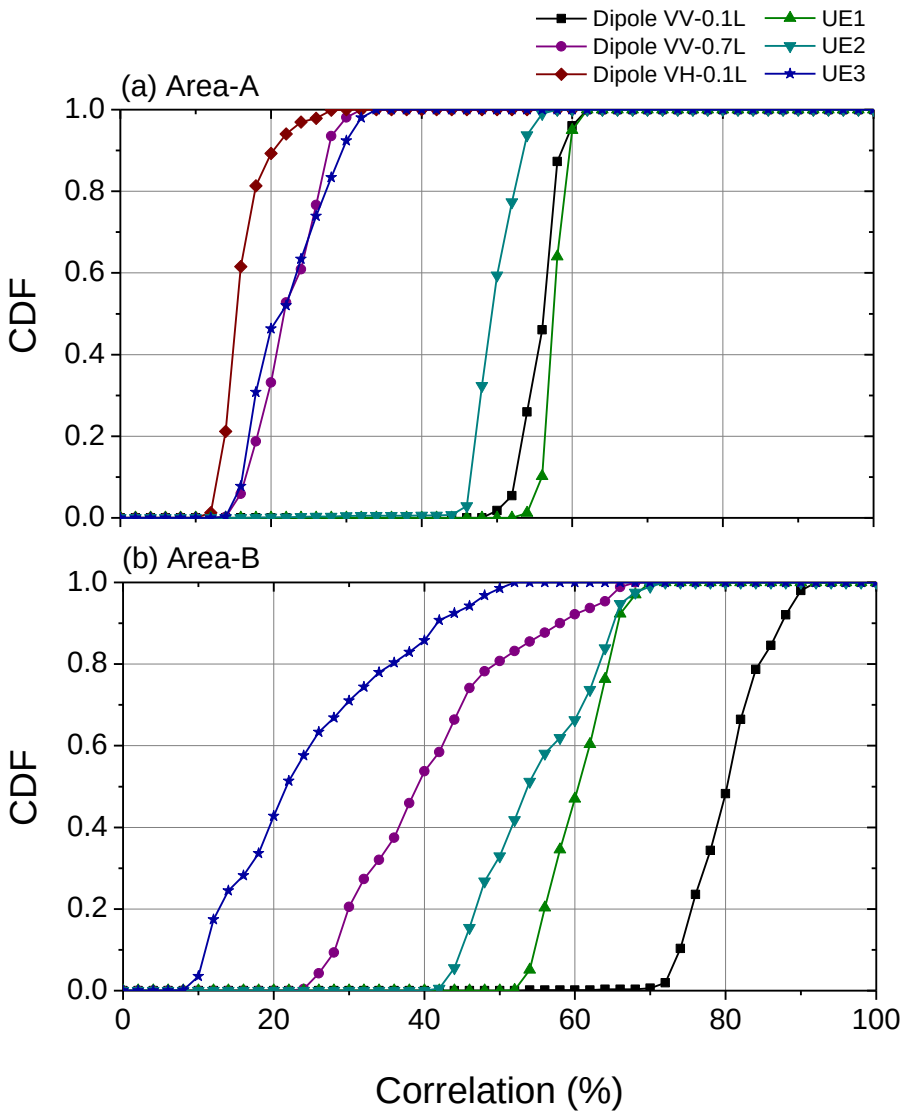

Figure 5. 8 CDFs of measured correlation characteristics over the test route in (a) area-A, and (b) area-B

In area-B, overall slops of CDFs are smaller and this may be caused by the effect of increased distance between transmitter and receiver [50]. It should be noted that only the correlation properties of co-polarized dipole array are increased significantly whereas the UE antennas experience similar correlation properties when we compare the correlation properties of AUTs in both area. As discussed in chapter 4, such effects were caused by LOS components in the radio channels. It can be reached to the fact that the LOS channel components are stronger in area-B than in area-A.

Figure 5.9 shows CDFs of measured throughputs over the test routes in both areas. In area-A, the throughput performance differences between co-polarized dipole array and dual-polarized dipole array is clearly observed similar to the results we observed in LOS route in chapter 4. This would mean that the channel characteristics of area-A is also LOS channel environment. It should be note that the UE3 antenna, which is polarization diversity antenna with very large gain imbalance outperforms than the other two UE antennas. This is consistent result as in the case we observed in the figure 3.15, which show the PDSCH throughput performance comparison of AUTs in MIMO OTA system under strong LOS channel. On the other hand, UE1 show the lowest throughput performance than UE2 and UE3 due to higher correlation. UE2 show slightly better throughput than UE1 thanks to larger horizontal gain than UE1 as we compared in the table 5.1.

Recalling the fact that the networks provide the rank adaptation, the analysis on the throughput results need to be done considering this effect. When we compare the throughput performance AUTs in both areas, the benefit of the closed loop MIMO scheduling is clearly observed. The co-polarized dipole antenna showed significantly lower throughput characteristics in area-A where the network schedules only the open-loop MIMO transmission mode. On the other hand, in area-B, even the LOS characteristics are stronger than in area-A, the throughput performance differences between the co-polarized dipole array and the dual-polarized or

UE antennas are much reduced thanks to the closed-loop MIMO scheduling capability supported by the network in area-B.

It is interesting to compare the UE antenna performance in area-B as we also be able to understand the effect of the closed-loop MIMO scheduling on the throughput performance. Now UE2 show slightly better throughput than UE3 in area-B. Even UE1 shows similar performance as UE3.

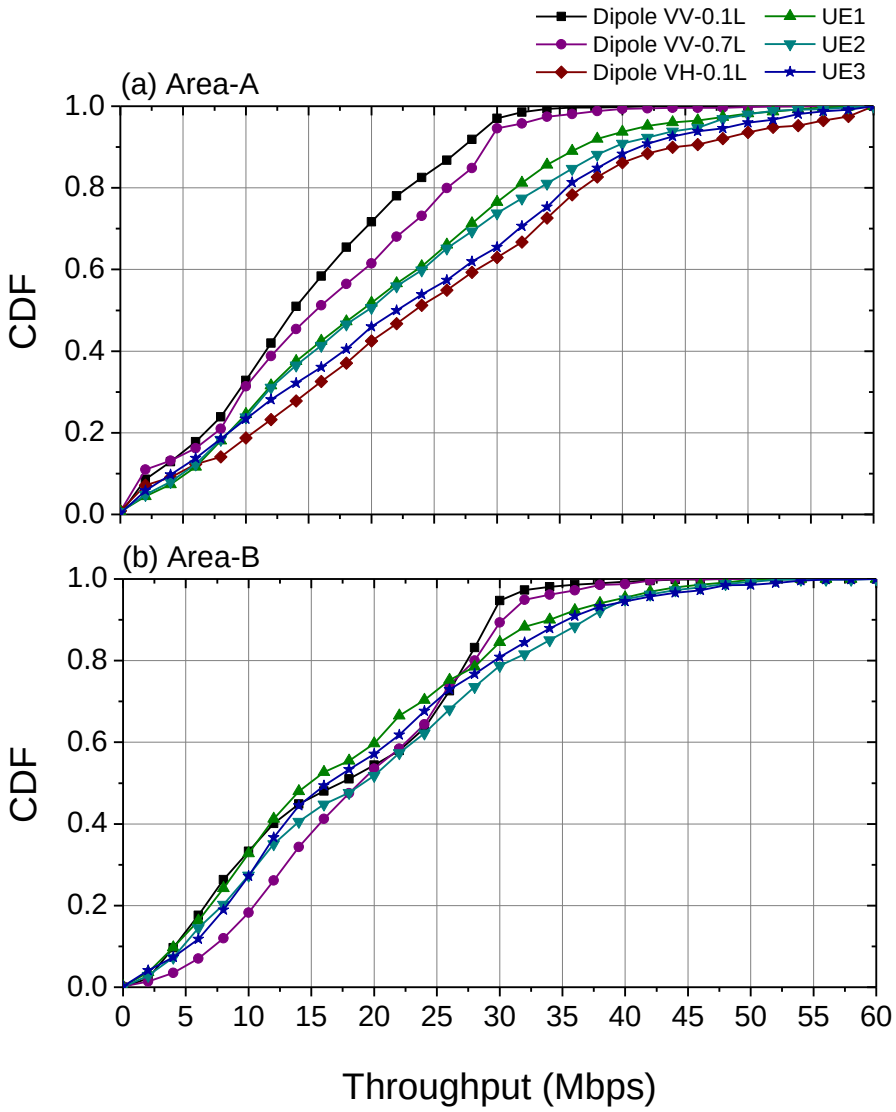

Figure 5.9 CDFs of measured throughput over the test route in (a) area-A, and (b) area-B

The judgment whether the closed-loop MIMO scheduling is beneficial or not can be done by comparing the probabilities of scheduled rank2 ratios experienced by the UEs in both areas. Figure 5.10 shows the ratio of scheduled rank2 ratios for UEs averaged over both test routes. It is clear that the network in area-A selected the rank2 by two to three times more frequently than the network in area-B. Note that the throughput results in area-A showed similar tendencies observed in our previous studies conducted in the trial network in Ottawa, particularly the NLOS route shown in figure 4.10 (b). On the other hand, due to the fact that the scheduler of the network in area-B selected the spatial multiplexing more conservatively, the devices in area-B were operating in the transmission diversity mode more frequently than in area-A. Such behavior of the network reduced the performance differences between bad and good antennas in area-B. It should be noted that the co-polarized dipole antenna almost selected only rank1 at all times because the maximum throughput was almost 32 Mbps, which is the theoretical limit of rank1 through at MCS=28 in case of CFI=2.

Figure 5.11 shows the throughput averaged within the same rank for both of areas. It is interesting to note that there are no remarkable differences in average throughput within the same rank between bad and good UEs. Clearly, the CDFs in figure 5.9 showed that the UE3 showed better throughput performance than the other UEs. This can be explained by the fact that the throughput performance is determined by the factor that how frequently the UEs are able to select the rank2 rather than rank1. Figure 5.10 proofs the fact that the UE3 is scheduled more rank2 in both areas. It should be note that if rank2 ratios are less than 40% as in area-B, the throughput gain will not be significant because rank 1 throughput will be more dominant factor to the total average throughput performance.

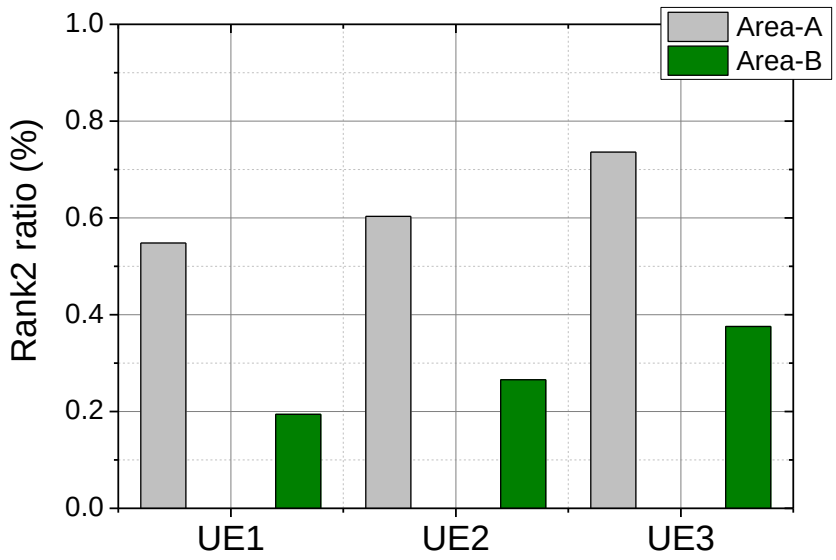

Figure 5.10 Rank2 selection ratio measured over both areas for UE antennas. The information is parsed from the downlink scheduling information logged during the measurements

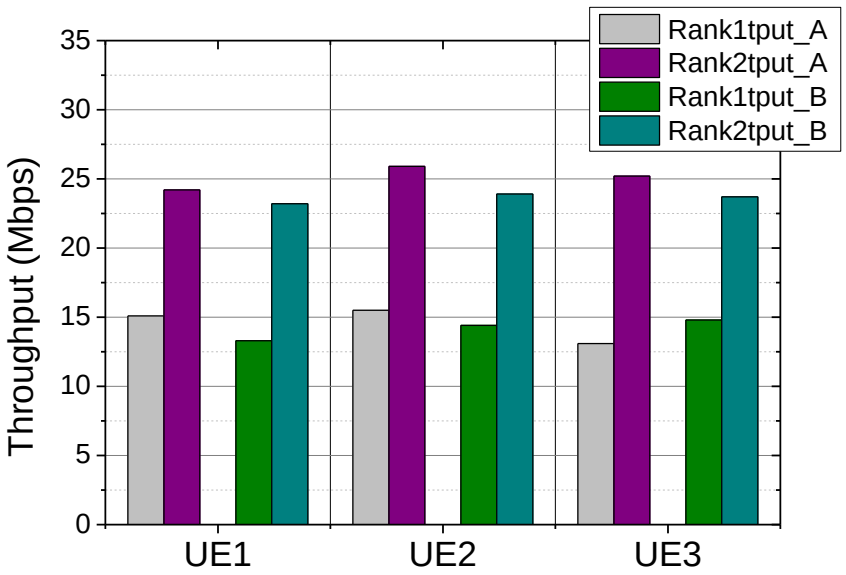

Figure 5. 11 Throughput averaged within the same rank for both of areas for UE antennas. The information is parsed from the downlink scheduling information logged during the measurements

5.4 Conclusions

In previous sections, antenna performance against commercial networks is analyzed based on channel statistics collected by AUTs.

Comparing between the throughput measurement results in the live networks and those in the MIMO OTA system, the following observations can be made:

In area-A against MIMO OTA LOS channel model with TM3 mode

1. *UE3 and VH-0.1λ showed similar throughputs overall. However, this is only true at high SNR ranges in MIMO OTA system with LOS channel model because the gain imbalance does not impact on the throughput only at high SNR range.*

2. *Co-polarized dipole clearly showed low throughput both in the live network and in MIMO OTA system when the radio channel contains LOS components.*

- *In area-B against MIMO OTA LOS channel model for TM2 mode*

3. *When comparing the throughput ranges below 30 Mbps taking into account for TM2, co-polarized dipole antenna showed better throughput than UE antennas in area-B. In MIMO OTA system, co-polarized dipole antenna showed best throughput in LOS channel model for TM2 mode.*

Due to the fact that there are a number of factors that impact on the device performance, isolation of such parameters from the measurement data is very important and non-trivial task, or sometimes it is not even possible. The benefit of MIMO OTA system is that such comparison tests of AUTs in various radio channel conditions can be done in a controlled lab environment with repeatable way. Then it would save a lot of resources and time with no doubt.

REFERENCES

[1] http://www.ic1004.org/.

[2] http://www.cost2100.org/.

[3] Vodafone, Proposed SID revision for study item: Measurement of radiated performance for MIMO and multi-antenna reception for HSPA and LTE terminals, 3GPP TSG-RAN 54, RP-111754, Berlin, Germany, Dec. 6th-9th, 2011.

[4] http://www.ctia.org/.

[5] Kyosti, Pekka, Nuutinen, Jukka-Pekka, Jamsa, Tommi, “MIMO OTA test concept with experimental and simulated verification,”, Proceedings of the Fourth European Conference on Antennas and Propagation (EuCAP), pp. 1-5, 2010.

[6] Karasawa, Y.; Iwai, H., “Modeling of signal envelope correlation of line-of-sight fading with applications to frequency correlation analysis,” IEEE Transactions on Communications, Vol. 42 , Issue: 6, pp. 2201-2203, 1994.

[7] Baum, D.S., Hansen, J., Salo, J., "An interim channel model for beyond-3G systems: extending the 3GPP spatial channel model (SCM)," in Proc. of the 61st IEEE Veh. Technol. Conf. (VTC '05), Stockholm, Sweden, vol. 5, pp. 3132-3136, May 2005.

[8] P. Kyosti et al., IST-4-027756 WINNER II Deliverable 1.1.2. v.1.2, WINNER II Channel Models, IST-WINNER2, Tech. Rep., 2007.

[9] Guidelines for evaluation of radio interface technologies for IMT-Advanced, ITU-R Report M.2135," ITU-R, Tech. Rep., 2008.

[10] R4-101024, Way Forward on MIMO OTA Study Item, NTT DOCOMO, AT&T, Telecom Italia, CMCC, Orange, Vodafone, Nokia, Motorola, LG Electronics, Samsung.

[11] R. Vaughan and J. B. Andersen, Channels, *Propagation and Antennas for Mobile Communications*. The IEE, London, UK, 2003.

[12] S. Laurent, I.P. Klaus, E.M.Preben, “From Antenna Spacings to Theoretical Capacities- Guidelines for Simulating MIMO Systems,” The 13th IEEE Internaltional Symposium on Personal, Indoor and Mobile Radio Communications, 2002, Vol. 2, pp: 587-592.

[13] http://www.info.fundp.ac.be/~lsc/Research/IEEE_80211_HTSG_CMSC/distribution_terms.html.

[14] Measurement of radiated performance for MIMO and multi-antenna reception for HSPA and LTE terminals, 3GPP TR 37.976, v1.5.0, May, 2011.

[15] P. Kyösti, T. Jämsä, and Jukka-Pekka Nuutinen, “Channel Modelling for Multiprobe Over-the-Air MIMO Testing,” International Journal of Antennas and Propagation, Vol. 2012, Article ID 615954, 11 pages, doi:10.1155/2012/615954.

[16] C.Oestges, “Channel correlations and capacity metrics in MIMO dual-polarized Rayleigh and Ricean channels,” IEEE 60th Vehicular Technology Conference, 2004. VTC2004-Fall. Vol. 2, pp. 1453-1457, 2004.

[17] C. Oestges, B. Clerckx, *MIMO Wireless Communications: From Channel Models to Space-Time Code Design*. Academic Press, 2007.

[18] Lusina, P.; Kohandani, F., “Analysis of MIMO Channel Capacity Dependence on Antenna Geometry and Environmental Parameters,” IEEE 68th Vehicular Technology Conference, pp. 1-5, 2008.

[19] Ivrlac, M.T.; Nossek, J.A., “Quantifying diversity and correlation in Rayleigh fading MIMO communication systems,” Proceedings of the 3rd IEEE International Symposium on Signal Processing and Information Technology, pp. 158-161, 2003.

[20] Pedersen, K.I. Mogensen, P.E., Fleury, B.H., “Spatial channel characteristics in outdoor environments and their impact on BS antenna system performance,” IEEE Vehicular Technology Conference, Vol. 2, pp. 719-723, 1998.

[21] Kolmonen, V.-M.; Kermoal, J.-P.; Vainikainen, P., "Comparison of Correlation-Based and Ray-Based Radio MIMO Channel Models,Personal, Indoor and Mobile Radio Communications," IEEE 17th International Symposium on, pp. 1-5, 2006.

[22] R-114599, "Model Polarization, Power Normalization, and Correlation," Spirent Communications, Elektrobit, Satimo, 3GPP TSG-RAN WG4 OTA Ad-hoc Meeting, Aug, 2011.

[23] 3GPP Technical Report, TS 25.996 V8.0.0, Spatial channel model for Multiple Input Multiple Output (MIMO) simulations.

[24] Blumenstein, J.; Ikuno, J.C.; Prokopec, J.; Rupp, M., "Simulating the long term evolution uplink physical layer," Proceedings of ELMAR, pp. 141-144, 2011

[25] Stephenne, A.; Champagne, B., "Effective multi-path vector channel simulator for antenna array systems," IEEE Transactions on Vehicular Technology, Vol. 49, Issue 6, pp. 2370-2381, 2000.

[26] A. Yamamoto, T. Hayashi, K. Ogawa, K. Olesen, J.O. Nielsen, Naizheng Zheng and G.F. Pedersen, "Outdoor Urban Propagation Experiment of a Handset MIMO Antenna with a Human Phantom Located in a Browsing Stance," IEEE Proc. of 66th Vehicular Technology Conference (VTC 2007), Baltimore, Sept 30-Oct 3, 2007.

[27] Hagerman, B.; Werner, K.; Jin Yang, "MIMO Performance at 700MHz: Field Trials of LTE with Handheld UE," IEEE Vehicular Technology Conference (VTC Fall), 2011.

[28] Azremi, A.A.H.; Haneda, K.; Vainikainen, P., "Site-specific evaluation of a MIMO channel capacity for multi-antenna mobile terminals in proximity to a human hand," Proceedings of the 5th European Conference on Antennas and Propagation (EuCAP), pp, 538-542, 2011.

[29] Test Plan for Mobile Station Over the Air Performance-Method of Measurement for Radiated RF Power and Receiver Performance, Rev. 3.1, Jan. 2011.

[30] Dietrich, C.B., Jr.; Dietze, K.; Nealy, J.R.; Stutzman, W.L.,"Spatial, polarization, and pattern diversity for wireless handheld terminals," IEEE Transactions on Antennas and Propagation,” Vol.49, Issue 9, pp.1271-1281, 2001.

[31] Lusina, P.; Kohandani, F.; Ali, S.M., “Antenna parameter effects on spatial channel models,“ Communications, IET, Vol. 3, Issue 9, pp. 1463-1472, 2009.

[32] Anreddy, V.R.; Ingram, M.A., “Capacity of measured Ricean and rayleigh indoor MIMO channels at 2.4 GHz with polarization and spatial diversity,” Wireless Communications and Networking Conference, 2006. WCNC 2006. IEEE, Vol. 2, pp. 946-951, 2006.

[33] Dietrich, C.B., Jr.; Dietze, K.; Nealy, J.R.; Stutzman, W.L.,"Spatial, polarization, and pattern diversity for wireless handheld terminals," IEEE Transactions on Antennas and Propagation, Vol. 49, Issue 9, pp.1271-1281, 2001.

[34] Mattheijssen, P.; Herben, M.H.A.J.; Dolmans, G.; Leyten, L., "Antenna-pattern diversity versus space diversity for use at handhelds," IEEE Transactions on Vehicular Technology, Vol. 53, Issue 4, pp.1035-1042, 2004.

[35] Vaughan, R, "Switched parasitic elements for antenna diversity," IEEE Transactions on Antennas and Propagation, Vol. 47, Issue 2, pp. 399-405, 1999.

[36] Scott, N.L.; Leonard-Taylor, M.O.; Vaughan, R.G ,"Diversity gain from a single-port adaptive antenna using switched parasitic elements illustrated with a wire and monopole prototype," IEEE Transactions on Antennas and Propagation, Vol. 47, Issue 6, pp. 1066- 1070, 1999.

[37] Turkmani, A.M.D.; Arowojolu, A.A.; Jefford, P.A.; Kellett, C.J., "An experimental evaluation of the performance of two-branch space and polarization diversity schemes at 1800 MHz," IEEE Transactions on Vehicular Technology, Vol.44 , Issue 2, pp. 318- 326 , 1995.

[38] Miyazaki, N.; Nanba, S.; Konishi, S.,"MIMO-OFDM Throughput Performance on MIMO Antenna Configurations Using LTE-Based Testbed with 100 MHz Bandwidth," 72nd IEEE Vehicular Technology Conference Fall, pp.1- 5, 2010.

[39] R. Vaughan and J. B. Andersen, Channels, *Propagation and Antennas for Mobile Communications*. The IEE, London, UK, 2003.

[40] Sulonen, K.; Vainkainen, P.,"Effects of antenna radiation pattern on the performance of the mobile handset," IEEE International Symposium Antennas and Propagation Society, Vol.3, pp.354- 357, 2001.

[41] Stefania Sesia et al., *LTE The Long Term Evolution - From theory to practice*, WILEY, 2009.

[42] Pratt, T.G.; Srinivasan, R.; Son Nguyen, "Input-to-output cross polarization discrimination (IOXPD) dispersion model for mobile-to-mobile LOS wireless communications MIMO channels," Wireless Telecommunications Symposium, pp. 341- 347, 2008.

[43] 3GPP Technical Report, TS 36.521-1 V10.0.0, User Equipment (UE) conformance specification Radio transmission and reception Part 1: Conformance Testing; (Release 10).

[44] Eugene, C.H.Y.; Sakaguchi, K.; Araki, K, "Experimental and analytical investigation of MIMO channel capacity in an indoor line-of-sight (LOS) environment,"15th IEEE International Symposium on Personal, Indoor and Mobile Radio Communications, Vol.1, pp. 295- 300, 2004.

[45] Anreddy, V.R.; Ingram, M.A., "Capacity of measured ricean and rayleigh indoor MIMO channels at 2.4 GHz with polarization and spatial diversity," Wireless Communications and Networking Conference, 2006. WCNC 2006. IEEE, Vol. 2, pp. 946-951, 2006.

[46] Eugene, C.H.Y.; Sakaguchi, K.; Araki, K, "Experimental and analytical investigation of MIMO channel capacity in an indoor line-of-sight (LOS) environment," 15th IEEE International Symposium on Personal, Indoor and Mobile Radio Communications, Vol.1, pp. 295- 300, 2004.

[47] Takahashi, H.; Ofuji, Y.; Fukumoto, S.; Abeta, S.; Nakamura, T., Experimental Results on E-UTRA Downlink Throughput Using Polarization Diversity Antennas," IEEE 69th Vehicular Technology Conference, VTC Spring, pp. 1-6, 2009.

[48] Thiele, L.; Peter, M.; Jungnickel, V., "Statistics of the Ricean K-Factor at 5.2 Ghz in an Urban Macro-Cell Scenario," 17th International Symposium on Personal, Indoor and Mobile Radio Communications, pp. 1-5, 2006.

[49] 3GPP Technical Specification 36.321, Multiplexing and Channel Coding (FDD) (Release 8), www.3gpp.org.

[50] Jongho Kim; Young-Keun Yoon, "Correlation analysis of MIMO subchannels in LOS environments," 11th International Conference on Advanced Communication Technology, Vol. 1, pp. 335-337, 2009.

Appendix

Table A.1 2D Uniform Multi-path model based on Extended Pedestrian A(EPA) model

Cluster #	Delay [ns]	Power [dB]	AoD [˚]	AoA [˚]
1	0	0.0	N/A	0
2	30	-1.0	N/A	0
3	70	-2.0	N/A	0
4	90	-3.0	N/A	0
5	110	-8.0	N/A	0
6	190	-17.2	N/A	0
7	410	-20.8	N/A	0
Delay spread [ns]				45

Table A.2 SCME based Single spatial cluster with multi-path based on SCME Urban micro-cell model

Cluster#	Delay [ns]	Power [dB]	AoD[°]	AoA[°]
1	0/5/10	-3.0/-5.2/-7.0	6.6	0
2	285/290/295	-4.3/-6.5/-8.3	14.1	0
3	205/210/215	-5.7/-7.9/-9.7	50.8	0
4	660/665/670	-7.3/-9.5/-11.3	38.4	0
5	805/810/815	-9.0/-11.2/-13.0	6.7	0
6	925/930/,935	-11.4/-13.6/-15.4	40.3	0
Delay spread [ns]				294
Cluster AS AoD / AS AoA [°]				5/25 or 35
Cluster PAS shape				Laplacian
Total AS AoD / AS AoA [°]				18.2/25 or 35

Table A.3 SCME Urban Macro-cell channel Model

Cluster	Delay [ns]	Power [dB]	AoD[°]	AoA[°]
1	0,5,10	-3,-5.2,-7	82	66
2	360,365,370	-5.2,-7.4,-9.2	81	46
3	255,260,265	-4.7,-6.9,-8.7	80	143
4	1040,1045,1050	-8.2,-10.4,-12.2	99	33
5	2730,2735,2740	-12.1,-14.3,-16.1	102	-91
6	4600,4605,4610	-15.5,-17.7,-19.5	107	-19
Delay spread [ns]				839.5
Cluster AS AoD / AS AoA [°]				2 / 35
Cluster PAS shape				Laplacian
Total AS AoD / AS AoA [°]				7.8 / 62.6
XPR [dB]				9
Antenna type of transmitter at BS/ Antenna separation				Slanted dual polarized /40λ

Table A.4 SCME Urban Micro-cell channel Model

Cluster	Delay [ns]	Power [dB]	AoD[°]	AoA[°]
1	0, 5, 10	-3.0, -5.2, -7.0	6.6	0.7
2	285, 290, 295	-4.3, -6.5, -8.3	14.1	-13.2
3	205, 210,215	-5.7, -7.9, -9.7	50.8	146.1
4	660, 665,670	-7.3, -9.5, -11.3	38.4	-30.5
5	805, 810, 815	-9.0, -11.2, -13.0	6.7	-11.4
6	925, 930, 935	-11.4, -13.6, -15.4	40.3	-1.1
Delay spread [ns]				294
Cluster AS AoD / AS AoA [°]				5/ 35
Cluster PAS shape				Laplacian
Total AS AoD / AS AoA [°]				18.2 / 49.0
XPR [dB]				9
Ricean factor, K NLOS/LOS [dB]				0 / 0
Antenna type of transmitter at BS/ Antenna separation				Slanted dual polarized /0λ

국문요약

다중 편파 MIMO 안테나의 링크 성능 검증 방법에 관한 연구

연세대학교 대학원
전기전자공학과
조용상

본 논문에서는 다양한 종류의 안테나 다이버시티 방식에 대한 링크 성능 평가방법에 관한 연구를 수행하였다. 최근 새롭게 제안된 MIMO 무선 성능 평가 시스템인 Anechoic chamber 기반의 MIMO OTA 시스템을 이용하여 각각의 diversity 구조의 링크 성능을 실험적으로 검증하였으며 이를 이론 및 실제 필드 테스트 결과와 비교하였다.

우선적으로, 새로운 개념의 검증방식의 신뢰성을 검증하기 위해 MIMO OTA 시스템에서 생성된 2 차원 공간 무선 채널의 통계적 특성을 이론 및 실험적인 평가를 수행하였다. 검증을 위해 동일 편파 또는 이중 편파 특성을 갖는 다이폴 안테나 배열의 안테나 상관 지수를 MIMO OTA 시스템을 이용하여 실험적으로 평가 하였다. 이론적인 평가는 PAS 모델과 CDL 모델 기반의 WINNER II 채널 모델을 이용하였다. 검증 결과, MIMO 무선 채널의 2-D 분포함수가 Urban Macro 모델 또는 Uniform 모델과 같이 넓은 분포를 갖는 경우에만 MIMO OTA 시스템에서의 실험

결과와 PAS 모델로부터 얻은 결과가 일치하는 반면 CDL 모델 기반의 WINNER II 채널 모델로부터 얻은 결과는 Single cluster 모델에서도 일치함을 확인하였다.

안테나의 성능평가를 시스템의 링크 성능관점에서 안테나 특성이 이동 단말의 무선 네트워크 환경에서의 하향 링크 성능에 미치는 영향을 분석하는데 있어 안테나 상관지수 분석만으로는 한계가 있다. 본 논문에서는 CDL 모델로부터 구한 이론적인 MIMO 무선 채널용량과 유효 신호대 잡음비 모델링을 통해 LTE PDSCH 전송속도 예측이 가능하도록 기존의 모델을 일부 개선하였다.

제 1 장에서는 MIMO OTA 시스템을 실험적 방법 및 수치해석 방법을 통해 검증하였다. 또한, CDL 모델 기반의 채널 모델 및 LTE PDSCH 성능 예측 모델과 MIMO OTA 시스템을 이용하여 이중 편파 다이폴 안테나간의 상대적 기울기가 증가 할수록 NLOS 및 LOS 채널 환경에서 채널 용량 및 LTE PDSCH 성능이 향상됨을 이론 및 실험적으로 확인하였다.

제 2 장에서는 1 장에서 사용한 이론 및 실험 방법을 이용하여 LTE 이동 단말기의 MIMO 안테나에 대한 핸드 효과를 분석하였다. 이 분석을 통해 핸드 효과가 안테나의 효율을 저하시키는 동시에 상관 지수를 낮추는 효과가 존재하며 수신 신호의 레벨이 높은 일부 영역에서는 LTE PDSCH 성능 개선 효과가 있음을 이론 및 실험을 통해 확인하였다.

제 3 장에서는 다이폴 안테나 및 이동 단말기에 구현한 공간 다이버시티, 패턴 다이버시티, 편파 다이버시티 방식의 NLOS 및 LOS 채널 환경에서의 링크 성능 비교를 1, 2 장에서 사용한 이론 및 실험 방법을 통하여 비교 분석을 수행하였으며 이 결과를

통하여 특히 동일 편파 다이폴 안테나의 성능은 LOS 채널 환경에서 크게 저하되나 이중 편파 다이폴 안테나 및 이동 단말기에 구현한 공간 다이버 시티 안테나와 편광 다이버시티 안테나의 특성은 LOS 채널 환경에서 오히려 성능이 향상되는 특성을 보임을 확인하였다.

제 4 장 및 5 장에서는 LTE 네트워크에서 동일 편파 및 이중 편파 다이폴 안테나와 이동 단말 형태의 MIMO 안테나에 대한 LTE PDSCH 성능검증을 수행하였다. 3 장에서의 결과와 비교를 위해 NLOS 및 LOS 채널 환경을 갖는 두 곳의 옥외 필드시험 경로를 선정하여 시험을 진행하였으며 MIMO OTA 시스템 및 이론적인 분석 결과와 비교하였다. 3 장에서의 결론과 동일하게 동일 편파 다이폴 안테나는 LOS 채널 환경에서 크게 저하되며 이중 편파 다이폴 안테나 및 이동 단말기의 안테나는 LOS 환경에서 LTE PDSCH MIMO 데이터 전송 속도가 증가하는 특성을 보임을 확인하였다. 또한 이동 단말기의 안테나는 공통적으로 편광 다이버 시티 특성을 갖는다는 점을 실험 및 이론을 통해 검증하였다.

본 논문의 주요 성과로는 앞서 기술한 MIMO 안테나의 이론적인 성능 평가 모델에 유효 신호대 잡음비 모델을 통하여 안테나 성능이 LTE PDSCH 전송 속도에 미치는 영향을 분석하였으며 새로운 방식의 MIMO 안테나 링크성능 측정 방법인 MIMO OTA 시스템에 대하여 이론 및 실험을 통해 LTE 시험망과 상용 망에서의 안테나 성능 평가결과가 MIMO OTA 시스템에서의 평가 결과와 동일한 경향을 보임을 입증하였다.